UNIVERSITÀ
DEGLI STUDI
FIRENZE

DOTTORATO DI RICERCA IN SCIENZE DELLA TERRA

CICLO XXXI°

COORDINATORE Prof.ssa Lorella Francalanci

Incidence of orbital forcing on calcareous nannofossil assemblages new insights from lower-middle Eocene successions of the Basque-Cantabrian Basin (Spain)

Settore Scientifico Disciplinare GEO/01

Dottoranda
Dott.ssa Franceschetti Gloria

Tutore
Prof.ssa Monechi Simonetta

Co-Tutore
Prof. Aitor Payros Agirre

Coordinatore
Prof.ssa Francalanci Lorella

Anni 2015/2018

Contents

Chapter 3: Calcareous nannofossil response to astronomically driven climate changes on three Eocene deep-sea sections from the Basque-Cantabrian Basin, Spain

Chapter 4: Reassessing the Bartonian unit stratotypes: an integrated approach

Abstract

The Paleogene experienced the most profound climatic shift of the past 65 million years of Earth history, Earth's climate changing from a 'greenhouse' in the early Paleocene, to an 'icehouse' in the Oligocene. This transition resulted in significant re-organization of oceanic circulation, marine communities, and biogeochemical cycles. Particularly, climate changes occurred during the Eocene are forced (or thought to be forced) by variations of orbital parameters, especially by precession (21ky) and eccentricity (100ky), which can be detected by biotic proxies, like planktonic foraminifera, calcareous nannofossils and dinoflagellates (e.g., variation in their diversity, abundance and size), in hemipelagic and shallow waters.

The high abundance of calcareous nannofossils in pelagic marine sediments, makes this group one of the most useful tools to perform biostratigraphic, paleoecologic and paleoclimatic studies. Calcareous nannofossils, showing high evolutionary rate, result to be a good biostratigraphic marker, particularly for Cenozoic, when they reach high diversification.

In this PhD thesis, I investigate the relationships between orbital parameters and the variation of calcareous nannofossil abundances, expressed in eccentricity cycles of three different stratigraphic successions in the Basque-Cantabrian Basin (Spain): the Sopelana (early Ypresian), the Gorrondatxe (upper Ypresian) and the Oyambre sections (upper Lutetian).

Most of the studies applying such an approach, are focused on the Neogene and Quaternary, and only few studies have been carried out in older Cretaceous and Jurassic records. Up to now, no detailed studies have been performed with the aim to investigate precession and eccentricity cycles and their forcing on calcareous nannofossil aassemblages during the Eocene.

The three analyzed sections are constituted by rhythmic alternations of marls and limestones. A depositional-sedimentological model has been previously proposed for the three studied sections, on the base of geochemical proxies variation ($CaCO_3$ content, Oxygen and Carbon isotopes). For the Oyambre and Gorrondatxe sections, a detailed biostratigraphy was already

present, and the role of orbital forcing on sedimentation had been already highlighted by previous studies, while, for the Sopelana section there was a lack of this information.

Concerning the Sopelana section (**Chapter 2**), before analysing the influence of precession and eccentricity forcing on calcareous nannofossil abundances, I provide a detailed nannofossil biostratigraphy, and, by means of spectral analysis on $CaCO_3$ record, I highlight the role of the precession cycle in driving the deposition of marl-limestone couplets, and the effect of the eccentricity cycles on the sedimentation of bundles (each of which is composed by five marl-limestone couplets).

The variation of calcareous nannofossil abundances induced by orbital forcing has been investigated in **Chapter 3**. The statistical analyses (implemented with Principal Component Analysis and Cluster methods), based on the variation of calcareous nannofossil abundances, carried out in the Sopelana, Oyambre and Gorrondatxe sections, confirm the previous sedimentological models, adding new information regarding the sedimentary environments during the Eocene in the Basque-Cantabrian Basin. The performed analyses indicate that the major calcareous nannofossil assemblages variations occur at the maximum eccentricity, in correspondence of which we observe a decrease in oligotrophic and stable environments taxa and an increase in eutrophic and low salinity taxa. These observations confirm that the maximum eccentricity corresponds to the maximum seasonality, leading to an increase in nutrients supply from continents and a higher water mixing (upwelling).

A further work has been performed in the framework of the studies for the definition of the GSSP, considering that for the Paleogene two GSSPs are still pending (i.e., the base of Bartonian, middle Eocene, and the Priabonian, middle-upper Eocene). In our work, we focus on the definition of the Bartonian Stage. In **Chapter 4**, I report the results of a multidisciplinary study based on calcareous nannofossil, dinoflagellate, larger and smaller benthic foraminifera and magnetostratigraphy to assess potential correlations and placements for the Lutetian/Bartonian

boundary. The Bartonian unit stratotype is located at the Barton coastal section (Hampshire Basin, UK). In this work, I study the parastratotype section, located 7 km away at Alum Bay, since it shows a better exposure. Basing on the obtained results, the Alum bay section is within the nannoplankton Zones CNE14 and CNE15. The Base of *Rhombodinium draco*, (dinoflagellate), an important and correlatable event in the Tethys domain, is recognized within the section, which also coincides with the acme of *N. prestwichianus* (formerly indicated as the base of the Bartonian Stage in the Barton area), both of which are correlated with nannoplankton Zone NP16, spanning the upper Lutetian and lower Bartonian. The palaeomagnetic correlation with calcareous nannofossil data allows to assign the normal Chron at the base of the section to C19n, considered an approximation for the base of the Bartonian Stage according to the Geological Time Scale. The remaining portion of the section correlates to C18n and C18r. All analyses, therefore, support that the section is lower Bartonian in age, with the palaeomagnetic data indicating that the first 5 m of the section also contains the Upper Lutetian.

Introduction and aims of the thesis

The aim of this thesis work, in general terms, is to investigate whether orbitally forced climate change produced cyclic calcareous nannofossil abundance variations in Ypresian and Lutetian times (56-41 Ma). The effect of the orbital forcing on climate is to regulate seasonality and the amount of solar energy that reaches our planet. In this framework, we have studied the orbital influence on calcareous nannofossil assemblages in three different stratigraphic sections (Sopelana, Gorrondatxe and Oyambre) outcropping in the northern margin of the Iberian Peninsula (Basque-Cantabrian basin). In this study area, the effect of orbital forcing on sedimentation had previously been recognized and confirmed by several authors (e.g., Payros et al., 2009, 2011, 2012; Payros & Martínez-Braceras, 2014; Martínez-Braceras et al., 2017; Dinarès-Turell et al., 2018; Intxauspe-Zubiaurre et al., 2018). The sediments that make up the three studied sections are hierarchical and well organized alternations between marls and limestones. Depositional models based on sedimentological, mineralogical and geochemical analysis (Martínez-Braceras et al., 2017) have shown that the sedimentation of the Sopelana section (lower Ypresian, starved deep-sea basin) was regulated by variations in pelagic carbonate productivity. This parameter was proven to be mainly dependent on vertical seawater mixing, driven by seasonality and the resulting sea surface temperature. In the Gorrondatxe section (upper Ypresian, submarine fan fringe) variations in the rate of dilution of pelagic sediment with terrigenous inputs related to the intensity of seasonal rainfall on land, were the main controlling factor (Martínez-Braceras et al., 2017), while in the Oyambre section (upper Lutetian, upper carbonate slope) variations in pelagic carbonate productivity were determined by fluctuations in seawater salinity and nutrient content, as a response to changing rates of fresh water input, in line with seasonality-controlled rainfall intensity (Martínez-Braceras et al., 2017).

In this thesis, through the analyses of abundance variations and paleoecological affinities of the calcareous nannofossil assemblages, we aim to evaluate the importance of calcareous

nannofossils in the formation of marl and limestone alternations and their role in the deposition of calcium carbonate in different environmental settings, thus giving new insight into, and assessing the validity of, the previously proposed depositional models. A detailed description of the aims and objectives of this part of the work are provided in the following chapter (*Chapter 1- Aims, materials and methods*).

An additional study has been carried out in the framework of the investigations for the definition of Paleogene GSSPs, two of which are still pending formalization (the bases of the Bartonian, middle Eocene, and the Priabonian, middle-upper Eocene), in an effort to improve the Chronostratigraphic Time Scale. Traditionally, the Bartonian has been defined by the stratotypic Barton Clay Formation of the Barton area, Hampshire Basin, in the south of England. The stratotypes of both the Bartonian unit chronostratigraphic Stage (Curry, 1981) and the lithostratigraphic Barton Clay Formation (Hooker, 1986) are at the Barton coastal section. A similar section, but significantly thicker and much better exposed than the stratotype, occurs 7 km away at Alum Bay, Isle of Wight. The level chosen for the base of the Bartonian Stage by Curry (1981) is a single bed rich in *Nummulites prestwichianus*, but unfortunately this bed is scarcely correlatable outside of the Hampshire Basin, a condition that imposes strong limitation to its use for correlation. In order to resolve the correlation issue, the Alum Bay section was re-visited, in an effort to identify possible global markers capable of approximating the *Nummulites prestwichianus* level, and therefore provide possible useful tools to correlate the base of the Bartonian stage outside of the Hampshire Basin.

Several studies have been carried out since 70s in the Alum Bay section. Biostratigraphic studies on calcareous nannofossil were performed by Martini (1971) and Aubry (1983, 1986). Small benthic foraminifera were studied by Murray and Wright (1974) and more recently by Dawber et al. (2011). Dinoflagellate cysts were studied by Bujak (1980). The most recent study by Dawber et al. (2011) is an attempt to integrate all the previous biostratigraphic studies adding

magnetostratigraphic data. Taking these references as a starting point for our integrated approach based on calcareous nannofossils, dinoflagellates, larger and smaller benthic foraminifera and magnetostratigraphy, we aimed at assessing potential correlations and placements for boundaries of the Bartonian Stage. A detailed description of the objectives and adopted methodologies to this effort are described in the following chapter *(Chapter 1-Aims, materials and methods*).

State of the art

The Eocene Epoch (~55 to 34 Ma) was characterized by a long-term transition in global climate from a warm, ice-free "greenhouse" world to a cool "icehouse" world, with significant glaciation in the polar regions (Cramer et al., 2003; Lourens et al., 2005; Agnini et al., 2009; Galeotti et al., 2010; Leon-Rodriguez and Dickens 2010; Stap et al., 2010; Zachos et al., 2010; Sexton et al., 2011; Slotnick et al., 2012; Littler et al., 2014; Kirtland Turner et al., 2014; Lauretano et al., 2015, 2016; Westerhold et al. 2017, 2018). The onset of the Eocene is characterized by an extreme, rapid warming event called the Paleocene/Eocene Thermal Maximum (PETM) (Kennett and Stott, 1991), followed by a prolonged period of global warmth during the Ypresian (~55 to 50 Ma), known as the Early Eocene Climatic Optimum (EECO) (Zachos et al., 2001, Zachos et al., 2008; Dallanave et al., 2015; Payros et al., 2015; Westerhold et al., 2018; Lauretano et al., 2018). The late Paleocene-early Eocene long-term warming trend reached its peak during the EECO (~53-49 Ma; Kirtland Turner et al., 2014; Lauretano et al., 2015; Payros et al., 2015; Westerhold et al., 2018; Zachos et al., 2008, 2001), when the atmospheric CO_2 concentration and temperatures reached by far the most intense greenhouse conditions of the Cenozoic (Foster et al., 2017; Pagani et al., 2005; Zachos et al., 2008). This interval of persistent warmth followed a long-term drop in $\delta^{13}C$ between 58 and 52 Ma, linked to a reduction in the flux of organic carbon (Komar et al., 2011), and was associated with increasing pCO_2 (300-1700 ppmv) (Anagnostou et al., 2016;

Cui et al., 2017; Jagniecki et al., 2015) (Fig.1). After this early Eocene greenhouse period, a long-term cooling trend followed (Miller et al., 1987; Lear et al., 2000; Zachos et al., 2001). A substantial long-term decrease in global temperatures occurred through the middle and late Eocene, with cooling of up to 7°C in deep waters and high-latitude surface waters (Miller et al., 1987; Zachos et al., 2001, Zachos et al., 2008, Westerhold et al., 2018), culminating in the widespread glaciation of Antarctica shortly after the Eocene/Oligocene boundary (~34 Ma) during the Oi-1 event. However, this global cooling trend was temporarily interrupted 40 Ma during the Middle Eocene Climatic Optimum (MECO, Bohaty and Zachos, 2003; Bohaty et al., 2009; Edgar et al., 2010; Sluijs et al., 2013), which entailed an increase in atmospheric pCO_2 during ~500 kyr (Bijl et al., 2010), shoaling of the CCD (Bohaty et al., 2009; Pälike et al., 2012), and a 4–6 °C increase in surface and deep water temperatures.

The long-term Eocene climatic evolution was punctuated by short-term events of abrupt increase in global temperatures, named hyperthermal events. Hyperthermal events were associated with intense perturbations of the global carbon cycle and sea-surface and atmospheric temperatures, being recorded by intense dissolution in deep-sea sediments and negative excursions in carbon and oxygen stable isotope records (Galeotti et al., 2017; Littler et al., 2014; Lourens et al., 2005; Sexton et al., 2011; Zachos et al., 2010). During the largest negative carbon isotope excursion (CIE) at the Paleocene–Eocene Thermal Maximum (PETM), global temperatures rose 4 to 8°C (Kennett and Stott, 1991; Zachos et al., 2005). Geochemical evidence suggests that these transient events were driven by the input of vast amounts of ^{13}C-depleted carbon to the ocean-atmosphere system, most likely from the destabilization of light-carbon reservoirs (Deconto et al., 2012; Dickens et al., 1997; Frieling et al., 2016; Kennett and Stott, 1991; Littler et al., 2014; Nicolo et al., 2007; Sluijs et al., 2007; Zachos et al., 2008, 2010). The increase in pCO_2 contributed to the acidification of the oceans, which induced a rise in the level of carbonate compensation (CCD-Calcite Compensation Depth) and the lysoclyne, temporarily affecting calcareous organisms

such as planktonic and benthic foraminifera, calcareous nannofossil and dinoflagellates (Thomas and Zachos, 2000; Thomas et al., 2000, 2006; Cramer et al., 2003; Zachos et al., 2004; Lourens et al., 2005; Rohl et al., 2005; Nicolo et al., 2007; Coccioni et al., 2010, 2012; Westerhold et al., 2011, 2017, 2018).

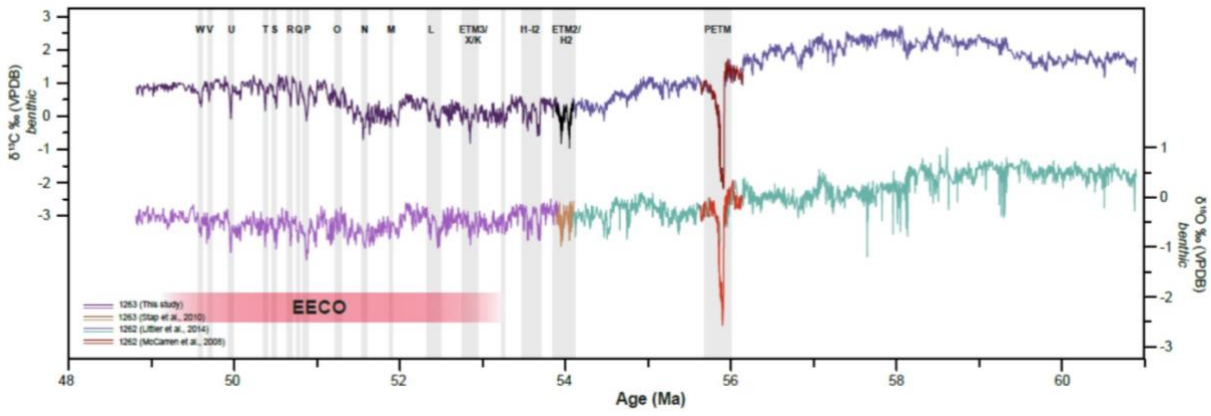

Fig. 1: Composite records of benthic $\delta^{13}C$ and $\delta^{18}O$ for the late Paleocene-early Eocene (modified from Lauretano et al., 2018). Vertical grey bands indicate the position of hyperthermal events. Labels for the events are from Westerhold et al. (2018), based on magnetostratigraphic information, and Lauretano et al. (2016), based on the alpha-numeric scheme by Cramer et al. (2003). Horizontal pink bar indicates the position of the Early Eocene Climatic Optimum (EECO; ~53-49 Ma).

Potential triggering mechanisms for the hyperthermal events include exceeding a temperature threshold as the Earth gradually warmed up, the impact of comets and extra-terrestrial objects, volcanism, or active tectogenesis (Svensen et al., 2004; DeConto et al., 2012; Luciani et al., 2017; Galeotti et al., 2017; Westerhold et al., 2018). However, studies on astronomical tuning of ocean sedimentary records have shown that most of the hyperthermal events and the $\delta^{13}C$ anomalies were related to periodic variations in insolation, which are regulated by changes in the Earth's orbital motion around the Sun (Cramer et al., 2003; Lourens et al., 2005; Westerhold et al., 2007; Galeotti et al., 2010; Laurin et al., 2016; Zeebe et al., 2017). Several studied have demonstrated that the periodic variations in the Earth orbital parameters

result in changes in climate over periods of tens to hundreds of thousands of years (e.g., Imbrie and Imbrie 1979; Imbrie et al. 1984). The Eccentricity of the orbit, Obliquity (axial tilt) and Precession of equinoxes are the main orbital elements considered in the so-called Milankovitch cycles. The precession of equinoxes is produced by a combined effect of the axial precession and precession of ellipse. It plays an important role in determining where on the orbit around the Sun the seasons occur (e.g. aphelio or perielio; Zachos et al., 2001). Obliquity is responsible for the variation of the inclination of the Earth axis, which amplifies or reduces the strength of the seasons, mainly at high latitudes. In addition, the shape of the Earth's orbit is regulated by its eccentricity, varying from more circular (low eccentricity) to more elliptical (high eccentricity), which implies that at minimum eccentricity there is virtually no difference in insolation between perihelion and aphelion. Eccentricity variations, changing the Earth-Sun distance, affect the intensity and length of the seasons. Climate change resulting from the variation of these orbital parameters has a direct impact on the Earth's marine environments and can consequently be recorded in deep-sea sedimentary records. The astronomical tuning of these sedimentary archives is a powerful tool to produce accurate time scales that have the advantage of creating continuous age models. The instance on which the Geological Time Scale (GTS) is based has progressively incorporated age-dated intervals with astronomical tuning, the Cenozoic Era being almost completely covered with an astronomical absolute time scale (ATS) (GTS2012; Ogg, 2012). Given that hemipelagic sedimentation in deep water environments is highly sensitive to climate change, calcareous limestone-mar alternations are ideal for cyclostratigraphic studies (Dinares-Turell et al., 2002; 2003; 2007; 2018; Wu et al., 2012; Jimenez Berrocoso et al., 2013; Payros & Martínez-Braceras, 2014; Eldrett et al., 2015; Martínez-Braceras et al., 2017; Westerhold et al., 2018). Orbital cyclicities have been identified in a wide variety of measurable geological parameters, which were initially restricted to lithological characters but subsequently incorporated physical, geochemical and paleontological characteristics of rock successions

(Berger et al., 1984; Gale and House, 1995; Gibbs et al. 2004). The cyclostratigraphic characteristics of these successions are generally considered to be the result of fluctuations in different sedimentary processes that are climatically regulated (Einsele et al., 1991), such as biological productivity of carbonate, dilution of carbonates by terrigenous inputs, and/or dissolution of carbonates in response to fluctuations of the CCD. Unfortunately, it is generally difficult to specify which environmental factors determine the relative significance of the abovementioned sedimentary processes in each succession.

The climate changes that occurred during the Eocene are well documented by variations of many temperature proxies ($\delta^{18}O$, Mg/Ca, Tex_{86}, Δ_{47} *clumped isotopes*) and biotic proxies (planktonic foraminifera, calcareous nannofossils and dinoflagellates) in hemipelagic and shallow water deposits. High-resolution studies on calcareous nannofossils highlight climate-driven evolutionary turnovers and the succession of biotic events, changes in richness and diversity mainly being related to abrupt and rapid variations in isotopic oxygen and carbon records (Thomas and Shackleton, 1996; Gingerich, 2003; Clyde et al., 2007; Sluijs et al., 2007a, 2007b, 2009; Dunkley Jones et al., 2013). Investigations of orbitally-driven climatic signals from nannofossil biotic records have generally been restricted to the late Quaternary (Marino et al., 2008, 2009; Beaufort et al., 1997, 2001; Bassinot et al., 1997; Maiorano et al., 2016). Fewer studies of orbital signals in nannofossil abundances have been carried out in older records. Cyclic patterns have been shown for *Discoaster* in the late Pliocene (Chepstow-Lusty et al., 1989; Gibbs et al., 2004) and for *Coccolithus pelagicus* and *Reticulofenestra pseudoumbilicus* in the Miocene (Beaufort and Aubry, 1990). In the Mesozoic, periodicities in nannofossil abundance have been observed in some studies (Erba et al., 1992; Herrle et al., 2003, Walsworth-Bell, 2001; Hay & Flogel, 2012; Giorgioni et al., 2015; Giorgioni et al., 2017).

References

Agnini, C., Macri, P., Backman, J., Brinkhuis, H., Fornaciari, E., Giusberti, L., Luciani, V., Rio, D., Sluijs, A., and Speranza, F. (2009). An early Eocene carbon cycle perturbation at 52.5Ma in the Southern Alps: Chronology and biotic response, Paleoceanogra- phy, 24, PA2209, https://doi.org/10.1029/2008pa001649.

Anagnostou, E., John, E.H., Edgar, K.M., Foster, G.L., Ridgwell, A., Inglis, G.N., Pancost, R.D., Lunt, D.J., Pearson, P.N., (2016). Changing atmospheric CO 2 concentration was the primary driver of early Cenozoic climate. https://doi.org/10.1038/nature17423

Aubry, M.-P., (1983). Biostratigraphie du Paléogène épicontinental de l'Europe du nord-ouest. Étude fondée sur les nannofossiles calcaires. Documents des Laboratoires de Géologie de la Faculté des Sciences de Lyon 89, 1–317.

Aubry, M.-P., (1986). Paleogene calcareous nannoplankton biostratigraphy of northwestern Europe. Palaeogeography, Palaeoclimatology, Palaeoecology 55, 267–334.

Beaufort, L., Aubry, M.-P., (1990). Fluctuations in the composition of Late Miocene calcareous nannofossil assemblages as a response to orbital forcing. Paleoceanography 5, 845–865.

Beaufort, L., de Garidel-Thoron, T., Mix, A.C., Pisias, N.G., (2001). ENSO-like forcing on oceanic primary production during the Late Pleistocene. Science 293, 2440–2444.

Beaufort, L., Lancelot, Y., Camberlin, P., Cayre, O., Vincent, E., Bassinot, F., Labeyrie, L., (1997). Insolation cycles as a major control of equatorial Indian ocean primary production. Science 278, 1451–1454.

Berger A. , J Imbrie, J Hays, J Kukla, B Saltzman (Eds) (1984). Milankovitch and Climate: Understanding the Response to Astronomical Forcing, Reidel Publishing Company, Dordrecht 895.

Berrocoso, Á. J., Elorza, J., & MacLeod, K. G. (2013). Proximate environmental forcing in fine scale geochemical records of calcareous couplets (Upper Cretaceous and Palaeocene of the Basque Cantabrian Basin, eastern North Atlantic). Sedimentary Geology, 284, 76-90.

Bijl, P.K., Houben, A.J.P., Schouten, S., Bohaty, S.M., Sluijs, A., Reichart, G.-J., Damsté, J.S.S., Brinkhuis, H., (2010). Transient middle Eocene atmospheric CO2 and temperature variations. Science 330, 819–821.

Bohaty, S.M., Zachos, J.C., (2003). Significant Southern Ocean warming event in the late middle Eocene. Geology 31, 1017–1020.

Bohaty, S.M., Zachos, J.C., Florindo, F., Delaney, M.L., (2009). Coupled greenhouse warming and deep-sea acidification in the middle Eocene. Paleoceanography 24, PA2207.

Bujak, J.P., Downie, C., Eaton, G.L., Williams, G.L., (1980). Dinoflagellate cysts and acritarchs from the Eocene of southern England. Special Papers in Palaeontology 24, 1–100.
Chepstow-Lusty, A., Shackleton, N.J., Backman, J., (1992). Upper Pliocene Discoaster abundance variations from the Atlantic, Pacific and Indian oceans: the significance of productivity pres- sure at low latitudes. Mem. Sci. Geol. 44, 357–373.

Clyde, W. C., Hamzi, W., Finarelli, J. A., Wing, S. L., Schankler, D., and Chew, A. (2007).: Basin-wide magnetostratigraphic framework for the Bighorn Basin, Wyoming, GSA Bulletin, 119, 848–859.

Coccioni, R., Bancala, G., Catanzarit, R., Fornaciari, E., Frontalini, F., Giusberti, L., ... & Sprovieri, M. (2012). An integrated stratigraphic record of the Palaeocene–lower Eocene at Gubbio (Italy): new insights into the early Palaeogene hyperthermals and carbon isotope excursions. Terra Nova, 24(5), 380-386.

Coccioni, R., Frontalini, F., Bancala` , G., Fornaciari, E., Jovane, L. and Sprovieri, M., (2010). The Dan–C2 hyperthermal event at Gubbio (Italy). Global implications, environmental effects, and cause(s). Earth Planet. Sci. Lett., 297, 298– 305.

Cramer, B. S., Wright, J. D., Kent, D. V., and Aubry, M.-P.(2003).: Orbital climate forcing of 13C excursions in the late Paleocene – Eocene (chrons C24n–C25n), Paleoceanography, 18, 1097, https://doi.org/10.1029/2003PA000909,.

Cui, Y., & Schubert, B. A. (2017). Atmospheric pCO2 reconstructed across five early Eocene global warming events. Earth and Planetary Science Letters, 478, 225-233.

Curry, D., Bartonian, (1981). In: Pomerol, C. (Ed.), Stratotypes of Paleogene stages. Bulletin d'Information des Géologues du Bassin de Paris (Mém. hors série), vol. 2. , pp. 23–36.

Dallanave, E., Agnini, C., Bachtadse, V., Muttoni, G., Crampton, J. S., Strong, C. P., ... & Slotnick, B. S. (2015). Early to middle Eocene magneto-biochronology of the southwest Pacific Ocean and climate influence on sedimentation: Insights from the Mead Stream section, New Zealand. Bulletin, 127(5-6), 643-660.

Dawber, C. F., Tripati, A. K., Gale, A. S., MacNiocaill, C., & Hesselbo, S. P. (2011). Glacioeustasy during the middle Eocene? Insights from the stratigraphy of the Hampshire Basin, UK. Palaeogeography, Palaeoclimatology, Palaeoecology, 300(1-4), 84-100.

DeConto, R.M., Galeotti, S., Pagani, M., Tracy, D., Schaefer, K., Zhang, T., Pollard, D., Beerling, D.J., (2012). Past extreme warming events linked to massive carbon release from thawing permafrost. Nature 484, 87–91. https://doi.org/10.1038/nature10929

Dickens, G.R., Castillo, M.M., Walker, J.C.G., (1997). A blast of gas in the latest Paleocene: Simulating first-order effects of massive dissociation of oceanic methane hydrate. Geology 25, 259.

Dinarès-Turell, J., Martínez-Braceras, N., Payros, A., (2018). High-resolution integrated cyclostratigraphy from the Oyambre section (Cantabria, N Iberian Peninsula): constraints for orbital tuning and correlation of middle Eocene Atlantic deep-sea records. Geochem. Geophys. Geosyst. 19, 2017GC007367. https://doi.org/10.1002/ 2017GC007367.

Dinarès-Turell, J., Baceta, J. I., Pujalte, V., Orue-Etxebarria, X., & Bernaola, G. (2002). Magnetostratigraphic and cyclostratigraphic calibration of a prospective Palaeocene/Eocene stratotype at Zumaia (Basque Basin, northern Spain). Terra Nova, 14(5), 371-378.

Dinarès-Turell, J., Baceta, J. I., Bernaola, G., Orue-Etxebarria, X., & Pujalte, V. (2007). Closing the mid-Palaeocene gap: toward a complete astronomically tuned Palaeocene Epoch and Selandian and Thanetian GSSPs at Zumaia (Basque Basin, W Pyrenees). Earth and Planetary Science Letters, 262(3-4), 450-467.

Dinarès-Turell, J., Baceta, J. I., Pujalte, V., Orue-Etxebarria, X., Bernaola, G., & Lorito, S. (2003). Untangling the Palaeocene climatic rhythm: an astronomically calibrated Early Palaeocene magnetostratigraphy and biostratigraphy at Zumaia (Basque basin, northern Spain). Earth and Planetary Science Letters, 216(4), 483-500.

Dunkley Jones, T., Lunt, D.J., Schmidt, D.N., Ridgwell, A., Sluijs, A., Valdes, P.J., Maslin, M., (2013). Climate model and proxy data constraints on ocean warming across the Paleocene-Eocene Thermal Maximum. Earth-Sci. Rev. 125, 123–145. https://doi.org/ 10.1016/j.earscirev.2013.07.004.

Edgar, K.M., Wilson, P.A., Sexton, P.F., Gibbs, S.J., Roberts, A.P., Norris, R.D., (2010). New biostratigraphic, magnetostratigraphic and isotopic insights into the Middle Eocene Climatic Optimum in low latitudes. Palaeogeogr. Palaeoclimatol. Palaeoecol. 297, 670–682.

Einsele, G., Ricken, W., & Seilacher, A. (1991). Cycles and events in stratigraphy.

Eldrett, J. S., Ma, C., Bergman, S. C., Lutz, B., Gregory, F. J., Dodsworth, P., ... & Ramezani, J. (2015). An astronomically calibrated stratigraphy of the Cenomanian, Turonian and earliest Coniacian from the Cretaceous Western Interior Seaway, USA: Implications for global chronostratigraphy. Cretaceous Research, 56, 316-344.

Erba, E., Castradori, D., Guasti, G., & Ripepe, M. (1992). Calcareous nannofossils and Milankovitch cycles: the example of the Albian Gault Clay Formation (southern England). Palaeogeography, Palaeoclimatology, Palaeoecology, 93(1-2), 47-69.

Foster, G.L., D.L. Royer, and D.J. Lunt, (2017). Future climate forcing potentially without precedent in the last 420 million years. Nature Communications, 8: p. 14845.

Frieling, J., Svensen, H.H., Planke, S., Cramwinckel, M.J., Selnes, H., Sluijs, A., (2016). Thermogenic methane release as a cause for the long duration of the PETM. Proc. Natl. Acad. Sci. U. S. A. 113, 12059–12064. https://doi.org/10.1073/pnas.1603348113

Gale, A. S., & House, M. R. (Eds.). (1995). Orbital forcing timescales and cyclostratigraphy. Geological Society.

Galeotti, S., Krishnan, S., Pagani, M., Lanci, L., Gaudio, A., Za- chos, J. C., Monechi, S., Morelli, G., and Lourens, L. (2010).: Orbital chronology of Early Eocene hyperthermals from the Contessa Road section, central Italy, Earth Planet. Sc. Lett., 290, 192–200, https://doi.org/10.1016/j.epsl.2009.12.021.

Galeotti, S., Moretti, M., Sabatino, N., Sprovieri, M., Ceccatelli, M., Francescone, F., ... & Monechi, S. (2017). Cyclochronology of the Early Eocene carbon isotope record from a composite Contessa Road-Bottaccione section (Gubbio, central Italy). Newsletters on Stratigraphy, 50(3), 231-244.

Gibbs, S., Shackleton, N., & Young, J. (2004). Orbitally forced climate signals in mid-Pliocene nannofossil assemblages. Marine Micropaleontology, 51(1), 39-56.

Gingerich, P. D. (2003).: Mammalian responses to climate change at the Paleocene-Eocene boundary: Polecat Bench record in the north- ern Bighorn Basin, Wyoming, in: Causes and Consequences of Globally Warm Climates in the Early Paleogene, edited by: Wing, S. L., Gingerich, P. D., Schmitz, B., and Thomas, E., Geo- logical Society of America Special Paper, Geological Society of America, Boulder, Colorado, 463–478,.

Giorgioni, M., Tiraboschi, D., Erba, E., Hamann, Y., & Weissert, H. (2017). Sedimentary patterns and palaeoceanography of the Albian Marne a Fucoidi Formation (Central Italy) revealed by high-resolution geochemical and nannofossil data. Sedimentology, 64(1), 111-126.

Giorgioni, M., Weissert, H., Bernasconi, S.M., Hochuli, P.A., Keller, C.E., Coccioni, R., Petrizzo, M.R., Lukeneder, A. and Garcia, T.I. (2015). Paleoceanographic changes during the Albian-Cenomanian in the Tethys and North Atlantic and the onset of the Cretaceous chalk. Global Planet. Change, 126, 46–61. doi:10.1016/j.gloplacha.2015.01.005.

Hay, W.W. and Flögel, S. (2012). New thoughts about the Cretaceous climate and oceans. Earth Sci. Rev., 115, 262–272.

Herrle, J.O., Pross, J., Friedrich, O., Hemleben, C., (2003). Short- term environmental changes in the Cretaceous Tethyan Ocean: micropalaeontological evidence from the Early Albian Oceanic Anoxic Event 1b. Terra Nova 15, 14–19.

Hooker J. J., C. King, The Bartonian unit stratotype (S. England), (2018). Assessment of its correlation problems and potential, Proc. Geol. Assoc. https://doi.org/10.1016/j.pgeola.2018.08.005.

Hooker, J.J., (1986). Mammals from the Bartonian (middle/late Eocene) of the Hampshire Basin, southern England. Bulletin of the British Museum (Natural History) (Geology) 39, 191–478.

Imbrie, J., & Imbrie, K. P. (1979). Ice ages: solving the mystery (2nd edn.). Harvard University Press, Cambridge.

Imbrie, J., Hays, J. D., Martinson, D. G., McIntyre, A., Mix, A. C., Morley, J. J., Pisias N.G.,Prell W.L., Shackleton, N. J. (1984). The orbital theory of Pleistocene climate: Support from a revised chronology of the marine delta18 O record. In Milankovitch and climate: Understanding the response to astronomical forcing (Vol. 1, p. 269).

Intxauspe-Zubiaurre, B., Martínez-Braceras, N., Payros, A., Ortiz, S., Dinarès-Turell, J., & Flores, J. A. (2018). The last Eocene hyperthermal (Chron C19r event,~ 41.5 Ma): Chronological and paleoenvironmental insights from a continental margin (Cape Oyambre, N Spain). Palaeogeography, Palaeoclimatology, Palaeoecology.

Jagniecki, E.A., Lowenstein, T.K., Jenkins, D.M., Demicco, R. V., (2015). Eocene atmospheric CO 2 from the nahcolite proxy. Geology 43, G36886.1. https://doi.org/10.1130/G36886.1

Kennett, J.P., Stott, L.D., 1991. Proteus and proto-oceanus: ancestral Paleogene oceans as revealed from Antarctic stable isotopic results; ODP 113. In: Barker, P.F., Kennett, J.P., et al. (Eds.), Proc. ODP Sci. Results, vol. 113, pp. 865–880.

Kirtland Turner, S., Sexton, P. F., Charles, C. D., and Norris, R. D. (2014).: Persistence of carbon release events through the peak of early Eocene global warmth, Nat. Geosci., 7, 748–751, https://doi.org/10.1038/ngeo2240,.

Komar, N., Zeebe, R.E., (2011). Oceanic calcium changes from enhanced weathering during the Paleocene-Eocene thermal maximum: No effect on calcium-based proxies. Paleoceanography 26. https://doi.org/10.1029/2010PA001979

Lauretano, V. , Zachos, J. C. and Lourens, L. J. (2018), Orbitally Paced Carbon and Deep-Sea Temperature Changes at the Peak of the Early Eocene Climatic Optimum. Paleoceanography and Paleoclimatology. Accepted Author Manuscript. . doi:10.1029/2018PA003422

Lauretano, V., Hilgen, F. J., Zachos, J. C., and Lourens, L. J. (2016)..: Astronomically tuned age model for the early Eocene carbon isotope events: A new high-resolution 13C benthic record of ODP Site 1263 between ⇠ 49 and ⇠ 54 Ma, Newsl. Stratigr., 49, 383–400, https://doi.org/10.1127/nos/2016/0077,

Lauretano, V., Littler, K., Polling, M., Zachos, J. C., and Lourens, L. J. (2015).: Frequency, magnitude and character of hyperthermal events at the onset of the Early Eocene Climatic Optimum, Clim. Past, 11, 1313–1324, https://doi.org/10.5194/cp-11-1313-2015,

Laurin, J., Meyers, S.R., Galeotti, S., Lanci, L., (2016). Frequency modulation reveals the phasing of orbital eccentricity during Cretaceous Oceanic Anoxic Event II and the Eocene hyperthermals. Earth Planet. Sci. Lett. 442, 143–156. https://doi.org/10. 1016/j.epsl.2016.02.047.

Lear, C.H., Elderfield, H., Wilson, P.A., (2000). Cenozoic deep-sea temperatures and global ice volumes from Mg/Ca in benthic foraminiferal calcite. Science 287, 269–272.

Leon-Rodriguez, L. and Dickens, G. R. (2010)..: Constraints on ocean acidification associated with rapid and massive carbon injections: The early Paleogene record at ocean drilling program site 1215, equatorial Pacific Ocean, Palaeogeogr. Palaeocl., 298, 409–420, https://doi.org/10.1016/j.palaeo.2010.10.029,

Littler, K., Röhl, U., Westerhold, T., Zachos, J.C., (2014). A high-resolution benthic stable isotope record for the South Atlantic: Implications for orbital-scale changes in Late Paleocene-Early Eocene climate and carbon cycling. Earth Planet. Sci. Lett. 401, 18– 30. https://doi.org/10.1016/j.epsl.2014.05.054

Lourens, L.J., Sluijs, A., Kroon, D., Zachos, J.C., Thomas, E., Röhl, U., Bowles, J., Raffi, I., (2005). Astronomical pacing of late Palaeocene to early Eocene global warming events. Nature 435, 1083–1087. https://doi.org/10.1038/nature03814

Luciani, V., D'Onofrio, R., Dickens, G. R., & Wade, B. (2017). Major early Eocene carbon cycle perturbations and changes in planktic foraminiferal assemblages from the southeast Atlantic Ocean (ODP Site 1263). In EGU General Assembly Conference Abstracts (Vol. 19, p. 8960).

Lunt, D.J., Ridgwell, A., Sluijs, A., Zachos, J.C., Hunter, S., Haywood, A., (2011). A modelbfor orbital pacing of methane hydrate destabilization during the Palaeogene. Nat.Geosci. 4, 775–778.

Maiorano, P., Girone, A., Marino, M., Kucera, M., & Pelosi, N. (2016). Sea surface water variability during the Mid-Brunhes inferred from calcareous plankton in the western Mediterranean (ODP Site 975). Palaeogeography, Palaeoclimatology, Palaeoecology, 459, 229-248.

Marino, M., Maiorano, P. and Lirer, F. (2008). Changes in calcareous nannofossil assemblages during the Mid-Pleistocene Revolution. Marine Micropaleontology, 69, 70-90.

Marino, M., Maiorano, P., Lirer, F. and Pelosi, N. (2009). Response of calcareous nannofossil assemblages to paleoenvironmental changes through the mid-Pleistocene revolution at Site 1090 (Southern Ocean). Palaeogeography, Palaeoclimatology, Palaeoecology, 280, 333-349.

Martínez-Braceras, N., Payros, A., Miniati, F., Arostegi, J., Franceschetti, G., (2017). Contrasting environmental effects of astronomically driven climate change on three Eocene hemipelagic successions from the Basque–Cantabrian Basin. Sedimentology 64 (4), 960-986. http://dx.doi.org/10.1111/sed.12334

Martini, E. (1971). Standard Tertiary and Quaternary calcareous nannoplankton zonation. In Proc. II Planktonic Conference, Roma 1970, Roma, Tecnoscienza (Vol. 2, pp. 739-785).

Miller, K.G., Fairbanks, R.G., Mountain, G.S., (1987). Tertiary oxygen isotope synthesis, sea-level history and continental margin erosion. Paleoceanography 2, 1–19.

Murray, J.W., Wright, C.A., (1974). Palaeogene Foraminiferida and palaeoecology, Hampshire and Paris Basins and the English Channel. Special Papers in Palaeontology 14, 1–129 20 pls.

Newsam, C., Bown, P. R., Wade, B. S., & Jones, H. L. (2017). Muted calcareous nannoplankton response at the Middle/Late Eocene Turnover event in the western North Atlantic Ocean. Newsletters on Stratigraphy, 50(3), 297-309.

Nicolo, M.J., Dickens, G.R., Hollis, C.J., Zachos, J.C., (2007). Multiple early Eocene hyperthermals: Their sedimentary expression on the New Zealand continental margin and in the deep sea. Geology 35, 699. https://doi.org/10.1130/G23648A.1

Ogg, J. G. (2012). The geomagnetic polarity timescale. In Gradstein, F. M., Ogg, J. G., Schmitz, M., & Ogg, G. (Eds.), A geological time scale (pp. 85–113). Amsterdam, the Netherlands: Elsevier B.V. https://doi.org/10.1016/B978-0-444-59425-9.00005-6

Pagani, M., Zachos, J.C., Freeman, K.H., Tipple, B., Bohaty, S., (2005). Marked Decline in Atmospheric Carbon Dioxide Concentrations During the Paleogene 600–603.

Pälike, H., Lyle, M.W., Nishi, H., Raffi, I., Ridgwell, A., Gamage, K., Klaus, A., Acton, G., Anderson, L., Backman, J., Baldauf, J., Beltran, C., Bohaty, S.M., Bown, P., Busch, W., Channell, J.E.T., Chun, C.O.J., Delaney, M., Dewangan, P., Dunkley Jones, T., Edgar, K.M., Evans, H., Fitch, P., Foster, G.L., Gussone, N., Hasegawa, H., Hathorne, E.C., Hayashi, H., Herrle, J.O., Holbourn, A., Hovan, S., Hyeong, K., Iijima, K., Ito, T., Kamikuri, S., Kimoto, K., Kuroda, J., Leon-Rodriguez, L., Malinverno, A., Moore Jr., T.C., Murphy, B.H., Murphy, D.P., Nakamura, H., Ogane, K., Ohneiser, C., Richter, C., Robinson, R., Rohling, E.J., Romero, O., Sawada, K., Scher, H., Schneider, L., Sluijs, A., Takata, H., Tian, J., Tsujimoto, A., Wade, B.S., Westerhold, T., Wilkens, R., Williams, T., Wilson, P.A., Yamamoto, Y., Yamamoto, S., Yamazaki, T., Zeebe, R.E., (2012). A Cenozoic record of the equatorial Pacific carbonate compensation depth. Nature 488, 609–614.

Payros, A., & Martínez-Braceras, N. (2014). Orbital forcing in turbidite accumulation during the Eocene greenhouse interval. Sedimentology, 61(5), 1411-1432.

Payros, A., Dinares-Turell, J., Bernaola, G., Orue-Etxebarria, X., Apellaniz, E. and Tosquella, J. (2011) On the age of the Early/Middle Eocene boundary and other related events: cyclostratigraphic refinements from the Pyrenean Otsakar section and the Lutetian GSSP. Geol. Mag., 148, 442–460.

Payros, A., Orue-Etxebarria, X., Bernaola, G., Apellaniz, E., Dinares-Turell,J.,Tosquella,J.andCaballero,F.(2009) Characterization and astronomically calibrated age of the first occurrence of Turborotalia frontosa in the Gorrondatxe section, a prospective Lutetian GSSP: implications for the Eocene time scale. Lethaia, 42, 255– 264.

Payros, A., Ortiz, S., Alegret, L., Orue-Etxebarria, X., Apellaniz, E., & Molina, E. (2012). An early Lutetian carbon-cycle perturbation: Insights from the Gorrondatxe section (western Pyrenees, Bay of Biscay). Paleoceanography, 27(2).

Payros, A., Ortiz, S., Millán, I., Arostegi, J., Orue-Etxebarria, X., & Apellaniz, E. (2015). Early Eocene climatic optimum: Environmental impact on the North Iberian continental margin. Bulletin, 127(11-12), 1632-1644

Rohl, U., Westerhold, T., Monechi, S., Thomas, E., Zachos, J.C. and Donner, B., (2005). The Third and Final Early Eocene Thermal Maximum: characteristics, Timing and Mechanisms of the ÔXÕ Event. Geol. Soc. Am., 37th Annual Meeting, Salt Lake City, USA, Abstract, 264.

Sexton, P. F., Norris, R. D., Wilson, P. A., Pälike, H., Westerhold, T., Röhl, U., Bolton, C. T., and Gibbs, S. (2011).: Eocene global warm- ing events driven by ventilation of oceanic dissolved organic carbon, Nature, 471, 349–352, https://doi.org/10.1038/nature09826,

Sexton, P.F., Norris, R.D., Wilson, P. a., Pälike, H., Westerhold, T., Röhl, U., Bolton, C.T., Gibbs, S.J., (2011). Eocene global warming events driven by ventilation of oceanic dissolved organic carbon. Nature 471, 349–352. https://doi.org/10.1038/nature09826

Slotnick, B. S., Dickens, G. R., Nicolo, M. J., Hollis, C. J., Cramp- ton, J. S., Zachos, J. C., and Sluijs, A. (2012).: Large-Amplitude Variations in Carbon Cycling and Terrestrial Weathering during the Latest Paleocene and Earliest Eocene: The Record at Mead Stream, New Zealand, J. Geol., 120, 487–505,.

Sluijs, A., Bowen, G., Brinkhuis, H., Lourens, L., Thomas, E., (2007a). The Palaeocene- Eocene Thermal Maximum Super Greenhouse: biotic and geochemical signatures. In: Age Models and Mechanisms of Global Change, Deep-Time Perspectives on Climate Change: Marrying the Signal From Computer Models and Biological Proxies. The Micropaleontological Society, Special Publicationspp. 323–349.

Sluijs, A., Brinkhuis, H., Schouten, S., Bohaty, S.M., John, C.M., Zachos, J.C., Reichart, G.J., Sinninghe Damsté, J.S., Crouch, E.M., Dickens, G.R., (2007b). Environmental precursors to rapid light carbon injection at the Palaeocene/Eocene boundary. Nature 450, 1218–1221. https://doi.org/10.1038/nature06400.

Sluijs, A., Schouten, S., Donders, T.H., Schoon, P.L., Röhl, U., Reichart, G.J., Sangiorgi, F., Kim, J.H., Sinninghe Damsté, J.S., Brinkhuis, H., (2009). Warm and wet conditions in the Arctic region during Eocene Thermal Maximum 2. Nat. Geosci. 2, 777–780. https://doi.org/10.1038/ngeo668.

Sluijs, A., Zeebe, R.E., Bijl, P.K., Bohaty, S.M., (2013). A middle Eocene carbon cycle conundrum. Nat. Geosci. 6, 429–434.

Stap, L., Lourens, L. J., Thomas, E., Sluijs, A., Bohaty, S., and Zachos, J. C. (2010).: High-resolution deep-sea carbon and oxygen isotope records of Eocene Thermal Maximum 2 and H2, Geology, 38, 607–610, https://doi.org/10.1130/g30777.1,.

Svensen H, Planke S, Malthe-Sorenssen A, Jamtveit B, Myklebust R, Rasmussen Eidem T, Rey SS. (2004). Release of methane from a volcanic basin as a mechanism for initial Eocene global warming. Nature 429, 542–545. (doi:10.1038/nature02566)

Thomas, E. and Shackelton, N. J. (1996): The Paleocene-Eocene benthic foraminiferal extinction and stable isotope anomalies, in: Correlation of the Early Paleogene in Northwest Europe, edited by: Knox, R. W. O. B., Corfield, R. M., and Dunay, R. E., Geological Society Special Publication, 401–441.

Thomas, E. and Zachos, J.C., (2000). Was the late Paleocene thermal maximum a unique event? Geol. Fo¨r. Stock. fo¨r., 122, 169–170.

Thomas, E., Brinkhuis, H., Huber, M. and Ro¨ hl, U., (2006). An ocean view of the early Cenozoic Greenhouse World. Oceanography (Spec. Vol. Ocean Drilling), 19, 63–72.

Thomas, E., J.C. Zachos, and T. J. Bralower, (2000). Deep-Sea Environments in the Absence of Polar Ice Caps: The Case of The Early Eocene. In Warm Climates in Earth History, B.T. Huber, K.G. MacLeod, S.L. Wing (Eds.), Cambridge Univ. Press, p.132-160

Thomas, E., Zachos, J.C. and Bralower, T.J., (2000). Deep-sea environments on a warm Earth: latest Paleocene–early Eocene. In: Warm Climates in Earth History (B. Huber, K. MacLeod and S. Wing eds), pp. 132–160. Cambridge University Press, Cambridge.

Walsworth-Bell, B., (2001). Jurassic Calcareous Nannofossils and Environmental Cycles. PhD Thesis, University College London, UK. 140 pp.

Westerhold, T., Ro¨hl, U., Donner, B., McCarren, H.K. and Zachos, J.C., (2011). A complete high-resolution Paleocene benthic stable isotope record for the central Pacific (ODP Site 1209). Paleoceanography, 26, PA2216.

Westerhold, T., Röhl, U., Donner, B., Frederichs, T., Kordesch, W. E. C., Bohaty, S. M., ... & Zeebe, R. E. (2018). Late Lutetian Thermal Maximum—Crossing a Thermal Threshold in Earth's Climate System?. Geochemistry, Geophysics, Geosystems, 19(1), 73-82.

Westerhold, T., Röhl, U., Donner, B., Zachos, J. C., (2018). Global Extent of Early Eocene Hyperthermal Events – a new Pacific Benthic Foraminiferal Isotope Record from Shatsky Rise (ODP Site 1209). Paleoceanography and Paleoclimatology. doi: 10.1029/2017PA003306

Westerhold, T., Röhl, U., Frederichs, T., Agnini, C., Raffi, I., Zachos, J. C., & Wilkens, R. H. (2017). Astronomical calibration of the Ypresian time scale: Implications for seafloor spreading rates and the chaotic behaviour of the solar system. Climate of the Past, 13(9), 1129-1152.

Westerhold, T., Röhl, U., Laskar, J., Raffi, I., Bowles, J., Lourens, L.J., Zachos, J.C., (2007). On the duration of magnetochrons C24r and C25n and the timing of early Eocene global warming events: implications from the Ocean Drilling Program Leg 208 Walvis Ridge depth transect. Paleoceanography 22, PA2201. https://doi.org/10.1029/ 2006PA001322.

Wu, H., Zhang, S., Feng, Q., Jiang, G., Li, H., & Yang, T. (2012). Milankovitch and sub-Milankovitch cycles of the early Triassic Daye Formation, South China and their geochronological and paleoclimatic implications. Gondwana Research, 22(2), 748-759

Zachos, J.C., Dickens, G.R., Zeebe, R.E., (2008). An early Cenozoic perspective on greenhouse warming and carbon-cycle dynamics. Nature 451, 279–283. https://doi.org/10.1038/nature06588

Zachos, J.C., Kroon, D., Blum, P., Bowles, J., Gaillot, P., Hasegawa, T., Hathorne, E.C., Hodell, D.A., Kelly, D.C., Jung,J.-H., Keller, S.M., Lee, Y.S., Leusch- ner, D.C., Liu, Z., Lohmann, K.C., Lourens, L., Monechi, S., Nicolo, M., Raffi, I., Riesselman, C., Ro¨ hl, U., Schellenberg, S.A., Schmidt, D.N., Sluijs, A., Thomas, D.J., Thomas, E. and Vallius, H., (2004). Proceedings of the Ocean Drilling Program, Initial Reports Volume 208 [Online]. Available from World Wide Web. http.//www-odp.tamu.edu/publications/208_IR/208ir.htm

Zachos, J.C., Pagani, M., Sloan, L., Thomas, E., Billups, K., (2001). Trends, rhythms, and aberrations in global climate 65 Ma to present. Science 292, 686–693.

Zachos, J.C., Röhl, U., Schellenberg, S.A., Sluijs, A., Hodell, D.A., Kelly, D.C., Thomas, E., Nicolo, M., Raffi, I., Lourens, L.J., McCarren, H., Kroon, D., (2005). Rapid acidification of the ocean during the Paleocene-Eocene thermal maximum. Science 308, 1611–5. https://doi.org/10.1126/science.1109004.

Zeebe, R. E., Westerhold, T., Littler, K., & Zachos, J. C. (2017). Orbital forcing of the Paleocene and Eocene carbon cycle. Paleoceanography, 32(5), 440-465.

Chapter 1

Aims, materials and methods

1.1 Aims of the work

Using a combined sedimentological-cyclostratigraphic approach, the present thesis work aims at analyzing the variation of calcareous nannoplankton assemblages induced by changes in Earth's orbital parameters (i.e. orbital forcing) in Eocene times. To this end, three stratigraphic succession of the Basque-Cantabrian Basin (N Spain), each representing a specific paleoenvironmental settings, were studied: the Sopelana, Oyambre and Gorrondatxe sections, for which orbital forcing on sedimentation had been previously recognized (Payros et al., 2009, 2011, 2012, 2015; Payros & Martinez-Braceras, 2014; Martinez-Braceras et al., 2017; Dinares-Turell et al., 2018).

Thanks to the collaboration with the Department of Stratigraphy and Paleontology ofthe University of the Basque Country, it has been possible to study the biostratigraphy of the Sopelana section and to analyze the role played by high-frequency orbital forcing (100 ky eccentricity cycles and 21 ky precession cycles) on the abundance and distribution of marine planktonic communities in well-defined biostratigraphic intervals. Furthermore, the variation in calcareous nannofossils assemblages throughout three short (100 ky) eccentricity cycles (one per each of the studied sections) and their constituent 21 ky precession cycles was also analyzed.

This thesis work included high-resolution quantitative, statistical, and qualitative analysis of calcareous nannofossils. The data and interpretations provide evidence to elaborate on the depositional models previously proposed for the formation of marl-limestone alternations in the Basque-Cantabrian Basin during the Eocene. In addition, the main environmental factors which drove the variations of the calcareous nannofossil assemblages can be deciphered, as well as the

role of orbital forcing on marine planktonic communities in relation to high-frequency climatic change.

Additionally, a further goal of this thesis is to carry out a multidisciplinary study on the stratotypic Bartonian deposits of the Barton area (Hampshire basin, South England) in an effort to improve the biostratigraphic and chronological knowledge of the Bartonian Stage, the Global Stratotype Section and Point (GSSP) of which is still pending definition. To tackle the chronostratigraphic problems of the Bartonian classic unit stratotype (Barton section), as expressed in the introduction of this thesis, the parastratotypic Alum Bay section (thicker and better exposed than the Barton section) was studied, with the aim of recognizing possible stratigraphic marker events that can approximate the base of the Bartonian stage and might be easily correlated outside the Hampshire Basin.

1.2 Materials

Three outcropping stratigraphic sections from the northern paleo-margin of the Iberian Peninsula, currently belonging to the Basque Cantabrian Basin (Spain), were studied: the Sopelana (lower Ypresian), Gorrondatxe (upper Ypresian) and Oyambre (upper Lutetian) sections (Fig. 1). These sections consist of well hierarchized marl and limestone couplets.

The Sopelana section (starved deep-sea basin), composed by about 30 m of alternating marls and limestones, outcrops on the coast of Biscay Gulf 10 km north of Bilbao city, close to the Sopelana village. The Gorrondatxe section (submarine fan fringe) is exposed in a beach cliff 2 km south-west of Sopelana. This section is composed by a 120 m thick succession that includes the Global Stratotype Section and Point (GSSP) for the base of the Lutetian Stage, and it built up of alternating hemipelagic limestones and marls intercalated with thin-bedded turbidites. The last Spanish investigated section is represented by the Oyambre coastal succession (upper carbonate slope), exposed in a coastal cliff and located approximately 100 km west of Sopelana and

Gorrondatxe. This section is composed by 130 m of late Lutetian and early Bartonian hemipelagic (marl-limestone sediments) and turbiditic deposits.

The Alum Bay section, located in the Hampshire basin (South of England), has been studied to tackle the chronostratigraphic problems encountered at the stratotypic Barton coastal section. The Alum Bay section, outcropping on the westernmost tip of the Isle of Wight (Fig. 1), about 3 km west of Totland village, is composed of 90 m of sand-clay deposits. In this area the Eocene sediments (black in Fig.1) are juxtaposed to the older Paleogene deposits (light blue in Fig.1), that here shows a setting varying from steeply dipping to vertical.

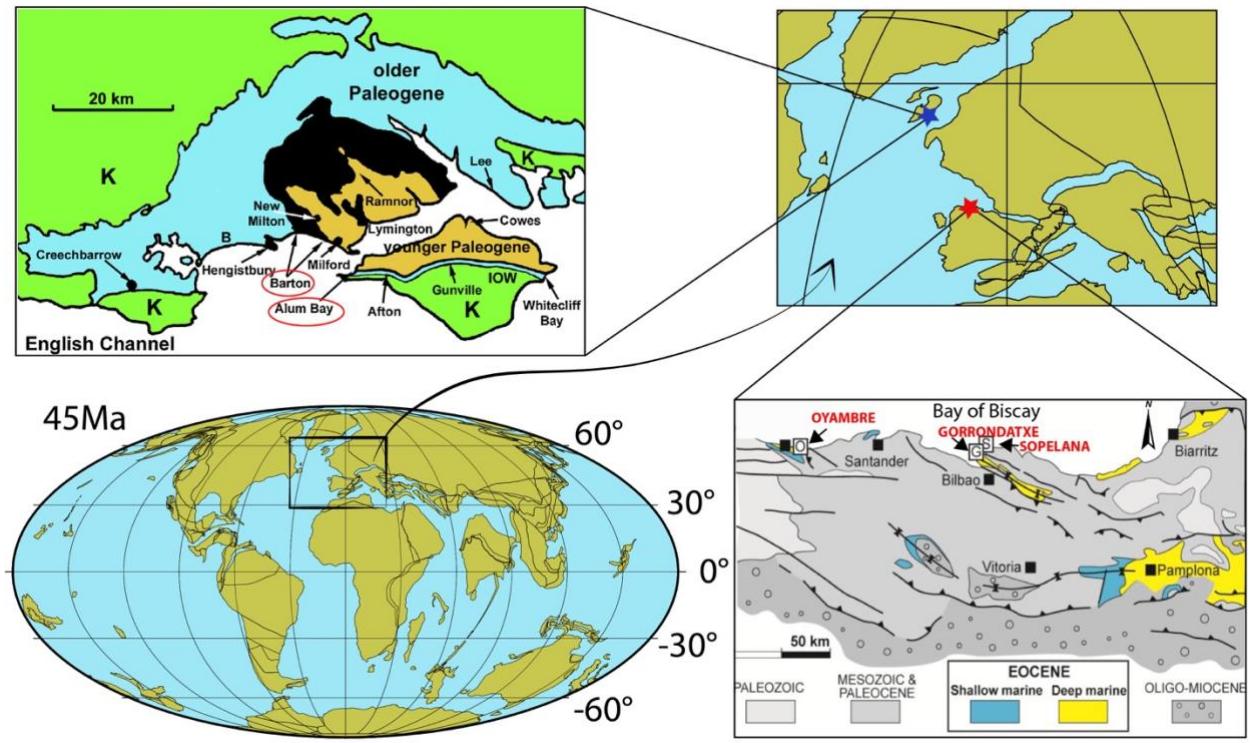

Fig. 1.1: Map with location of the northern paleo-margin of the Iberian Peninsula (red star) and the Hampshire basin (blue star) at 45 Ma, paleogeographic reconstruction with Mollweide projection (from http: // www. Odsn.de); on the lower right, geological map of the Basque-Cantabrian basin, with the distribution of Eocene deposits (coloured) and the location of the three studied sections: Oyambre (O), Gorrondatxe (G) and Sopelana (S) (modified from Martinez-Braceras et al., 2017); on the upper left, geological map of the Hampshire basin showing

distribution of Eocene deposits (black), and location of the Barton and Alum Bay sections (red circles).

1.3 Methods

1.3.1 Calcareous nannofossils

Calcareous nannofossils are one of the most powerful biostratigraphic tools in marine carbonate sediments, especially in open ocean settings (Agnini et al., 2017). They are a group of calcifying, unicellular algae (phylum or division Haptophyta, class Prymnesiophyceae) (Young et al. 2003). Calcareous nannofossils are a main component of open-ocean primary production (Milliman, 1993; Winter et al., 1994; Rost and Riebe-sell, 2004), dominating the output of carbonate in the ocean (Ziveri et al., 1999; Hay, 2004). They are common in some Mesozoic and Cenozoic rocks, especially in deep-sea deposits, and often constitute the main bulk of chalky sediments (Romein, 1979; Aubry, 1998; Bown et al., 2004; Gibbs et al., 2012; Agnini et al., 2017).

Global temperatures vary in association with climate change, and such changes might affect the abundance of phytoplankton in general, leading to species-specific coccolithophore responses. As an example, new information is emerging about the contribution of different coccolithophore species to total calcification (Balch 2018). Therefore changes in calcareous nannofossil assemblages represent a powerful paleontological tool for the investigation of past climate change.

In the Spanish sections the calcareous nannofossil analyses have been performed on 270 samples, with an average sampling resolution of about 1.5 kyr, resulting in approximately 15 samples per 21 ky couplet. However, owing to differences in sedimentation rate among sections, samples were collected every 2 to 3 cm in the Sopelana section, every 10 to 14 cm of hemipelagic deposits in the Gorrondatxe section, and every 7 to 8 cm in the Oyambre section. In total, 57 samples were collected in Sopelana (23 in marls, 34 in limestones), 122 in Gorrondatxe (71 in

marls, 51 in limestones) and 88 in Oyambre (28 in marls, 60 in limestones). Twenty seven samples were collected in the Alum Bay section, with a variable resolution varying from 50 cm to 6 m. More detailed descriptions of the studied sections will be provided in the following chapters *(Chapter 2, 3 and 4).*

The 270 samples collected in the Spanish section are prepared following the decantation method proposed by Flores and Sierro (1997). Quantitative analyses were performed using polarized light microscope "Zeiss Axioplan 2 imaging" at 1250X magnification, counting at least 500 specimens per sample. The counts have been reported as a percentage and the variations in relative and absolute abundance of the forms were calculated.

The 27 samples from the Alum Bay section were processed from raw sediments to prepare standard smear slides (Bown and Young, 1998). Taxonomy follows Perch-Nielsen (1985), Bown (2005) and Fornaciari et al. (2010).

1.3.2 Planktonic foraminifera

Planktonic foraminifera analysis has been performed on three thin-section of the Sopelana section from indurated limestones at 11.40 m, 11.60 m, 16.20 m in order to pinpoint the Base of *Morozovella formosa*, a significant biostratigraphic marker event of the Eocene period.

1.3.3 Calcium carbonate content

A total of 643 samples with an average sampling resolution of 4.5 cm, have been analyzed from the 31 m of Sopelana section, for their $CaCO_3$ content using a Bernard calcimeter, available in the facilities of the University of the Basque Country. The values are given with precision ranging between 1 and 5%.

1.3.4 Spectral analysis

We have applied the Fourier Transform to perform the spectral analysis of the Sopelana calcium carbonate content. This procedure is used to identify periodicity in analyzed the sedimentary record. We have performed the spectral analysis using the free software Past 3.1 (Hammer et al., 2001) applying the function “REDFIT spectral analysis”.

1.3.5 Statistical analyses of calcareous nannofossil data

To capture changes in calcareous nannofossil assemblages and recognize the causes and environmental gradients within the dataset, a statistical approach was used by means of Cluster analysis and Principal Component Analysis (PCA), which were performed using the free software PAST (Paleontological Statistics Software Package for Education and Data Analysis – Hammer et al., 2001). Multivariate statistical analysis applications are not directly applicable to the compositional data because of the problem of false and induced correlations (Pearson, 1897). Thus, before performing the statistical analysis, all the data were log-standardized, because percentage counts represent a closed set (Pearson, 1897; Buccianti & Esposito, 2004).

1.3.5.1 Cluster analysis

Cluster analysis is a multivariate method which aims at classifying a sample of data (taxa) on the basis of a set of measured variables into a number of different groups, so that similar data are placed in the same group. The hierarchical clustering produces a dendrogram showing the data cluster. The similarity measure (distance) among taxa is given by Pearson correlation coefficient, and they are grouped by complete linkage (furthest-neighbor method). In this case, the distance between two clusters is defined to be the maximum distance between members. This allows the identification of clusters with high internal affinity (Krzanowski, 1988). Therefore, the better the

groups are merged and separated from the others, the greater the possibility that these groups of taxa (or samples) are characterized by an ecological and natural affinity**.**

1.3.5.2 Principal component analysis (PCA)

Through the PCA the major components of the calcareous nannofossil assemblage can be identified, graphically plotting the factors that explain the maximum variance, which were interpreted from a paleoecological point of view. This multivariate, statistical method allows the analysis of the nannoflora community, instead of changes in abundance of single taxa. This method also permits a better interpretation of complex sets of data, and the reduction of a large data matrix composed of several variables to a small number of factors, representing the main modes of variations (Fukunaga, 1990). Only the species with average relative abundance higher than 3% were considered for PCA.

1.3.6 Carbon and Oxygen isotopes

The carbon and oxygen data used in this thesis work to compare the calcareous nannofossil variations in three different short eccentricity cycle in Sopelana, Oyambre and Gorrondatxe sections, derive from Martinez-Braceras et al., (2017).

References

Agnini, C., Monechi, S., & Raffi, I. (2017). Calcareous nannofossil biostratigraphy: historical background and application in Cenozoic chronostratigraphy. Lethaia, 50(3), 447-463.

Aubry, M. P. (1998). Early Paleogene calcareous nannoplankton evolution: a tale of climatic amelioration. Late Paleocene-Early Eocene climatic and biotic events in the marine and terrestrial records, 158-203.

Berrocoso, Á. J., Elorza, J., & MacLeod, K. G. (2013). Proximate environmental forcing in fine scale geochemical records of calcareous couplets (Upper Cretaceous and Palaeocene of the Basque Cantabrian Basin, eastern North Atlantic). Sedimentary Geology, 284, 76-90.

Blunden, J., & Arndt, D. S. (2015). State of the Climate in 2014, Bulletin American Meteorology. Society, 96, S1–S267.

Bown, P. (1998). Calcareous nannofossil biostratigraphy (pp. 1-315). Chapman and Hall; Kluwer Academic.

Bown, P. R. (2005). Calcareous nannoplankton evolution: a tale of two oceans. Micropaleontology, 51(4), 299-308.

Bown, P. R., Lees, J. A., & Young, J. R. (2004). Calcareous nannoplankton evolution and diversity through time. In Coccolithophores (pp. 481-508). Springer, Berlin, Heidelberg.

Buccianti, A., & Esposito, P. (2004). Insights into Late Quaternary calcareous nannoplankton assemblages under the theory of statistical analysis for compositional data. Palaeogeography, Palaeoclimatology, Palaeoecology, 202(3-4), 209-227.

Dinarès-Turell, J., Martínez-Braceras, N., Payros, A., (2018). High-resolution integrated cyclostratigraphy from the Oyambre section (Cantabria, N Iberian Peninsula): constraints for orbital tuning and correlation of middle Eocene Atlantic deep-sea records. Geochem. Geophys. Geosyst. 19, 2017GC007367. https://doi.org/10.1002/ 2017GC007367.

Einsele, G., Ricken, W., & Seilacher, A. (1991). Cycles and events in stratigraphy.

Erba, E., Castradori, D., Guasti, G., & Ripepe, M. (1992). Calcareous nannofossils and Milankovitch cycles: the example of the Albian Gault Clay Formation (southern England). Palaeogeography, Palaeoclimatology, Palaeoecology, 93(1-2), 47-69.

Flores, J. A., & Sierro, F. J. (1997). Revised technique for calculation of calcareous nannofossil accumulation rates. Micropaleontology, 321-324.

Fornaciari, E., Agnini, C., Catanzariti, R., Rio, D., Bolla, E. M., & Valvasoni, E. (2010). Mid-latitude calcareous nannofossil biostratigraphy and biochronology across the middle to late Eocene transition. Stratigraphy, 7(4), 229.

Fukunaga (1990). Introduction to Statistical Pattern Recognition (2nd edition), Academic Press, New York (1990)

Gibbs, S. J., Bown, P. R., Murphy, B. H., Sluijs, A., Edgar, K. M., Pälike, H., ... & Zachos, J. C. (2012). Scaled biotic disruption during early Eocene global warming events. Biogeosciences, 9(11), 4679-4688.

Hammer, Ø., Harper, D. A. T., & Ryan, P. D. (2001). PAST-Palaeontological statistics. www. uv. es/~ pardomv/pe/2001_1/past/pastprog/past. pdf, acessado em, 25(07).

Hay, W.W., (2004). Carbonate fluxes and calcareous nannoplankton. In: Thierstein, H.R., Young, J.R. (Eds.), Coccolithophores. From Molecular Processes to Global Impact. Springer-Verlag, Berlin, pp. 509–528.

Krzanowski W.J. (1988) Principles of multivariate analysis, Oxford University Press.

Martínez-Braceras, N., Payros, A., Miniati, F., Arostegi, J., Franceschetti, G., 2017. Contrasting environmental effects of astronomically driven climate change on three Eocene hemipelagic successions from the Basque–Cantabrian Basin. Sedimentology 64 (4), 960-986. http://dx.doi.org/10.1111/sed.12334. Milliman JD (1993). Production and accumulation of calcium carbonate in the ocean: budget of a nonsteady state. Global Biogeochem Cy 7: 927–957.

Payros, A., Dinarès-Turell, J., Monechi, S., Orue-Etxebarria, X., Ortiz, S., Apellaniz, E., & Martínez-Braceras, N. (2015). The Lutetian/Bartonian transition (middle Eocene) at the Oyambre section (northern Spain):

Implications for standard chronostratigraphy. Palaeogeography, Palaeoclimatology, Palaeoecology, 440, 234-248.

Payros, A., & Martínez-Braceras, N. (2014). Orbital forcing in turbidite accumulation during the Eocene greenhouse interval. Sedimentology, 61(5), 1411-1432.

Payros, A., Dinares-Turell, J., Bernaola, G., Orue-Etxebarria, X., Apellaniz, E. and Tosquella, J. (2011) On the age of the Early/Middle Eocene boundary and other related events: cyclostratigraphic refinements from the Pyrenean Otsakar section and the Lutetian GSSP. Geol. Mag., 148, 442–460.

Payros, A., Orue-Etxebarria, X., Bernaola, G., Apellaniz, E., Dinares-Turell,J.,Tosquella,J.andCaballero,F.(2009) Characterization and astronomically calibrated age of the first occurrence of Turborotalia frontosa in the Gorrondatxe section, a prospective Lutetian GSSP: implications for the Eocene time scale. Lethaia, 42, 255– 264.

Payros, A., Ortiz, S., Alegret, L., Orue-Etxebarria, X., Apellaniz, E., & Molina, E. (2012). An early Lutetian carbon-cycle perturbation: Insights from the Gorrondatxe section (western Pyrenees, Bay of Biscay). Paleoceanography, 27(2).

Payros, A., Ortiz, S., Millán, I., Arostegi, J., Orue-Etxebarria, X., & Apellaniz, E. (2015). Early Eocene climatic optimum: Environmental impact on the North Iberian continental margin. Bulletin, 127(11-12), 1632-1644

Pearson, K. (1897). Mathematical contributions to the theory of evolution.—on a form of spurious correlation which may arise when indices are used in the measurement of organs. Proceedings of the royal society of london, 60(359-367), 489-49.

Perch-Nielsen, K. (1985). Cenozoic calcareous nannofossils. Plankton stratigraphy, 427-554.

Romein, A. J. T. (1979). Lineages in early Paleogene calcareous nannoplankton (Doctoral dissertation, Utrecht University).

Rost, B., Riebesell, U., (2004). Coccolithophores and the biological pump: responses to environmental changes. In: Thierstein, H.R., Young, J.R. (Eds.), Coccolithophores. From Molecular Processes to Global Impact. Springer-Verlag, Berlin, pp. 99–125.

Winter, a., Jordan, r.w., and Roth, p.h., (1994). Biogeography of living coccolithophores in ocean waters. In: A. Winter and W.G. Siesser Coccolithophores. Cambridge University Press: 161-177.

Young, J.R., Geisen, M., Cros, L., Kleijne, A., Sprengel, C., Pro-bert, I. & Østergaard, J. (2003). A guide to extant coccolithophore taxonomy. Journal of Nannoplankton ResearchSpecial Issue 1,1–121.

Ziveri, P., Young, J. R., & Van Hinte, J. E. (1999). Coccolithophore export production and accumulation rates.

Chapter 2

Calcareous nannofossil biostratigraphy and cyclostratigraphy of the Ypresian Sopelana section (Basque-Cantabrian Basin)*

Abstract

The lower Eocene Sopelana section (Basque-Cantabrian basin) is characterized by 30 m of a rhythmic alternation between pelagic marls and limestones organized in thirteen well defined bundles, each of which generally contains five limestone-marl couplets. This hierarchical arrangement strongly suggests that the formation of the couplets was driven by astronomical precession cycles (21 ky each) and that of the bundles by eccentricity cycles (100 ky). The studied section was assigned to the early Ypresian *Morozovella subbotinae* planktonic foraminiferal Zone. The aims of this study were to investigate the orbitally controlled sedimentary cyclicity of the Sopelana section using geochemical proxies, to obtain a detailed chronology based on calcareous nannofossil biostratigraphy and to characterize the nannofloral assemblage changes. The geochemical analysis, based on the carbonate content of the beds, was performed with a resolution of 1-1.5 ky and allowed reliable identification of orbital cycles as the main forcing mechanism that controlled sedimentation.

*This chapter is based on manuscript in preparation for submission to *Geologica Acta*

FRANCESCHETTI G.[1], MARTINEZ- BRACERAS N.[2], P AYROS A.[2], MONECHI S.[1]

[1] Dipartimento di Scienze della Terra, Università degli Studi di Firenze, Via La Pira 4, 50121, Firenze, Italy

[2] Department of Stratigraphy and Paleontology, Faculty of Science and Technology, University of the Basque Country (UPV/EHU), Ap. 644, E48080 Bilbao, Spain.

The calcareous nannofossil content constrains more accurately the age of the Sopelana section. *Rhomboaster* and *Fasciculithus* are present from the base of the section suggesting the assignment of the lowermost part of the section to CNE1 Zone (lowermost Ypresian, just above the P/E boundary). The *Rhomboaster-Tribrachiatus* lineage is well documented, and the section spans from CNE1 to CNE3 and from NP10 to NP11 Zones (Martini et al. 1971). According to the biochronology of calcareous nannofossil events, the studied interval represents approximately 1 Ma, confirming the age obtained by counting short eccentricity bundles.

The bio-litho-cyclostratigraphic data of the Sopelana section can be readily correlated with the coeval Zumaia section, located 60 km to the east. This correlation confirms that the studied beds are the result of supra-regional sedimentary processes, rather than manifestations of local diagenesis, demonstrating the homogeneity of the sedimentary and biotic processes throughout the Basque-Cantabrian basin in early Ypresian times.

2.1 Introduction

Pelagic calcareous limestone-marl couplets are often interpreted as a result of periodic climatic fluctuations related to changes in the Earth's orbital parameters (Elder et al., 1994; House,1995; Dinarés-Turell et al., 2010, 2018). The cyclicity has often been attributed to a combination of several paleo-environmental factors in the water column (Einsele & Ricken, 1991). These factors are related with fluctuations in the input of terrigenous sediments (dilution cycles; Moiroud et al., 2012), supply of calcareous biogenic sediment produced by calcareous plankton (productivity cycles; Boulila et al., 2010; Jimenez Berrocoso et al., 2013), the degree of saturation in calcium carbonate of the sea water (dissolution cycles; Dean & Gardner, 1986), and the accessibility of oxygen in the sea bottom and the degree of organic matter preservation (redox cycles; Einsele & Ricken, 1991). The small seasonal effect induced by these variations can be amplified by climate systems and recorded as cyclic sedimentary successions, as is likely to be occurred in the

Sopelana section. However, diagenetic processes acting after deposition can distort or sometimes completely delete the primary environmental signal. Nonetheless, previous studies carried out in older materials (Maastrictian and Paleocene) in outcrops adjacent to Sopelana section, excluded the role of diagenetic processes in the formation of the marl and limestone couplets (Pujalte et al., 1998; Dominguez et al., 2007; Berrocoso et al., 2012; Dinarès-Turell et al., 2013; Batenburg et al., 2014). Recent studies (Boulila et al., 2010; Berrocoso et al., 2013) have demonstrated that several proxies (carbonate content, manganese content, magnetic susceptibility, bulk carbon and oxygen stable isotopes) obtained through high-resolution sampling ($<10^4$ years) can help to determine the dominant forcing mechanisms on pelagic sedimentation. The paleoenvironmental fluctuations and periods of the orbital perturbations predicted by the Milankovitch theory have various hierarchical ranks with a range of 20-400 ky. The precession cycles (19-23 ky), obliquity of the Earth's rotation axis (41-54 ky) and eccentricity of the orbit around the Sun (98-123 ky and 413 ky) produce cyclic fluctuations of insolation due to different interaction between several parameters in the Earth's climate system. Only few studies have analyzed the effect of Milankovitch cycles on calcareous nannofossils and the majority are restricted to the Pliocene (Gibbs et al., 2004). Our main objectives are the definition of calcareous nannofossil biostratigraphy, not present for this section yet; the evaluation of possible orbital forcing influence, based on spectral analysis of the calcium carbonate content, in the marls-limestone couplets of the Ypresian Sopelana section, and the investigation of possible variation in the calcareous nannofossil abundance in these lithologies.

2.2 Geological setting and previous works

The Sopelana section (43°23'32.57"N, 2°59'25.60"W) is exposed at the costal cliff of the Arnakatxa beach, near the city of Bilbao (Biscay province, Basque Country, northern Spain). The Paleogene sediments were deposited at an estimated water depth of about 1000-1500 m in an

E-W elongated offshore basin, called the Basque-Cantabrian basin, opening westwards into the Bay of Biscay (Payros et al., 2006) (Fig. 2.1).

The studied sediments belong to the stratigraphic succession of the Basque-Cantabrian Basin, which is included within the Cantabrian Cordillera developed during the Alpine Orogeny (Muñoz, J. A., 2002). Alpine materials outcropping in the Basque-Cantabrian basin border the Cantabrian Sea to the north, and the basins of the Duero and Ebro to the south. To the east the Pamplona fault tectonically bounds these sediments and to the west they are connected to the Asturian Massif. According to Feullieé and Rat (1971), the Alpine materials are divided into three zones: the Peri-Asturian Domain, the Navarro-Cántabro Domain and the Basque Arc. The Sopelana succession is comprised within the latter one, in which materials deposited in the NW of the basin outcrop.

A previous biostratigraphic study using planktonic foraminifera assigned the Sopelana Eocene section to the *Morozovella subbotinae* Zone (Elorza et al., 1984), which corresponds to E3-E4 Zone of the Wade et al. (2011) Zonation. No calcareous nannofossil analyses were performed previously in this section. Martinèz-Braceras et al. (2017) studied a portion of the Sopelana section in order to decipher which environmental factors governed the formation of the rhythmic alternation. These authors, demonstrated that the sedimentary cyclicity observed in the Ypresian Sopelana section (Basque-Cantabrian Basin) was produced by variations in the Earth's orbital parameters. The limestone marl couplets observed along the section are the expression of precession cycles, whereas the hierarchical arrangement in bundles, composed of five marl-limestone couplets, is the expression of short eccentricity cycles. Based on an integrated study (using oxygen and carbon isotopes and mineralogical analysis), a depositional model was proposed for the Sopelana section by Martinez-Braceras et al. (2017). The model suggests that limestones were formed during periods of high pelagic carbonate productivity under warm seawater and slow circulation conditions, linked to periods of low seasonality (Norther

Hemisphere- summers at aphelion); on the contrary, marls accumulated when pelagic carbonate productivity decreased during periods with cooler waters and active circulation, linked to high seasonality conditions (summers at perihelion). Unfortunately, only a low resolution planktic foraminifera biostratigraphy has been produced in the Sopelana section to date (Elorza et al., 1984). In this work we present calcareous nannofossil biostratigraphy results integrated with the cyclostratigraphy model.

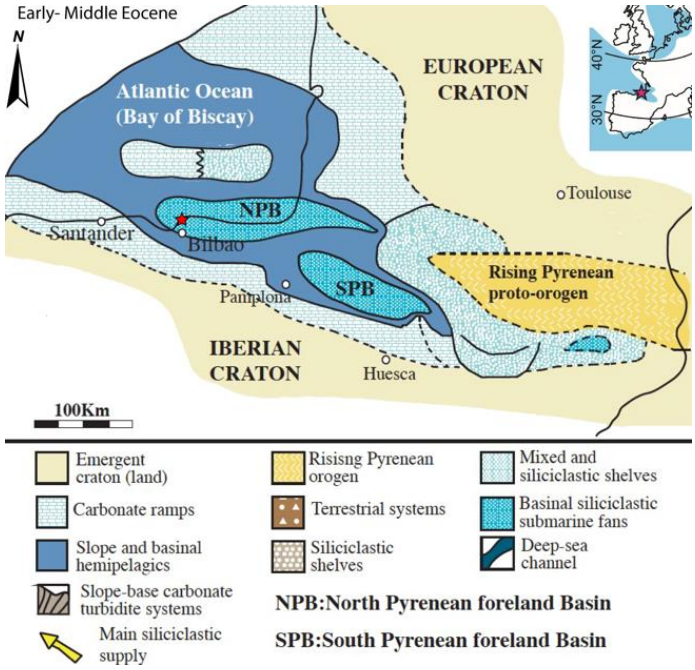

Fig. 2.1: Pyrenean and Basque-Cantabrian paleogeographic setting during early-middle Eocene times (modified from Pujalte et al., 2002), the red star showing the location of the Sopelana section.

2.2.1 Materials

The thickness of the studied Eocene section is 31 m (Fig. 2.2A and B). The base of the section (lowermost Ypresian, Elorza et al., 1984) is characterized by the presence of slightly deformed limestone beds that are due to the soft nature of the intervening PETM interval. The first 15 m of the section are characterized by a rhythmic alternation of grey hemipelagic limestones and reddish marls which define couplets approximately 40-50 cm thick. The upper portion of the section (15 to 31 m) is represented by rhythmic alternations of grey hemipelagic limestones and

marlstones, which define couplets about 50-60 cm thick, although the boundary between the two lithologies is not as distinct as in the lower part of the succession (Fig. 2.2C and B). Some intercalations of thin-bedded turbidites (2-10 cm) and slumps are present in this interval. The slumps are characterized by a clay matrix and contorted, sub-angular fragments of hemipelagic limestone beds, possibly linked to downslope transportation from a submarine slope. Despite the occurrence of turbidites and slumps, the marl-limestone couplets have been observed to be organized in 13 plurimetric bundles, each composed of five marl-limestone couplets (Martinez-Braceras et al., 2017). The astronomical control on the Eocene deposits was demonstrated in Martinez-Braceras et al. (2015 & 2017). Furthermore, siimilar hemipelagic cycles due to orbital forcing were also found in the Maastrichtian-Thanetian interval of the Sopelana (Pujalte et al., 1998; Dominguez et al., 2007; Batenburg et al., 2014; Berrocoso et al., 2013).

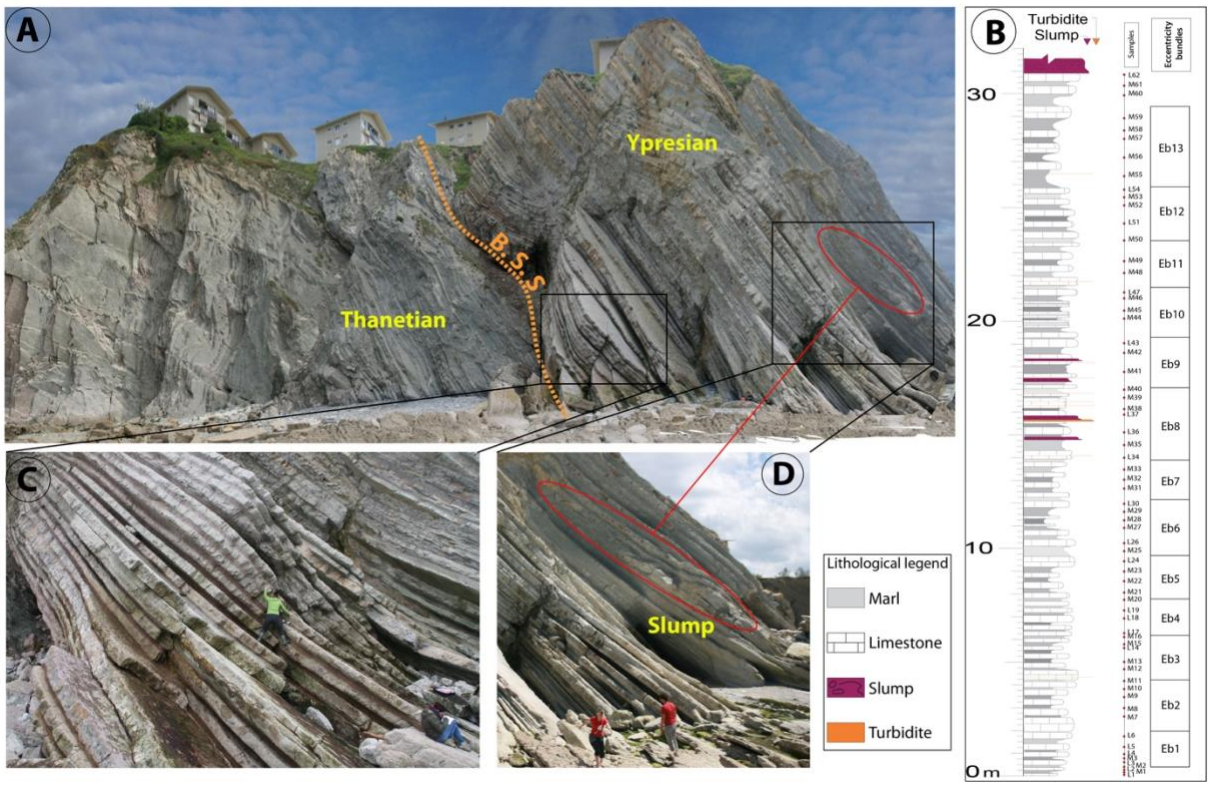

Fig. 2.2: (A) Overview of the Sopelana section. B.S.S.: Base of the studied section. (B) Lithostratigraphic log of the section, showing the position of the samples collected for the calcareous nannofossil analysis and the eccentricity bundles (coded Eb) recorded. (C) Zoom into

the basal portion (0-15m) of the section, in which the marl-limestone couplets are clearly defined. (D) Zoom into the upper part of the succession, showing a slump in the red circle.

2.3 Methods

2.3.1 Calcareous nannofossils

For the calcareous nannofossil biostratigraphic study 65 samples were collected from the 31 m thick Sopelana Eocene section. The average sampling interval was about 50 cm, but was reduced to a few centimeters (2 cm) in the lower part of the section, in order to increase the sampling resolution to better characterize the biostratigraphy in correspondence of the base of the section. Slides for coccolithophore analysis were prepared according to Flores and Sierro (1997) and analyzed under a Zeiss microscope at a magnification of 1250X. Quantitative analyses were performed by counting at least 500 specimens per sample. In order to detect rare, but biostratigraphically significant, species (such as *Rhomboaster contortus* and *Tribrachiatus orthostylus*), three random traverses (~9 mm^2) were analysed on each smear-slide. The mid latitude Zonation of Agnini et al. (2014) was applied and compared with the Martini (1971) and Okada and Bukry (1980) Zones. The standard taxonomy for Paleogene calcareous nannofossils was adopted (Perch-Nielsen 1985; Bown 2005), and that of Monechi et al. (2000), Von Salis et al., (2000) and Alegret et al., (2009) for *Rhomboaster*.

2.3.2 Planktonic foraminifera

Based on available planktonic foraminiferal information (Elorza et al., 1984), a preliminary study was designed to pinpoint the Base of *Morozovella formosa*, which is a significant biostratigraphic marker event. To this end, three thin sections were prepared from samples collected at 11.40 m, 11.60 m and 16.20 m.

2.3.3 $CaCO_3$ content

To determine $CaCO_3$ content along the succession, a total of 643 samples were collected at an average sampling resolution of 4.5 cm. Calcium carbonate was measured using an Automatic Calcimeter (Aquitaine Technique Innovation, Bordeaux) at the University of the Basque Country following the method of Bernard.

2.3.4 Cyclostratigraphic methodology

An important tool used in cyclostratigraphic studies is spectral analysis. It represents a statistical method of examining cyclicity in a time series. The spectral analysis cannot explain why a connection between climatic variations and sediment composition exists, but can provide a proof that this connection exists (Weedon, 2003). The method used here to perform the spectral analysis of the Sopelana calcium carbonate content data is the Fourier Transform. To perform the spectral analysis Past 3.1 software was used (http://folk.uio.no/ohammer/past/), which is frequently used in paleontological and cyclostratigraphical analyses. The "REDFIT spectral analyses" extension of the program uses a simple algorithm Lomb periodogram, showing values very similar to those of a "Fast Fourier Transform" (FFT). To this end, the Sopelana calcium carbonate content data were implemented in the software together with the relative stratigraphic position (age equivalent). The program allows calculation of confidence intervals based on the chi-squared distribution in order to demonstrate that the peaks are statistically distinct from the background noise (Weedon, 2003). A confidence level of 99% was established. Two separate frequency spectrum analysis were performed: one, with data up to 14.71m, which marks the level of the occurrence of the first slump, and the second spectrum for the remaining 16.47 meters (upper part of the section) in which turbidites and slumps are intercalated.

2.4. Results

2.4.1 Calcareous nannofossil biostratigraphy

The calcareous nannofossil content is abundant and diversified. The species richness is low but relatively consistent throughout, varying between 25 and 39 species (average of 27 species). Preservation varies from poor to moderate.

The nannofossil assemblages of the Sopelana section mainly consist of placoliths represented by *Coccolithus pelagicus* and *Toweius*. Among nannoliths *Discoaster* and *Braarudosphaera* are the most prominent taxa. Reworking is present in few samples and consists of rare specimens of Cretaceous and Paleocene specimens (Plate 1).

The calcareous nannofossil assemblages from the Sopelana section show a decrease in the total number of nannofossils (N/mm^{-2}) with decreasing age. The samples up to 14 show approximately 2250 specimens mm^{-2}, whereas in the uppermost part of the section an average of approximately 2000 specimens mm^{-2} has been observed. However, the quantitative analysis shows that the calcareous nannofossil abundance and assemblage composition do not change significantly throughout the section and from marls to limestones (Fig. 2.3). *Coccolithus* and *Discoaster* constitute nearly half of the assemblages throughout the entire section. However, *Coccolithus* shows an evident decrease in abundance from 12.40 m upwards. *Sphenolithus* does not vary in abundance throughout the section. *Braarudosphaera* and *Toweius* have a similar abundance pattern, both increasing in abundance within the interval 15-18m. *Zyghrablithus bijugatus* shows an abundance of about 12% up to 11 m, but decreases to 8% in the uppermost part of the section reaching the lowest value at 22 m (2%). We observe only few differences between the two lithologies. In the limestone lithology *Discoaster* and *Sphenolithus* seem to be more abundant, whereas the genera *Toweius* and *Braarudosphaera* seem to show a significant increase in the marly hemicouplets.

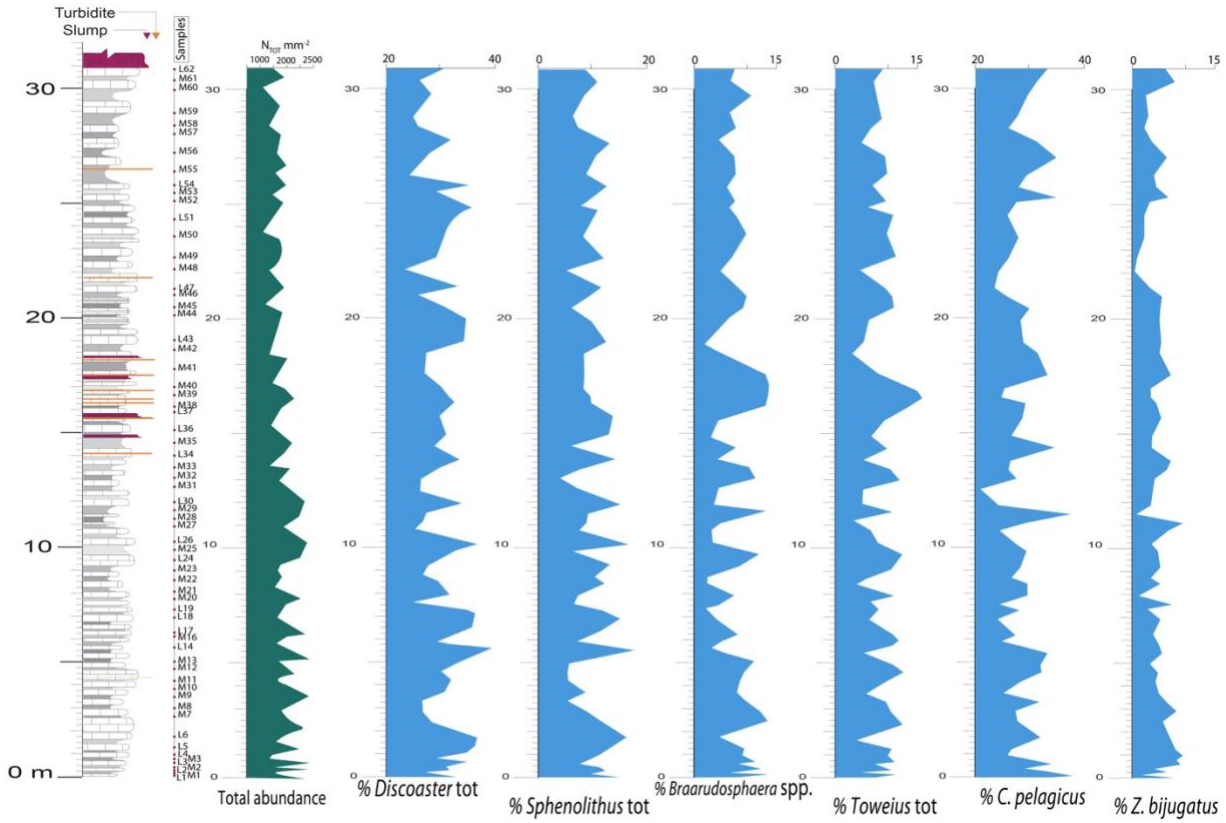

Fig. 2.3: Abundance patterns of selected calcareous nannofossil species (light blue diagrams) and total abundance pattern (N_{TOT} mm^{-2}, green diagram).

Most of the markers used in the standard zonations of Martini (1971), Okada and Bukry (1980) and Agnini et al. (2014) have been identified. Their identification and distribution throughout the section, as well as the assemblage composition, allowed the identification of the Zones CNE1 to CNE3 (lower Ypresian) of the scheme of Agnini et al. (2014) (Fig. 2.4). The occurrence of *Fasciculithus tympaniformis* and *Rhomboaster bramlettei* in the lowermost part of the section (0 to 5.25 m) and the Base of *Discoaster salisburgensis* at 1.55 m allows this interval to be assigned to the uppermost part of Zone CNE1 (*F.tympaniformis* Top Zone) and to the lower part of NP10 Zone. The base of Zone CNE2 (*Toweius eminens* Partial Range Zone) is marked by the Top of *F. tympaniformis* at 5.25 and by the Base of *Tribrachiatus ortostylus* at 27.75 m. Few secondary events, but useful for correlation between the Agnini et al. (2014) and Martini (1971) zonations, have been identified in this Zone, such as the Base of *D. diastypus* at 6.65m, the Base of *R.*

contortus at 7.25 and the Base of *D. barbadiensis* at 8.25m. The base of CNE3 Zone (*T. orthostylus* Base Zone) is marked by the Base *T. orthostylus* at 27.75 m. A secondary event, the Base of *Sphenolithus radians*, is recorded at 29 m, which is particularly useful to approximate the base of Zone NP11 in case *Tribrachiathus* is missing (Agnini et al., 2006).

In summary, the Sopelana section spans Zones CNE1 to CNE3. This interval corresponds to Zones NP10-NP11 of Martini (1971) (Fig. 2.4). The *Rhomboaster-Tribrachiatus* lineage is well documented and characterized by the classical succession of events (Fig. 2.4), demonstrating the stratigraphic continuity of the section.

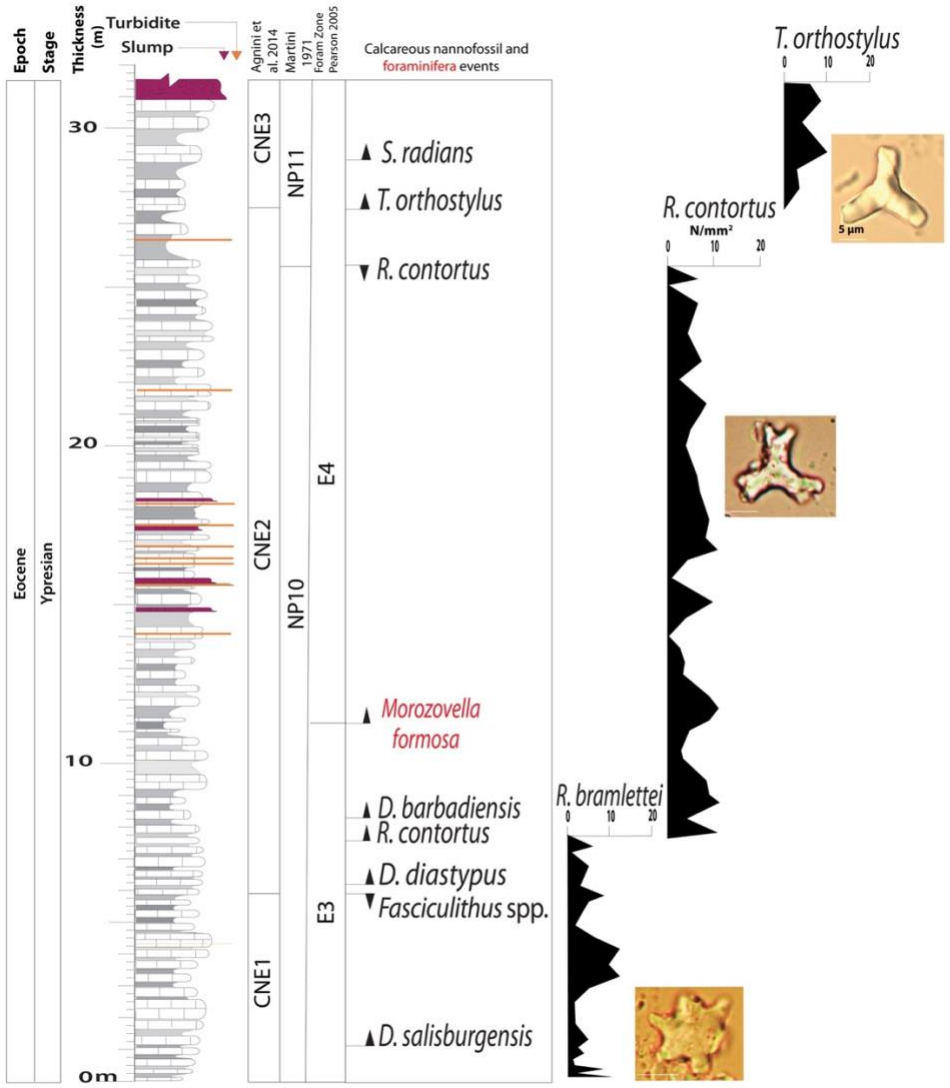

Fig. 2.4: Detailed stratigraphic log of the Sopelana section; the orange lines represent turbidites, while slump beds are marked in violet. Biostratigraphic results and abundance n/mm^2 of *Rhomboaster* and T*ribrachiatus* have been reported.

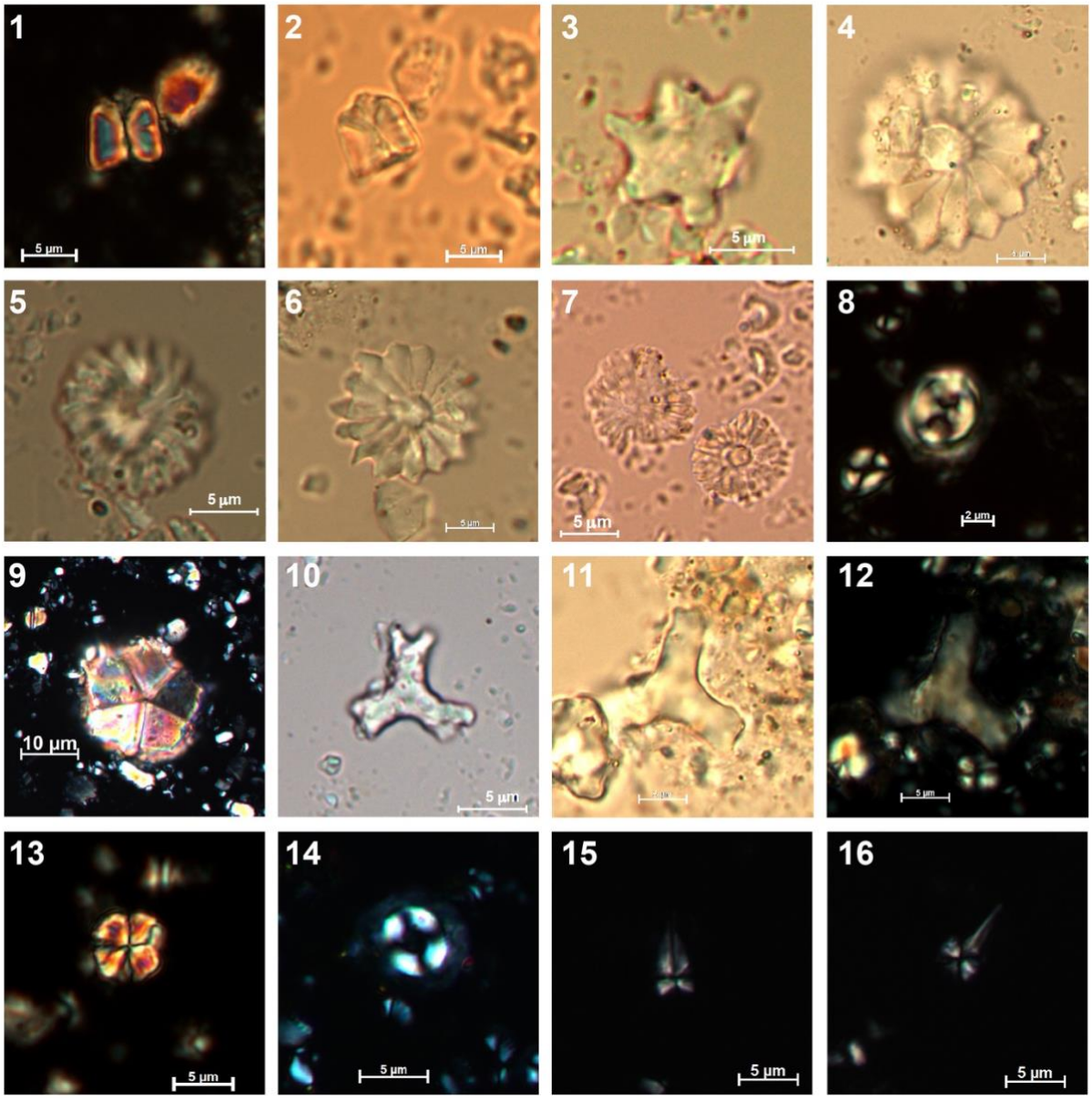

Plate 1: Calcareous nannofossils: 1-2. *Fasciculithus tympaniformis* Hay and Mohler in Hay et al. 1967. Crossed nicols and Parallel light. 3. *Rhomboaster bramlettei* (Brönnimann and Stradner 1960) Proto Decima et al. 1975. Parallel light. 4. *Discoaster salisburgensis* Stradner, 1961. Parallel light. 5. *Discoaster diastypus* Bramlette and Sullivan 1961. Parallel light. 6. *Discoaster barbadiensis* Tan Sin Hok 1927 emend. Bramlette and Riedel 1954. Parallel light. 7. *Discoaster multiradiatus* Bramlette and Riedel 1954. Parallel light. 8. *Toweius eminens* (Bramlette & Sullivan, 1961) Perch-Nielsen, 1971. Crossed nicols. 9. *Braarudosphaera bigelowii* (Gran & Braarud 1935) Deflandre, 1947. 10. *Rhomboaster contortus* (Stradner, 1958) Bukry 1972. Parallel light. 11-12. *Tribrachiatus orthostylus* Shamrai 1963. Parallel light and crossed nicols. 13. *Sphenolithus moriformis* (Bronnimann and Stradner 1960) Bramlette and Wilcoxon, 1967. Crossed nicols 0°. 14. *Ericsonia formosa* (Kamptner 1963) Haq 1971. Crossed nicols. 15-16. *Sphenolithus radians* Deflandre in Grassé 1952. Crossed nicols 0° and 45°.

2.4.2 Planktonic foraminifera biostratigraphy **

The analysis of the thin sections yielded a typical Ypresian assemblage. In the sample from 11.40 m *Subbotina* species are frequent, while species of morozovellids and acarinids are rare. The assemblage includes *Morozovella gracilis, Subbotina roesnaensis, Morozovella subbotinae, Acarinina wilcoxensis* and *Subbotina linaperta.* The sample from 11.60 m is composed of *Acarinina soldadoensis, Acarinina coalingensis, Acarinina esnaensis, Morozovella formosa, Morozovella aequa*, and *Planorotalites pseudoscitulus.* The sample from 16.20 m is similar to the previous samples but shows the richest fauna, with abundant *Subbotina* and chiloguembelinae. The taxa include *Acarinina coalingensis, Morozovella margino dentata, Morozovella subbotinae, Morozovella* cf. *gracilis, Subbotina eocaena, Subbotina linaperta, Planorotalites pseudoscitulus,* and *Morozovella formosa* (Fig. 2.5). The first occurrence of *M. formosa* at 11.60 m marks the base of Zones E4 (Wade et al., 2011) and P6a (Berggren et al., 1995). Consequently, the boundary between the zones E3 and E4 has been placed at 11.50 m (Fig. 2.4). This result is in agreement with the previous study by Elorza et al., (1984), which assigned the studied section to *Morozovella subbotinae* Zone (Berggren, 1969).

**I knowledge for this paragraph Isabella Premoli Silva that kindly helped me with foraminifera analysis.

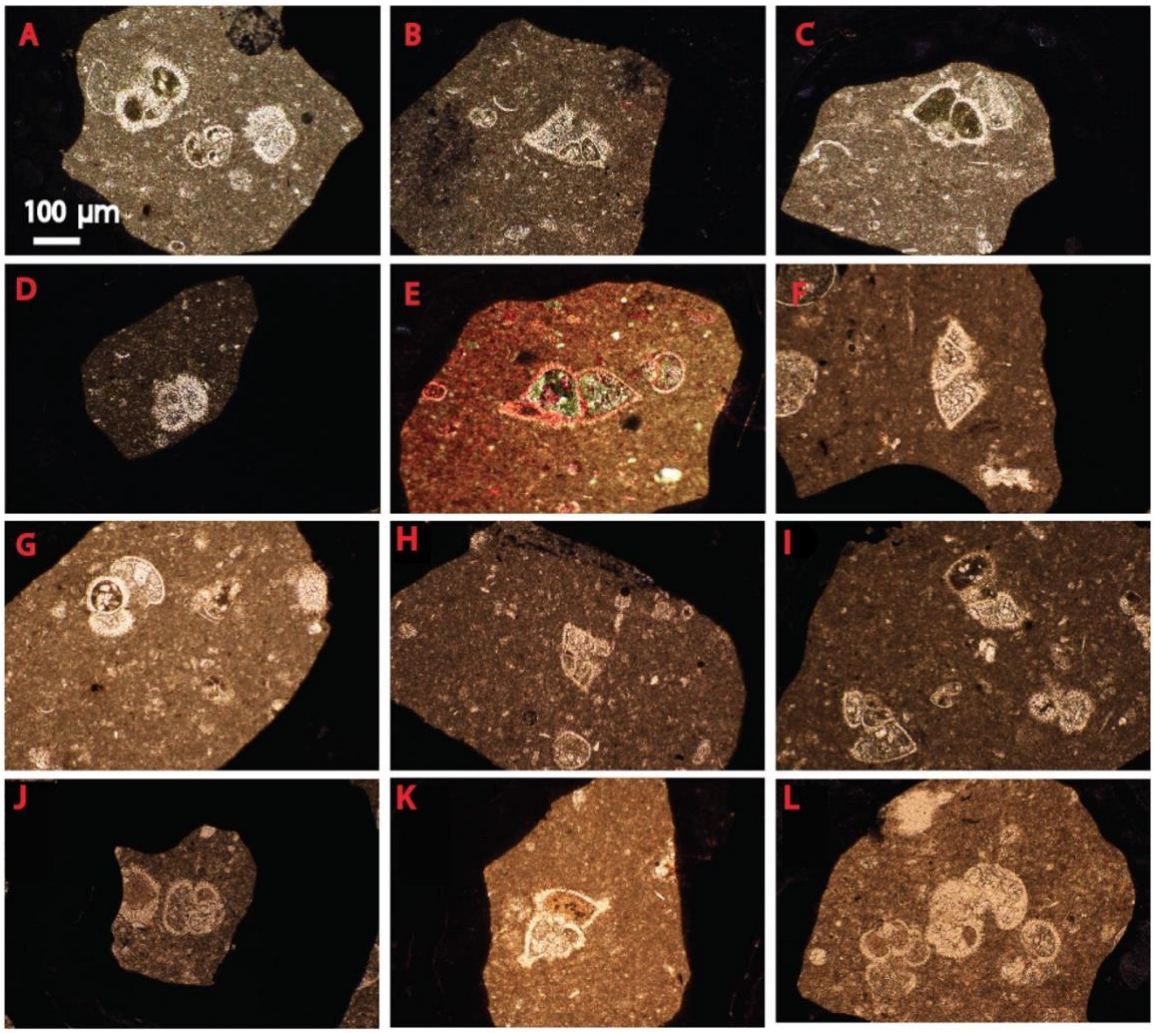

Fig. 2.5: Images of selected planktonic foraminifera taxa from samples of the Sopelana section. Scale bar 100 µm A: *Acarinina soldadoensis- A.coalingensis- A.esnaensis*; B: *Morozovella formosa*; C: *M. aequa;* D: *A. coalingensis*; E: *Planorotalites pseudoscitulus*; F: *M. gracilis*; G: *S. roesnaesensis*; H: *M. subbotinae*; I: *A. wilcoxensis* (on the left)- *Morozovella sp.* (on the right) J: *A. coalingensis*; K: *M. marginodentata*; L: *S. eocaena*.

2.4.3 $CaCO_3$ content

The $CaCO_3$ content shows a greater variability in the percentage of carbonate (40-80%) in the first 15 m of the section, while above this point, up to the top of the section, the calcium carbonate content shows a narrower variability range, stabilizing its values at about 65-75%, implying a lower variability between the marly and limy lithologies (Fig. 2.6). On outcrop, it is well visible a hierarchically arrangement of marl-limestone lithologies in couplets, five of which

forming a bundles. Couplets marking the bundle boundaries show less variability in $CaCO_3$ content between the marly and limy lithologies, whereas, couplets in the middle of the bundle are generally characterized by higher $CaCO_3$ content.

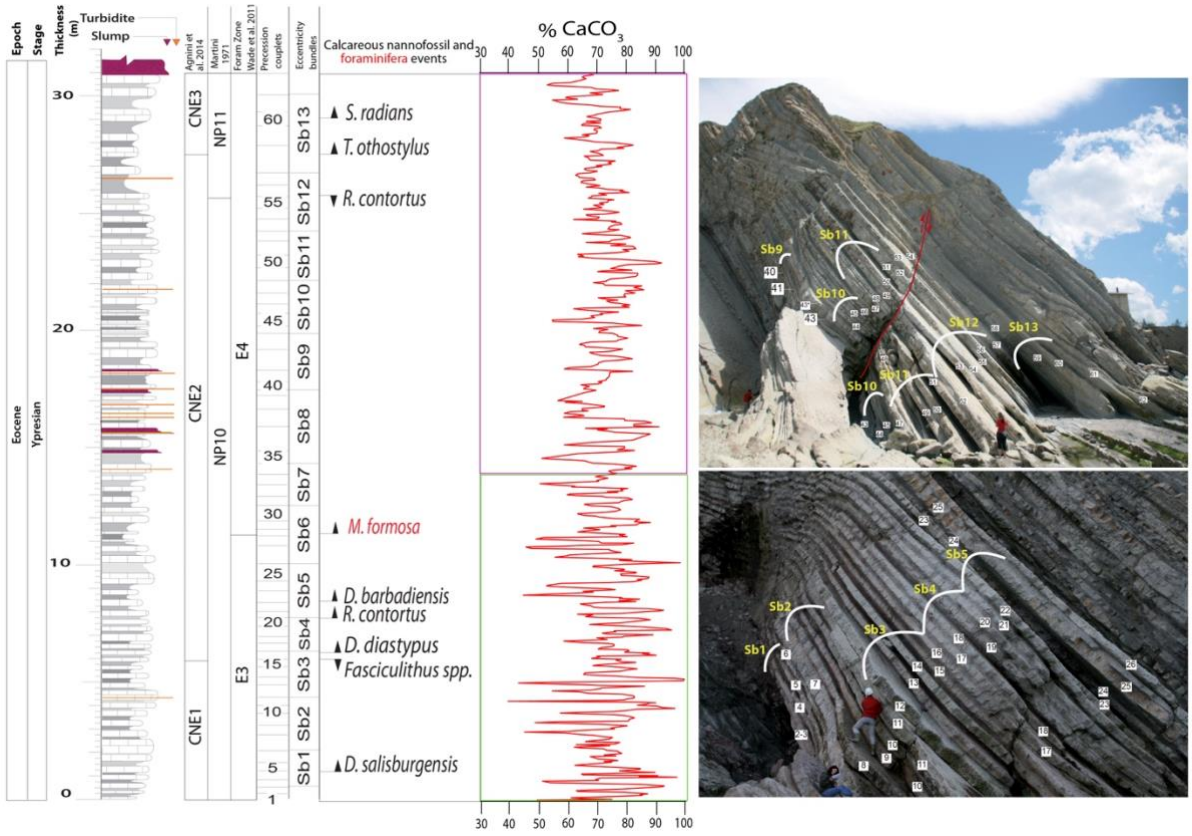

Fig. 2.6: $CaCO_3$ content in the Sopelana section. In the second part of the section, from 15 meters up to the top (purple rectangle), the variability of the calcium carbonate content is reduced, whereas the number and magnitude of slumps and turbidites increase.

2.4.4 Power spectral analysis

The frequency spectrum of the first 14.71 m shows three significant peaks exceeding the confidence level of 99%, which respectively represent frequencies of 0.023, 0.025 and 0.027 cycles/cm (Fig. 2.7a). The frequency spectrum generated for the uppermost 16.42 meters shows one single noticeable peak that exceeds the confidence level of 99%, with a frequency of 0.019

cycles/cm and a period of 51.50 cm. A peak of lesser power is also present in the spectrum, with a frequency of 0.022 and a period of 45.44 cm (Fig. 2.7b).

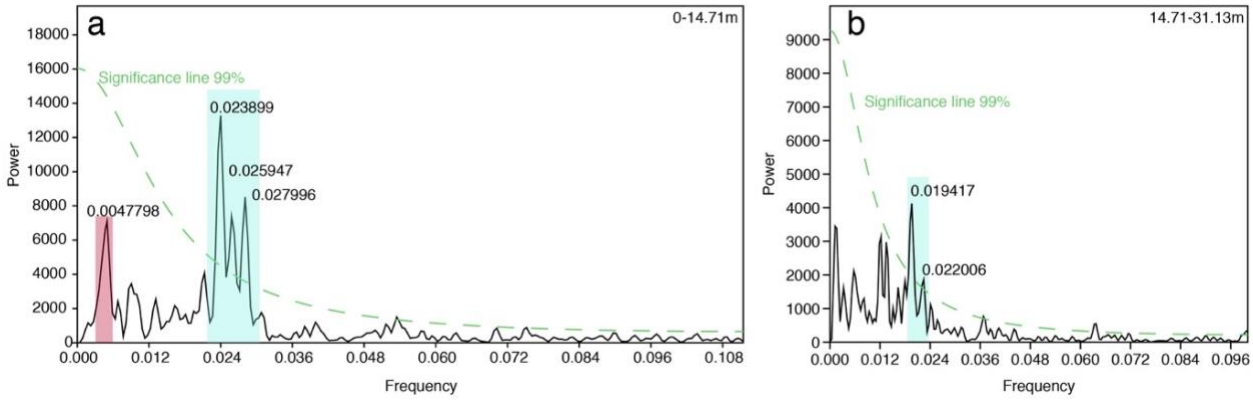

Fig. 2.7: Results of the REDFIT spectral analyses carried out on the $CaCO_3$% records of the Sopelana section. a) Results from the lower segment (from the base of the section up to 14.71 m). b) Results from the uppermost segment (from 14.71 to 31.13 m). The 99% confidence level is indicated with a green dashed line. Short eccentricity and precession bands have been marked in red and light blue, respectively.

2.5. Discussion

2.5.1 Abundance changes of calcareous nannofossil assemblages

Discoaster and *Sphenolithus*, are interpreted as inhabitants of warm waters (Haq and Lohmann, 1976; Haq 1980; Lohmann and Carlson, 1981), perhaps with a shallow water preference (Perch-Nielsen, 1985), and as being adapted to stable, low-nutrient environments (Aubry 1992, Bralower 2002) are more abundant in limestone-rich lithology. On the other hand, *Toweius* and *Braarudosphaera*, are more abundant in marly lithology. The first taxon is interpreted as adapted to meso-eutrophic conditions and cooler waters (Young 1994; Bralower 2002, Dedert et al., 2012, Schneider et al., 2013). The second one is an opportunistic taxon (r-strategist), usually associated with near shore settings, hyposaline water (Bukry, 1974, Liebrand et al. 2018) and eutrophic environments (Bartol et al., 2008; Cunha and Shimabukuro, 1997; Švábenická, 1999). Therefore, according to taxa paleoecology affinity, the marly lithology could be reflect a slight higher

fertility, whereas limestones could be the expression of stable environments and oligotrophic conditions.

The total calcareous nannofossil abundance and 5-pt moving average of the calcium carbonate variations show a good correlation throughout the section even though sample resolution of the two proxies is quite different (Fig. 2.8).

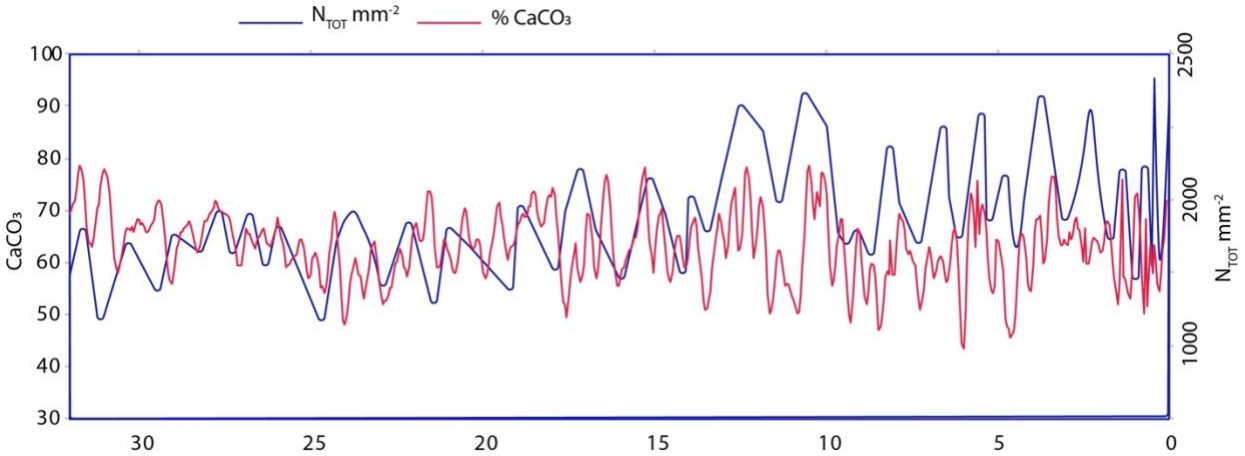

Fig. 2.8: $CaCO_3$ content 5-pt moving average (red line) and total calcareous nannofossil abundance per mm^2 (blue line).

In the first 20 m of the section, the limestone hemicouplets contain more than 2000 nannofossils per square mm, while marly hemicouplets show a decrease in the total abundance of calcareous nannofossils. However, in the uppermost 10 m the correlation between total abundance of calcareous nannofossil and $CaCO_3$ content is not straightforward. Despite the difference, it can be generally considered that a high value of calcium carbonate content may reflect high total abundance of calcareous nannofossil. Given that quantitative calcareous nannofossil variations seem to be correlated with the lithological alternation, the marl-limestone couplets could be interpreted as the response to changes in the characteristics of water masses, probably as a consequence of changes in insolation intensity.

2.5.2 Cluster analysis and principal component

To better capture the changes in calcareous nannofossil assemblages, a statistical approach was used. Principal component analysis (PCA) and cluster analysis were performed on the log-ratio transformation data (Kucera et al., 1998) using the statistical software PAST (Hammer et al., 2001). The PCA is often used for examining paleontological data (Buccianti et al, 2006; Marino et al., 2008; Bordiga et al., 2015; Agnini et al., 2016), as it can identify hypothetical variables (expressed as components) that explain much of the variance into a multidimensional dataset. The first principal component (PC1) takes into account the majority of the variability in any tested dataset.

Only the 11 taxa with abundance higher than 3% were used for the PCA analysis, which include *Chiasmolithus, C. pelagicus, Discoaster, Ericsonia, Markalius, Sphenolithus, Toweius, Rhomboaster/Tribrachiatus, Zyghrablithus, Braarudosphaera* and *Thoracosphaera.* The PCA results show that calcareous nannofossil taxa can be subdivided into two main groups (Fig. 2.9). The two populations are distinguished because of their different positions along the *x* axis (PC1). Definition of a third population is less clear, but a possible discrimination from the other two can be hypothesized because of its different position along the *y* axis (PC2). The PC1 variable contains the 73.2% of variance, while the PC2 variable represents 13.3%, both together accounting for 86.5% of the variance in the data set.

The first cluster of species composed by *Toweius, Chiasmolithus, Braarudosphaera* and *Thoracosphaera* is placed in high value of PC2 and range from -4 to +4 PC1 values. This cluster contains taxa with affinity to eutrophic environments and cooler water (Bybell and Gartner, 1972; Bralower, 2002; Persico & Villa, 2004; Villa, et al., 2008; Bown et al., 2004, 2005; Self-Trail et al., 2012; Agnini et al., 2016). The second cluster shows low value of x axis and high values of y axis. This cluster is composed by *Ericsonia, Discoaster, Rhomboaster/Tribrachiatus* and *Sphenolithus*. This group of taxa have affinity to oligotrophic, stable conditions (stratified water)

and warmer water (Bukry, 1973; Wei & Wise, 1990; Wei et al., 1992; Bralower, 2002; Villa et al., 2008).

Thus, basing on the analyses of the component's matrix (Fig. 2.10) we can hypothesize that PC2 reflects ecological parameters related to nutrients, whereas based on the placement of the second population to high values of PC1, this major component may reflect the temperature. Based on our analyses of PC1 and PC2, and in agreement with the literature, *C. pelagicus* seems to be a mesotrophic and temperate-warm taxon (Wei & Wise, 1990; Persico & Villa, 2004; Villa et al., 2008), whereas *Z. bijugatus* and *Markalius* could be interpreted as meso-oligotrophic taxa. Our ecological attribution for *Z. bijugatus* is supported by the literature, as it has been interpreted as a K specialist more adapted to stable settings and oligotrophic conditions (Aubry, 1998; Bralower, 2002; Tremolada and Bralower, 2004; Agnini et al., 2007, 2016; Self-Trail et al., 2012).

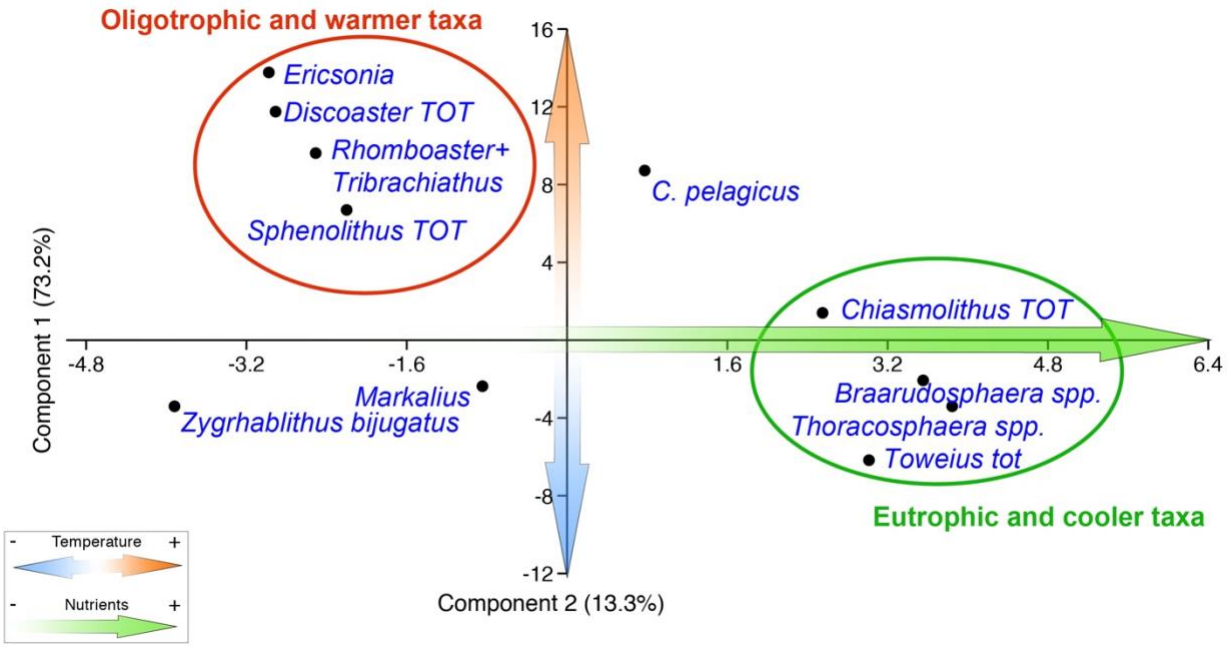

Fig. 2.9: Principal component analysis (PCA) scatter plot of log-ratio transformation data of calcareous nannofossil taxa in terms of the first and second component.

Plotting each component (PC1 and PC2) versus the respective stratigraphic position of samples, PC1 and PC2 show clear variations through the section and in the two different lithologies. It is visible a high positive and negative loadings of Factor 1 in limestones and in the marls, respectively, whereas a positive and negative loadings of Factor 2 are visible respectively in the marls and limestones (Fig. 2.10). The different correlation between PC1 and PC2 in the two different lithologies across the entire section can support our hypothesis suggesting that the marls can reflect eutrophication and cooler waters, whereas limestones may reflect periods with oligotrophy and warmer sea waters.

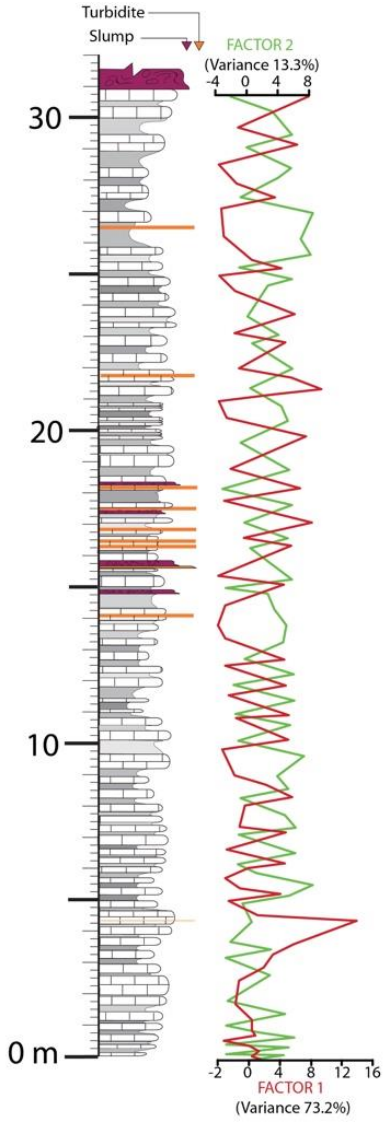

COMPONENT'S MATRIX

SPECIES	Component 1
C. pelagicus	8
Chiasmolithus spp.	1
Braarudospaera spp.	-4
Toweius spp.	-7
Discoster spp.	12.3
Sphenolithus spp.	7.8
Ericsonia	14.2

SPECIES	Component 2
C. pelagicus	0.89
Chiasmolithus spp.	3
Braarudospaera spp.	3.4
Toweius spp.	3.1
Discoster spp.	-3
Sphenolithus spp.	-2.3
Ericsonia	-3.1

Fig. 2.10: Correlation between PCA Factor 1 (red line) and Factor 2 (green line) and lithology at the Sopelana section. On the right of the figure we report the Factor 1 and Factor 2 component's matrix.

The cluster analysis was performed with the same data-set used for the PCA analysis. The cluster analysis was performed using paired group as algorithm and Rho as similarity measure, and it was used to define the ecological assemblages. The Qmode results show different groups of taxa at different similarity levels can be identified (Fig. 2.11). Group A (*Toweius, Chiasmolithus, Braarudosphaera* and *Thoracosphaera)* is characterized by taxa considered to be adapted to high nutrient levels and cool water. Group B (*Z. bijugatus and Markalius*) is composed by taxa with affinity for meso-oligotrophic conditions. Group C (*Ericsonia, Discoaster, C. pelagicus, Rhomboaster/Tribrachiatus* and *Sphenolithus)* is characterized by species that are the major components of the calcareous nannoflora in the Sopelana section, all being considered to be adapted to meso-oligotrophic environments under temperate-warm water conditions.

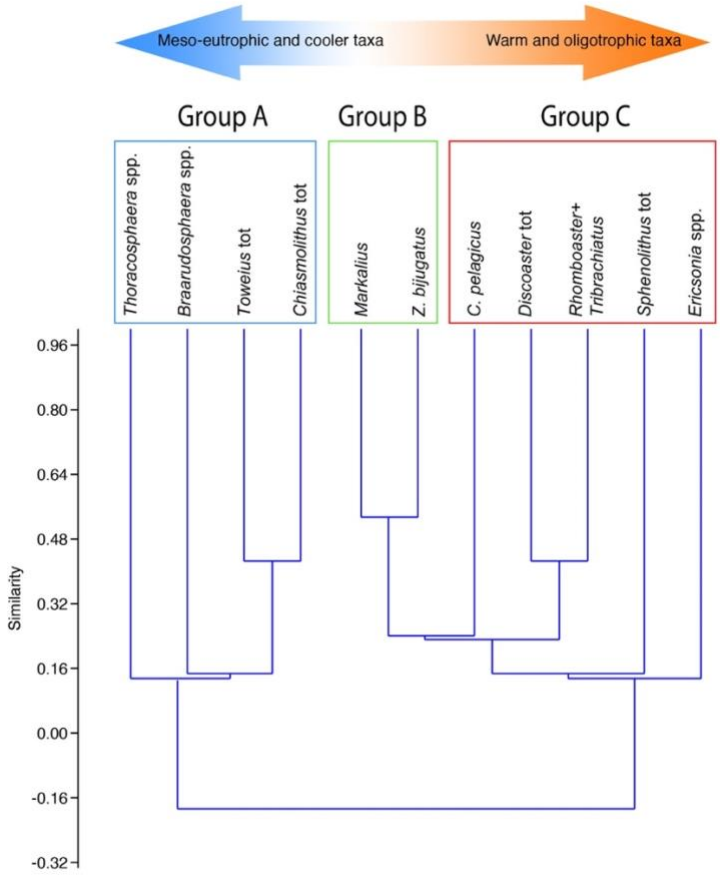

Fig. 2.11: Ecological clusters of calcareous nannofossil assemblages from the Sopelana section. A cluster analysis (paired group as algorithm, Rho as similarity measure) was used to define the ecological assemblages. The potential affinity of each cluster, from warm to cool water environments, is indicated.

The cluster analysis on R-mode was also performed. The cluster analysis is used here to identify groups of samples on the base of abundance variations of taxa. This cluster analysis was performed using Ward as algorithm. The Ward's method associates similar samples on the base of taxa distribution and the similarity index is expressed as Euclidean distances. Four distinctive clusters of samples at different similarity levels can be recognized (Fig. 2.12). Group A includes samples collected near the base of the section (i.e. close to the Paleocene/Eocene boundary). Group B is composed of samples up to the first turbidite layer at 14 m. Group C contains the samples collected in the interval 14-20 m, which contains turbidites and slumps. Group D includes the samples collected in the uppermost part of the section.

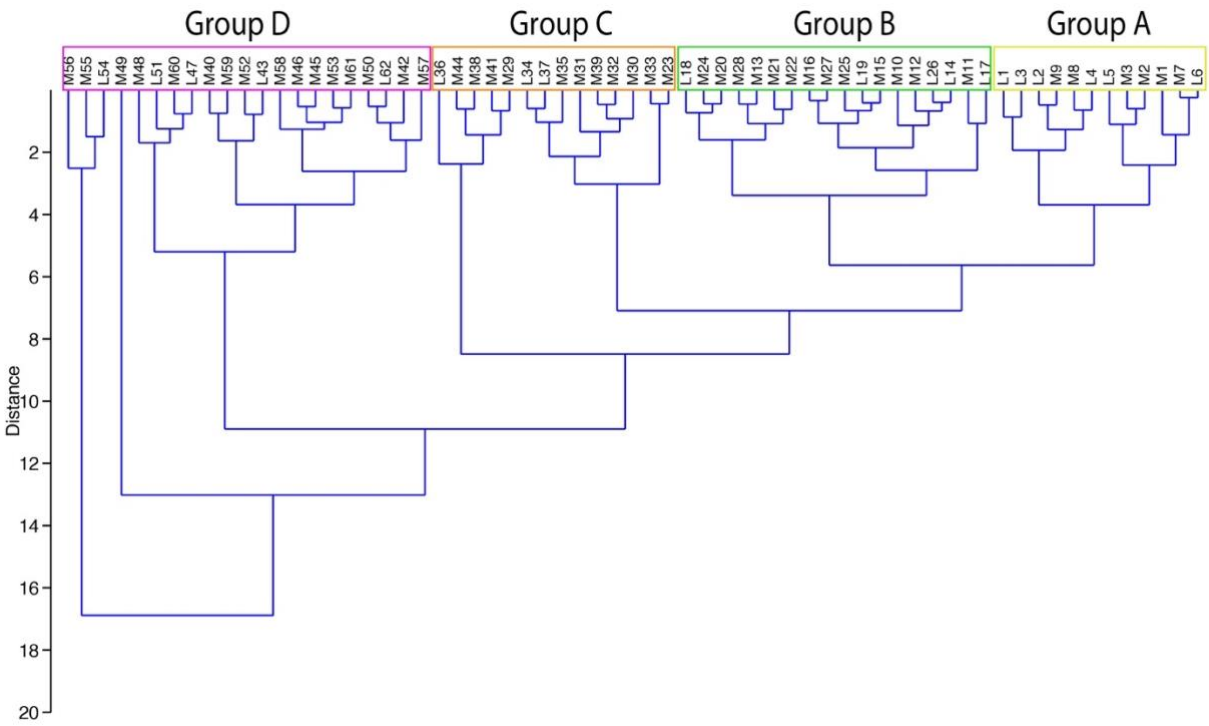

Fig. 2.12: Hierarchical cluster analysis of the investigated samples in the Sopelana section.

2.5.3 Milankovitch cyclicity at the Sopelana section

Spectral analysis of the geochemical data has been used in order to find possible periodicities in the lithological rhythms that may be linked to palaeoclimatic drivers.

The spectrum from the 0-14.71 m interval (Fig. 2.7a) shows periodicities of 41.84, 38.54 and 35.71 cm respectively (1/0.023; 1/0.025 and 1/0.027). The thickness of each marl-limestone couplet in the first part of the section varies between a minimum of 21 cm measured in the first couplet and a maximum value of 70 cm in the 25th couplet, with an average thickness of about 42 cm (an average frequency of 0.0239). In addition to the organization in marl-limestone couplets, a hierarchical organization in bundles, constituted generally of 5 marl-limestone couplets, was observed in the Sopelana section, with an average thickness of 210 cm (i.e., a frequency of 0.0047 cycles/cm). A sharp peak is recorded at this frequency in the spectrum, although it does not exceed the confidence level set at 99% (Fig. 2.7a).

Regarding the power spectrum of the 14.71-31.13 m interval, the frequency of 0.019 cycles/cm corresponds to a period of 51.50 cm. The thickness of the marl-limestone couplets of the second part of the section varies between a minimum of 34 cm recorded in the couplet 37 and a maximum of 113 cm recorded in couplet 56, with an average thickness of approximately 57 cm, which is in line with the spectral results. In this second part of outcrop visual definition of bundles is less evident, so that in the frequency spectrum no peak appears that can be related to the thickness of a bundle (Fig. 2.7b)**.** The power spectrum of the calcium carbonate content shows periodicities that can be related to those of the orbital variations known from the Milankovitch theory, suggesting the climatic origin of the limestone–marl couplets. The strongest signal seems to be associated to the thickness of limestone-marl couplets, which are the sedimentary expression of precession cycle (Martinez-Braceras et al., 2017).

2.5.4 Chronological inferences

Combining the cyclostratigraphic data and the succession of calcareous nannofossil events identified in Sopelana, it is possible to obtain compare the Sopelana results with chronological assignments by Agnini et al. (2014). The most significant calcareous nannofossil bioevents are the Top of *Fasciculithus* spp., marker of the boundary between the zones CNE1 and CNE2, and the Base of *T. orthostylus*, marker of the base of Zone CNE3. According to correlation and calibration to the Geomagnetic Polarity Time Scale (GPTS), Agnini et al., (2014) attributed an age of 54.71 Ma to the former and 53.67 Ma to the latter, meaning that Zone CNE2 has an estimated duration of 1.04 Myr. These bioevents occur at 5.25 and 27.75 m in the Sopelana section, respectively. Between both levels 46 marl-limestone couplets have been identified, each of which would accordingly have an average duration of 22.6 ky, which agrees with the duration of the precession band (18-24 ky) (Laskar et al., 2004). In the same interval, there are 10 bundles with an average duration of 100 ky, which corresponds to the duration of short eccentricity cycles. Integrating the nannofossil biostratigraphic data with the outcomes cyclostratigraphy it is finally possible estimate the age of the base and the top of the section, as well as the age of target and important bioevents: according to the fact that a limestone-marl couplet corresponds to a single precession cycle (22.6 ky, on average) and considering as tie-point the Top of *Fasciculithus* (54.71 Ma), it follows that the base of the section results to have an age of 55.04 Ma. Considering the first 15 m of the section are unaffected by turbidite beds and slump, the age inferred for the base of the section is reliable. Besides, the uppermost portion of the section, from about 15 m up to the top, is affected by the presence of turbidite beds and slump, that might have obscured the orbital forcing signal. Therefore the calculation of the age for the top, is affected by a larger uncertainty. Nonetheless, using as tie-point the most recent bioevent (Base of *S. radians*, dated 53.53 Ma), we calculate an age of 53.49 Ma, therefore constraining the age of the stratigraphic succession.

2.6 Summary and conclusions

The most important results are reviewed in the following main points.

a) The calcareous nannofossil biostratigraphy shows the continuous deposition of the lower Eocene Sopelana section. The Sopelana section spans from CNE1 (upper part of Zone NP10 Zone) to CNE3 (lower part of Zone NP11).

b) The PCA of the calcareous nannofossil assemblages shows two distinctive taxa clusters. Oligotrophic and warm water taxa were distinct from eutrophic and cooler taxa. The PC1 component (73.2%) reflects the temperature, while the second component PC2 (13.3%) reflects the ecological parameter of nutrients.

c) The marlstone-limestone couplets are the expression of primary deposition and are associated with the variation in fertility and productivity cycles.

d) High fertility seems to be documented in marly beds by the increase in abundance of eutrophic taxa, such as *Braarudosphaera* and *Toweius*.

e) According to spectral analysis the cycles identified are in tune with Milankovitch frequencies; the periodicities may be related to precession (21 ky) and short eccentricity cycles (100 ky). The age defined by counting the precession and eccentricity cycles is confirmed by calcareous nannofossil chronology.

f) According to our cyclostratigraphic interpretation, we estimate an age for the base of the investigated section of 55.04 Ma, and an age (even if affected by larger uncertainty) of 53.49 Ma for the top of the section.

Acknowledgements

Research funded by projects CGL2015-65404-R (MINECO/FEDER, Spanish Government/EU) and IT-930-16 (Basque Government). GF was funded by the Erasmus+ programme of the European Commission and by doctoral grant of the University of Florence. SM was funded by University of Florence (2007-11). NMB benefitted by a predoctoral research grant of the Basque Government.

References

Agnini, C., Muttoni, G., Kent, D. V., & Rio, D. (2006). Eocene biostratigraphy and magnetic stratigraphy from Possagno, Italy: the calcareous nannofossil response to climate variability. Earth and Planetary Science Letters, 241(3-4), 815-830.

Agnini, C., Fornaciari, E., Rio, D., Tateo, F., Backman, J., and Giusberti, L (2007): Responses of calcareous nannofossil as- semblages, mineralogy and geochemistry to the environmen- tal perturbations across the Paleocene/Eocene boundary in the Venetian Pre–Alps, Mar. Micropaleontol., 63, 19–38, doi:10.1016/j.marmicro.2006.10.002.

Agnini, C., Fornaciari, E., Raffi, I., Catanzariti, R., Pälike, H., Backman, J., & Rio, D. (2014). Biozonation and biochronology of Paleogene calcareous nannofossils from low and middle latitudes. Newsletters on Stratigraphy, 47(2), 131-181.

Agnini, C., Spofforth, D., Dickens, G., Rio, D., Pälike, H., Backman, J., ... & Dallanave, E. (2016). Stable isotope and calcareous nannofossil assemblage records for the Cicogna section: toward a detailed template of late Paleocene and early Eocene global carbon cycle and nannoplankton evolution. Climate of the Past Discussions, 11(5), 4329-4389.

Alegret L., Ortiz S., Orue-Etxebarria X., Bernaola G., Baceta J.I., Monechi S., Apellaniz E. and Pujalte V. (2009). The Paleocene-Eocene Thermal Maximum: new data from the microfossil turnover at the Zumaia section, Spain. Palaios, 24: 318-328.

Angori, E., & Monechi, S. (1996). High-resolution calcareous nannofossil biostratigraphy across the Paleocene/Eocene boundary at Caravaca (southern Spain). Israel J. Earth Sci, 44, 197-206.

Aubry, M.P., (1998). Late paleogene calcareous nannoplankton evolution: a tale of climatic deterioration. In: Prothero, D.R., Berggren, W.A. (Eds.), Eocene–Oligocene Climatic and Biotic Evolution. Princeton University Press, pp. 272–309.

Bartol M. (2008) Unusual Braarudosphaera bigelowii and Micrantholithus vesper enrichment in the early miocene sediments from the slovenian corridor, a seaway linking the central paratethys and the mediterranean; paleogeography, paleoclimatology, paleoecology, Palaeogeography Palaeoclimatology Palaeoecology, 267, pp. 77-88

Batenburg Sietske J., Andrew S. Gale, Mario Sprovieri, Frederik J. Hilgen, Nicolas Thibault, Myriam Boussaha, Xabier Orue-Etxebarria (2014); An astronomical time scale for the Maastrichtian based on the Zumaia and Sopelana sections (Basque country, northern Spain). Journal of the Geological Society ; 171 (2): 165–180. doi: https://doi.org/10.1144/jgs2013-015

Berggren, W. A. (1969). Paleogene biostratigraphy and planktonic foraminifera of northern Europe. In Proc. I. Internat. Conf. Plankt. Microfoss. Geneva (Vol. 1, pp. 121-160).

Berggren, W. A., Kent, D. V., Swisher III, C. C., & Aubry, M. P. (1995). A revised Cenozoic geochronology and chronostratigraphy.

Berggren, W.A., and Pearson, P.N., (2005). A revised tropical to subtropical Paleogene planktonic foraminiferal zonation. Journal of Foraminiferal Research, 35, 279-298.

Berrocoso, Á. J., Elorza, J., & MacLeod, K. G. (2013). Proximate environmental forcing in fine scale geochemical records of calcareous couplets (Upper Cretaceous and Palaeocene of the Basque-Cantabrian Basin, eastern North Atlantic). Sedimentary Geology, 284, 76-90.

Bordiga, M., Henderiks, J., Tori, F., Monechi, S., Fenero, R., Legarda-Lisarri, A., and Thomas, E. (2015): Microfossil evidence for trophic changes during the Eocene-Oligocene transition in the South Atlantic (ODP Site 1263, Walvis Ridge), Clim. Past, 11, 1249–1270, doi:10.5194/cp-11-1249-2015.

Boulila, S., De Rafaelis, M., Hinnov, L. A., Gardin, S., Galdrun, B., Collin, P. (2010): Orbitally forced climate and sea-level changes in the Paleoceanic Tethyan domain (marl-limestone alternations, Lower Kimmerifgian, SE FRance). Palaeogeogr. Palaeoclimatol. Palaeoecol., 292, 57–70.

Bown, P.R., (2005). Paleogene calcareous nannofossils from Kilwa and Lindi areas of coastal Tanzania (Tanzania Drilling Project 2003–2004). J. Nannoplankton Res. 27, 21–95.

Bown, P. R., Lees, J. A., & Young, J. R. (2004). Calcareous nannoplankton evolution and diversity through time. In Thierstein, H. R., & Young, J. R. (Eds.), Coccolithophores: From Molecular Processes to Global Impact (pp. 481–508). Berlin: Springer-Verlag

Bralower, T.J., (2002). Evidence of surface water oligotrophy during the Paleocene-Eocene Termal Maximum: nannofossil assemblage data from ocean drilling program Site 690, Maud Rise, Weddell Sea. Paleoceanography 17 (2), 1029–1042. https://doi.org/ 10.1029/2001PA000662.

Buccianti, A., Mateu-Figueras, G., and Pawlowsky-Glahn, V. (2006).: Compositional data analysis in the geosciences: From theory to practice, Geol. Soc. London, London, Spec. Publ., 264, 1–206, doi:10.1144/GSL.SP.2006.264.01.16.

Bukry, D. (1973). Coccolith and silicoflagellate biostratigraphy, Tasman Sea and southwest Pacific Ocean, Deep Sea Drilling Project Leg 21. In Burns, R. E., Andrews, J. E., et al., Initial Reports of the Deep Sea Drilling Project (Vol. 21, pp. 885–893). Washington, DC: US Government Printing Office.

Bukry, D., (1974). Coccoliths as paleosalinity indicators: evidence from Black Sea. AAPG Mem. 20, 353–363.

Bybell, L.M., Gartner, S., (1972). Provincialism among mid-Eocene calcareous nannofossils. Micropaleontology 18, 319–336. http://dx.doi.org/10.2307/1485011

Cuevas, J., Eguiluz, L., Ramón-Lluch, R., Tubía, J.M., (1982): Sobre la existencia de una deformación tectónica compleja en el flanco N del sinclinal de Oiz-Punta Galea. Nota preliminar. Lurralde. Investigación y espacio, 47 61.

Cunha, A. S., & Shimabukuro, S. (1997). Braarudosphaera blooms and anomalous enrichments of Nannoconus: evidence from the Turonian South Atlantic, Santos Basin, Brazil. Journal of Nannoplankton Research, 19(1), 51-55.

Dedert, M., Stoll, H. M., Kroon, D., Shimizu, N., Kanamaru, K., & Ziveri, P. (2012). Productivity response of calcareous nannoplankton to Eocene Thermal Maximum 2 (ETM2). Climate of the Past, 8(3), 977-993.

Dinarès-Turell, J., Martínez-Braceras, N., Payros, A., (2018). High-resolution integrated cyclostratigraphy from the Oyambre section (Cantabria, N Iberian Peninsula): constraints for orbital tuning and correlation of middle Eocene Atlantic deep-sea records. Geochem. Geophys. Geosyst. 19, 2017GC007367. https://doi.org/10.1002/ 2017GC007367.

Dinarès-Turell, J., Stoykova, K., Baceta, J.I., Ivanov, M., Pujalte, V., (2010). Highresolution intraand interbasinal correlation of the Danian–Selandian transition (Early Paleocene): the Bjala section (Bulgaria) and the Selandian GSSP at Zumaia (Spain). Palaeogeography, Palaeoclimatology, Palaeoecology 297, 511–533.

Domínguez, E., Echeberria, J., Gómez-Urtasun, I., Ibisate, R., Martínez- García, B. & Elorza, J. (2007): Espesores y contenido de CaCO3 en los pares marga-caliza del Daniense (Sopelana, Arco Vasco). Geogazeta, 41, 67–70.

Elder, W.P., Gustason, E.R., Sageman, B.B., (1994). Correlation of basinal carbonate cycles to nearshore parasequences in the Late Cretaceous Greenhorn seaway, Western Interior U.S.A. GSA Bulletin 106, 892–902.

Eldrett, J. S., Ma, C., Bergman, S. C., Ozkan, A., Minisini, D., Lutz, B., ... & Kelly, A. E. (2015). Origin of limestone–marlstone cycles: astronomic forcing of organic-rich sedimentary rocks from the Cenomanian to early Coniacian of the Cretaceous Western Interior Seaway, USA. Earth and Planetary Science Letters, 423, 98-113.

Elorza, J.J., Orue-Etxebarria, X. and Lamolda, M.A. (1984) Existencia de una fracturacion intensa en el area de Sopelana-Meñakoz. I Congreso Español de Geologia, 3, 177.

Feuillée, P. & Rat, P. (1971): Structures et paléogéographies pyrénéo-¬¬cantabriques. En: Histoire Structural du golfe de Gascogne (J. Debyser, X. Le Pichon, L. Montardet, Eds.), Publ. l´inst. Français Pétrole, Coll. Et Sémin, Ed.Technip., 2: 1-¬¬48.

Flores, J. A., & Sierro, F. J. (1997). Revised technique for calculation of calcareous nannofossil accumulation rates. Micropaleontology, 321-324.

Gibbs, S., Shackleton, N.J., Young, J., (2004). Orbitally forced climate signals in mid-Pliocene nannofossil assemblages. Mar. Micropaleontol. 51, 39–56. doi:10.1016/j.marmicro.2003.09.002.

Hammer, Ø., Harper, D.A.T., Ryan, P.D., (2001). PAST: paleontological statistics software package for education and data analysis. Palaeontol. Electron. 4, 1–9.

Haq, B. U. (1980). Biogeographic history of Miocene calcareous nannoplankton and paleoceanography of the Atlantic Ocean. Micropaleontology, 414-443.

Haq, B.U., Lohmann, G.P., (1976). Early Cenozoic calcareous nannoplankton biogeography of the Atlantic Ocean. Mar. Micropaleontol. 1, 119–194. https://doi.org/10.1016/ 0377-8398(76)90008-6.

House, M.R., Gale, A.S. (Eds.), (1995). Orbital Forcing Timescales and Cyclostratigraphy. Spec. Publ.-Geol. Soc. Lond., vol. 85. 204 pp.in Stratigraphy (Eds G. Einsele, W. Ricken and A. Seilacher), pp. 23-47. 8 Springer-Verlag, New York.

Kucera, M. and Malmgren, B. A. (1998).: Logratio transformation of com- positional data – a resolution of the constant sum constraint, Mar. Micropaleontol., 34, 117–120.

Laskar, J., Robutel, P., Joutel, F., Gastineau, M., Correia, A. C. M., & Levrard, B. (2004). A long-term numerical solution for the insolation quantities of the Earth. Astronomy & Astrophysics, 428(1), 261-285.

Liebrand, D., Raffi, I., Fraguas, Á., Laxenaire, R., Bosmans, J. H., Hilgen, F. J., ... & Bown, P. R. (2018). Orbitally forced hyperstratification of the Oligocene South Atlantic Ocean. Paleoceanography and Paleoclimatology.

Lohmann, G. P., & Carlson, J. J. (1981). Oceanographic significance of Pacific late Miocene calcareous nannoplankton. Marine Micropaleontology, 6(5-6), 553-579.

Marino, M., Maiorano, P., and Lirer, F. (2008): Changes in calcareous nannofossil assemblages during the Mid- Pleistocene Revolution, Mar. Micropaleontol., 69, 70–90, doi:10.1016/j.marmicro.2007.11.010.

Martínez-Braceras, N., Payros, A., Miniati, F., Arostegi, J., Franceschetti, G., (2017). Contrasting environmental effects of astronomically driven climate change on three Eocene hemipelagic successions from the Basque–Cantabrian Basin. Sedimentology 64 (4), 960-986. http://dx.doi.org/10.1111/sed.12334

Martini, E., (1971): Standard Tertiary and Quaternary calcareous nannoplankton zonation. In: Farinacci, A. (Ed.), Proceedings 2nd International Conference Planktonic Microfossils Roma: Rome (Ed. Tecnosci.) 2, 739–785.

Moiroud, M., Martinez, M., Deconinck, J., Monna, F., Pellenard, P., Riquier, L. and Company, M. (2012) High-resolution clay mineralogy as a proxy for orbital tuning: Example of the Hauterivian-Barremian transition in the Betic Cordillera (SE Spain). Sed. Geol., 282, 336-346.

Monechi S., Angori E. and VonSalis K. (2000). Calcareous nannofossil turnover around the Paleocene-Eocene transition at Alamedilla (Southern Spain). Bull. Soc. géol. Fr., 4, 477-489).

Muñoz, J.A. (2002) Alpine Tectonic I: the Alpine system north of the Betic Cordillera. Tectonic setting; The Pyrenees. The Geology of Spain (W. Gibbons y T. Moreno, Eds.), Geol. Soc. (London), 370-385.

Okada, H., Bukry, D., 1980. Supplementary modification and introduction of code numbers of the low-latitude coccolith biostratigraphic zonation (Bukry, 1973; 1975). Mar. Micropaleontol. 5, 321–325. https://doi.org/10.1016/0377-8398(80)90016-X.

Payros, A., Orue-Etxebarria,X. and Pujalte,V., (2006). Covarying sedimentary and bioticfluctuations in Lower-Middle Eocene Pyrenean deep-sea deposits: palaeoenvironmental implications.Palaeogeogr., Palaeoclimatol., Palaeoecol., 234, 258– 276.

Perch-Nielsen, K. (1985): Mesozoic calcareous nannofossils. In: Bolli, H.M., Saunders, J.B., et al. (eds) Plankton Stratigraphy. Cambridge University Press, Cambridge, 329–426.

Persico, D., & Villa, G. (2004). Eocene–Oligocene calcareous nannofossils from Maud Rise and Kerguelen Plateau (Antarctica): paleoecological and paleoceanographic implications. Marine Micropaleontology, 52(1–4), 153–179, doi: 10.1016/j.marmicro.2004.05.002

Pujalte, V., Baceta, J.I., Orue-Etxebarria, X. & Payros, A. (1998): Paleocene strata of the Basque Country, western Pyrenees, northern Spain: facies, and sequence development in a deep-water starved basin. In: de Graciansky, P.-C., Hardenbol, J., et al. Mesozoic and Cenozoic Sequence Stratigraphy of European Basins. SEPM Special Publications, 60, 311–328.

Pujalte, V., Baceta, J.I., Payros, A., (2002): Chapter 13: Tertiary: Western Pyrenees and Basque–Cantabrian region. In: Gibbons, W., Moreno, T. (Eds.), The Geology of Spain. Geol. Soc., London, pp. 293–301.

Schneider, L. J., Bralower, T. J., Kump, L. R., & Patzkowsky, M. E. (2013). Calcareous nannoplankton ecology and community change across the Paleocene-Eocene Thermal Maximum. Paleobiology, 39(4), 628-647.

Self-Trail, J. M., Powars, D. S., Watkins, D. K., and Wand- less, G. (2012): Calcareous nannofossil assemblage changes across the Paleocene-Eocene thermal maximum: Evidence from a shelf setting, Mar. Micropaleontol., 92–93, 61–80, doi:10.1016/j.marmicro.2012.05.003.

Serrano, A., Martínez del Olmo, W. (1990): Tectónica salina en el dominio Cántabro- Navarro: evolución, edad y origen de las estructuras salinas. InF. Orti et al. eds. Form. Evap. Cuenca Ebros. ENRESA. GPPG., Univ. Barcelona. Pp. 39-53.

Švábenická, L. (1999). Braarudosphaera-rich sediments in the turonian of the bohemian cretaceous basin, Czech Republic Cretaceous Research, 20, pp. 773-782.

Thunnel, R., Rio, D., Sprovieri, R., Raffi, I., (1991). Limestone–marl couplets: origin of the early Pliocene Trubi marls in Cala- bria, Southern Italy. Journal of Sedimentary Petrology 61, 1109 – 1122.

Tremolada, F. and Bralower, T. J. (2004).: Nannofossil assemblage fluctuations during the Paleocene–Eocene Thermal Maximum at Sites 213 (Indian Ocean) and 401 (North Atlantic Ocean): palaeoceanographic implications, Mar. Micropaleontol., 52, 107–116, doi:10.1016/j.marmicro.2004.04.002.

Villa, G., Fioroni, C., Pea, L., Bohaty, S., & Persico, D. (2008). Middle Eocene–late Oligocene climate variability: Calcareous nannofossil response at Kerguelen Plateau, Site 748. Marine Micropaleontology, 69(2), 173–192, doi: 10.1016/j.marmicro.2008.07.006.

Von Salis K., Monechi S., Bybell L. M., Self-Trail J. and Young J., (2000). Remarks on the calcareous nannofossil markers Rhomboaster / Tribrachiatus around the Paleocene/Eocene Boundary. Geological Soc. of Sweden.GFF, 122,1,138-140.

Wade,B.S.,Pearson,P.N.,Berggren,W.A.andPa€like,H. (2011) Review and revision of Cenozoic tropical planktonic foraminiferal biostratigraphy and calibration to the geomagnetic polarity and astronomical time scale. Earth-Sci. Rev., 104, 111–142.

Weedon G., (2003): Time series analysis and cyclostratigraphy: Examining stratigraphic records of environmental cycles. Cambridge University.

Wei, W., & Wise Jr, S. W. (1992). Eocene-Oligocene calcareous nannofossil magnetobiochronology of the Southern Ocean. Newsletters on Stratigraphy, 119-132.

Wei, W., Wise Jr., S.W., (1990). Biogeographic gradients of middle Eocene– Oligocene calcareous nannoplankton in the South Atlantic Ocean. Palaeogeogr. Palaeoclimatol. Palaeoecol. 79, 29–61. doi:10.1016/0031- 0182(90)90104-F

Westphal, H., Munnecke, A., Böhm, F., & Bornholdt, S. (2008). Limestone–marl alternations in epeiric sea settings–witnesses of environmental changes or diagnesis. Special Paper–Geological Association of Canada, 389, 406.

Young J. (1994) Functions of coccoliths A. Winter, W. Sissler (Eds.), Coccolithophores, Cambridge University Press, pp. 63-82.

Chapter 3

Calcareous nannofossil response to astronomically driven climate changes on three Eocene deep-sea sections from the Basque-Cantabrian Basin, Spain *

Abstract

Several proxies can be used to study the origin of marl-limestone alternations in hemipelagic successions. The lithological hierarchical arrangement often reflects Milankovitch cycles of precession, obliquity and eccentricity, indicating that the ocean-climate system was strongly controlled by orbital forcing. Palaeoenvironmental changes induced by orbital forcing determine the characteristics of the marine communities, including calcareous nannoplankton. We present high-resolution records of changes in calcareous nannofossil assemblages across three short eccentricity cycles (100 ky) from three early-middle Eocene sections in the Basque-Cantabrian Basin (Sopelana, Gorrandatxe and Oyambre) each representing a distinct palaeogeographic setting. The results show that the variations in calcareous nannofossil assemblages observed in the three sections can be related to palaeoenvironmental variations related to eccentricity minima and maxima. In the Sopelana section (deep-sea basin) and in the Oyambre section (upper slope) the calcareous nannofossil changes were related primarily to temperature and secondarily to nutrients. In the Gorrondatxe section (submarine fan fringe) the calcareous nannofossil changes were mainly due to nutrients and to a lesser extent to salinity changes.

*This chapter is based on a manuscript in preparation for submission to *Paleogeography, Paleoclimatology, Paleoecology*

FRANCESCHETTI G.[1], MARTINEZ- BRACERAS N.[2], PAYROS A.[2,] BERNAOLA-BILBAO G. [3] MONECHI S.[1]
[1] Dipartimento di Scienze della Terra, Università degli Studi di Firenze, Via La Pira 4, 50121, Firenze, Italy
[2] Department of Stratigraphy and Paleontology, Faculty of Science and Technology, University of the Basque Country (UPV/EHU), Ap. 644, E48080 Bilbao, Spain. [3] Department of Mining and Metallurgical Engineering and Materials Science, University of the Basque Country (UPV/EHU), Rafael Moreno Pitxitxi 2, 48013 Bilbao, Spain.

3.1 Introduction

Changes in the Earth's orbital parameters (Milankovitch cycles) regulate the amount of solar energy that reaches our planet and annual seasonality. These periodic climatic fluctuations are often regarded as the main force driving the formation of hemipelagic marl-limestone alternations (Elder et al., 1994; House, 1995; Dinarès-Turell et al., 2003, 2010). The small seasonal effect induced by these variations can be amplified by climate systems and recorded as cyclic sedimentary successions. However, processes acting after deposition, such as diagenesis, can distort or sometimes completely delete the primary environmental signal (Westphal et al., 2004). Recent studies (Boulila et al., 2010; Berrocoso et al., 2013; Martinez-Braceras et al. 2017; Dinares-Turell et al., 2018) have demonstrated that several physical and chemical proxies (carbonate and manganese content, magnetic susceptibility or bulk carbon and oxygen stable isotopes) obtained through high-resolution sampling (<104 years) of hemipelagic successions can help to determine the dominant forcing mechanisms on sedimentation. The characteristics of the biotic assemblages (composition, abundance, diversity), despite being very sensitive to climatic and environmental change, have more rarely been used for the recognition of different scale Milankovitch variations (e.g., Erba et al., 1992; Gibbs et al., 2004; Marino et al., 2009). Calcareous nannofossils have been proven a useful tool for paleoceanographic and palaeonvironmental studies, but few papers have analysed the relationship between calcareous nannofossil variations and Milankovitch-scale forcing. Most of these studies have been focused on the Neogene and Quaternary (Backman et al., 1986; Backman and Pestiaux, 1987; Chepstow-Lusty et al., 1989; Beafort and Aubry, 1990; Hilgen, 1991; Shackleton et al., 1995; Shackleton et al., 1999; Gibbs et al., 2004; Marino et al., 2009, 2011) and highlighted the relationship between calcareous nannofossil assemblages and eccentricity and obliquity, the two cycles that have regulated climatic changes in the most recent part of Cenozoic. Fewer studies have been carried out in older records, such as in Cretaceous and Jurassic successions (Erba et al.,1992; Mattioli,

1997; Röhl et al., 2001, 2003; Weber et al., 2001; Cramer et al., 2003, Herrle et al., 2003 a,b; Suchéras-Marx et al., 2010; Giorgioni et al., 2017). To our knowledge, no detailed studies about the effect of Milankovitch cycles on Paleogene calcareous nannofossil assemblages have been performed to date. However, this period is probably the most relevant to ongoing climate change, as it was characterized by high concentrations of greenhouse gases and the warmest global temperatures over the last 80 Myr (Zachos et al., 2001).

In order to analyse the orbital influence on Eocene marine planktonic communities, we have studied the calcareous nannoplankton assemblages, at high resolution, of three sections in the Basque-Cantabrian basin, which represent different sedimentary environments from the northern margin of the Iberian Peninsula (deep-sea basin in Sopelana, upper slope in Oyambre and submarine fan fringe in Gorrondatxe). Orbital forcing on sedimentation due to precession (20 ky) and short eccentricity (100 ky) cycles has previously been demonstrated on the three sections (e.g., Payros et al., 2009, 2011, 2012; Payros & Martínez-Braceras, 2014; Martínez-Braceras et al., 2017; Dinarès-Turell et al., 2018; Intxauspe-Zubiaurre et al., 2018). Furthermore, Martínez-Braceras et al. (2017) suggested which specific climate-related environmental factors influenced on each of the Eocene hemipelagic successions, concluding that the intensity of the different processes varied depending on paleogeographic setting and eccentricity-modulated precessional seasonality. The aim of this study is to investigate the influence of Milankovitch cycles on calcareous nannofossils in order to check whether the fluctuations observed in the nannofloral content support the sedimentological model proposed by Martínez-Braceras et al. (2017). To this end, the calcareous nannofossil sampling has been conducted on the same levels (samples) of the previous geochemical analysis. These analyses have been performed on three specific short eccentricity cycles in the three different sections. These intervals have been selected because of their easy access, their well-developed eccentricity bundles and the high

clarity of the minimum and maximum eccentricity signals, this last factor being represented by a high lithological contrast between marls and limestones.

3.2 Geological setting of the studied area

The studied area, comprehending the Sopelana, Oyambre and Gorrondatxe sections is located in the Basque-Cantabrian Basin (BCB). The BCB is sited at the westernmost boundary of the Pyrenees and is a geological constituent of the Bay of Biscay-Pyrenean realm (Abalos 2016) (Fig. 3.1). Its tectonic evolution was determined by the interaction between the Iberian and the European plates (Roca 2011). The basin is bordered by the Landes high to the north, the Tertiary Ebro and Duero basins to the south, the Asturian massif to the west and the Pamplona Fault to the east.

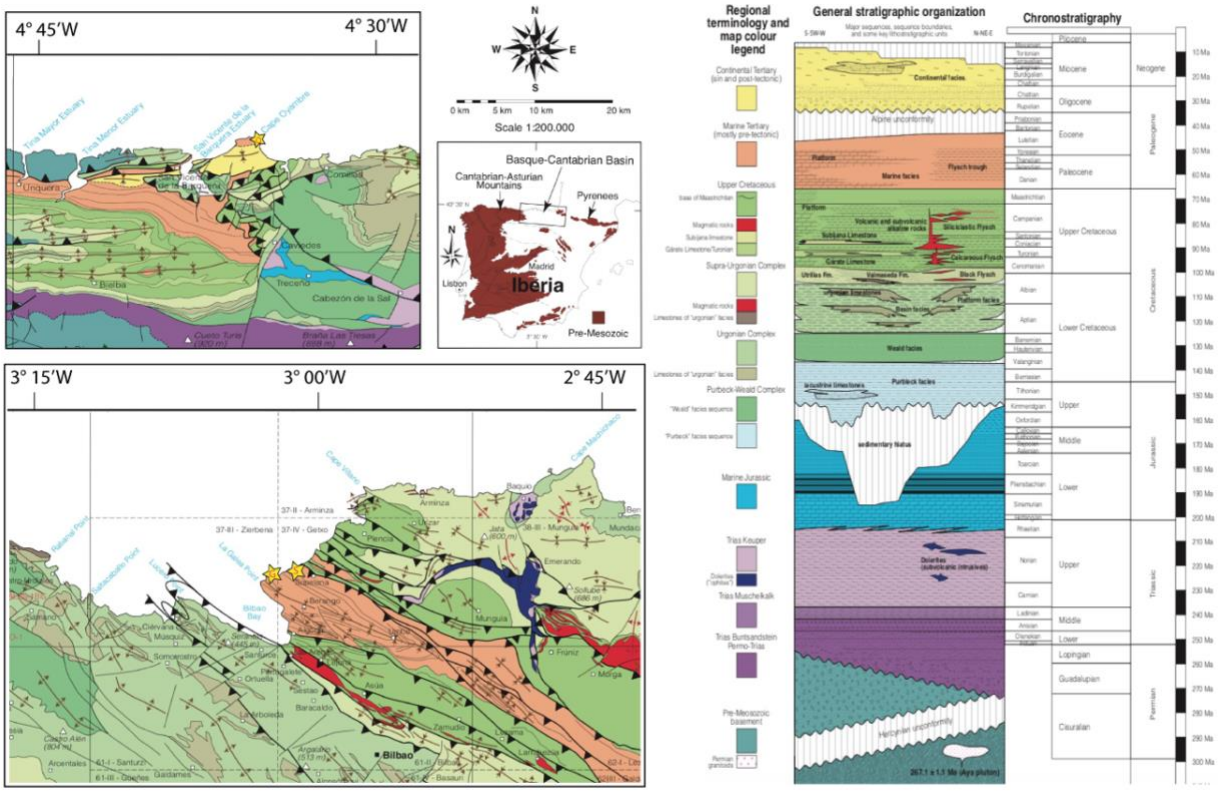

Fig. 3.1: Geological sketch map of the BCB showing into the yellow stars the location of the studied section, Sopelana (S), Gorrondatxe (G) and Oyambre (O). Modified after Abalos 2016.

Following the opening of the Central Atlantic Ocean and of the Bay of Biscay in the Triassic-early Cretaceous times a string of subsiding basins was formed. Subsequently, from the late Albian up to the Santonian intervals, all the sub basins coalesced into one single larger marine embayment, the Pyrenean basin, of which the Basque Basin represents the deepest part (Pujalte et al., 2002). The opening of the South Atlantic Ocean and the resulting northward shift of the African plate produced the collision and subduction of the Iberian plate under the European plate.

In the early Paleocene, as a result of an oblique convergence between the Iberian and the European plate, the Pyrenean domain was an east-west oriented embayment opening westward into the Atlantic Ocean at approximately 35°N latitude. It was surrounded on its north, south and east sides by shallow marine carbonate platform systems, and flanked by continental alluvial plains (Pujalte et al., 2002, Ortiz et al., 2012).

During Eocene times plate collision led to the progressive emergence of the Pyrenean axial zone and to the subdivision of the former single basin into the northern Pyrenean foreland basin (which extended into the Basque Basin) and the southern Pyrenean foreland basin. Thrusting and uplift during late Eocene and Miocene times reduced the marine areas and produced a basin inversion. Nowadays, Cenozoic deposits are associated with the main structures of the Basque-Cantabrian belt in several distinct outcrops (Fig. 3.2b). Thus, the early Palaeogene deep-water deposits of the Basque basin are exposed in the Biscay Syncline and in the Gipuzkoa Monocline. This complex evolution led to the development of the present-day tectono-stratigraphic setting (Fig.3.1).

3.2.1 Sopelana section

The Sopelana section (Lat. 43°23'24.2"N, Log. 2°59'32.4"W) is exposed at the cliff to the NE of the Atxabiribil beach, nearly 15 km north-west of Bilbao (Basque Country; Fig. 3.1). The Sopelana section is 31.5 m thick and was attributed to calcareous nannofossil zones CNE1 to CNE3 of Agnini

et al. (2014) (Franceschetti et al., in prep). The section is characterized by the alternation of weather-resistant limestones and recessive marls, but sediment gravity flow deposits become progressively more abundant upsection (Martinez-Braceras et al., 2017; Franceschetti et al., in prep.). According to the planktonic/benthonic ratio (Murray, 1976), the hemi-pelagic sediments accumulated at approximately 1500m water depth (Martınez-Braceras et al., 2015). Sixty three marl-limestone couplets, approximately 40-50 cm thick each, were identified and interpreted as the expression of 20 ky precession cycles. These couplets are organized in 13 well-defined plurimetric (average of 2.2 m) bundles, each of which generally contains five limestone-marl couplets, which were attributed to short (100 ky) eccentricity cycles. The studied eccentricity bundle 'Sb12' is 2.85 m thick and includes precession couplets 'Sc52' to 'Sc57' (Martinez-Braceras et al., 2017) (Fig. 3.1). A total of 57 samples (29 in limestone beds and 28 in marls) were collected along the studied interval.

3.2.2 Oyambre section

The Oyambre section is exposed along the costal cliff and wave-cut platform on the east side of Oyambre Cape (Lat. 43°24'13''N, Log. 4°37'24''W), which is situated near the village of San Vicente de la Barquera in the north-west of the Cantabria Province (Fig. 3.1). This section is composed of 130 m of upper Lutetian and lower Bartonian hemipelagic (marl-limestone sediments) and turbiditic deposits accumulated on an eastward-facing slope that progressively deepened from 500 to 900 m (Payros et al., 2015). The section has previously been studied by Dinarès-Turell et al. (2018), Intxauspe-Zubiaurre et al. (2018), Martinez-Braceras et al. (2017) and Payros et al. (2015). Based on the bio-magnetostratigraphic studies carried out by Payros et al. (2015), the section spans from Zone CNE12 to Zone CNE17 of Agnini et al. (2014). A cyclostratigraphic study of the lower part of the Acebosa Fm was carried out by Dinares-Turell et al. (2018) using magnetic susceptibility and color proxy records. Seventy three marl-limestone

couplets, organized into 15 bundles, were attributed to precession (20 ky) and short eccentricity (100 ky) cycles, respectively. This study showed a good correlation of the Oyambre cycles with those recognized at ODP Site 1260 and other oceanic records studied by Westerhold et al. (2015). The interval studied herein is about 6 m thick and extends from precession couplet 'Oc28' to 'Oc33', encompassing eccentricity bundle 'Ob7' completely (Fig. 3.2). A total of 88 samples were collected (60 in limestone beds and 38 in marl levels).

3.2.3 Gorrondatxe

The Gorrondatxe section is exposed along costal cliffs near the city of Bilbao (Biscay province, Basque Country; Lat. 43°22'46"N, Log. 3°00'5"W; Fig. 3.1). The 700-m-thick succession consists of upper Ypresian to middle Lutetian alternating hemipelagic limestones and marls with abundant intercalations of plane parallel, thin-bedded (<10 cm) siliciclastic turbidites. The intercalated siliciclastic turbidites are commonly tabular-shaped, flat-based and just few millimeters thick. No evidence of turbidite amalgamation or any large-scale vertical arrangement of facies was observed (Payros et al., 2009). According to these features, the Gorrondatxe materials were attributed to submarine fan fringe or basin plain settings approximately 1500 m deep (Payros et al., 2006). In the lower part of the Gorrondatxe section these authors defined 45 limestone-marls couplets, each 1.1-3 m thick, which were interpreted as the expression of 20 ky precession cycles. In addition, ten bundles, each 9.5-14-5 m thick and composed of four to six couplets, were defined and attributed to short (100 ky) eccentricity cycles. The interval studied herein corresponds to that previously studied by Payros & Martínez-Braceras (2014) for turbidite characteristics and by Martínez-Braceras et al. (2017) for hemipelagic composition. It is 13.5 m thick and extends from precession couplets 'Gc9' to 'Gc15' of eccentricity bundle 'Gb3' (Fig. 3.2). A total of 126 samples were collected for calcareous nannofossil analysis (72 in marls, 54 in limestones).

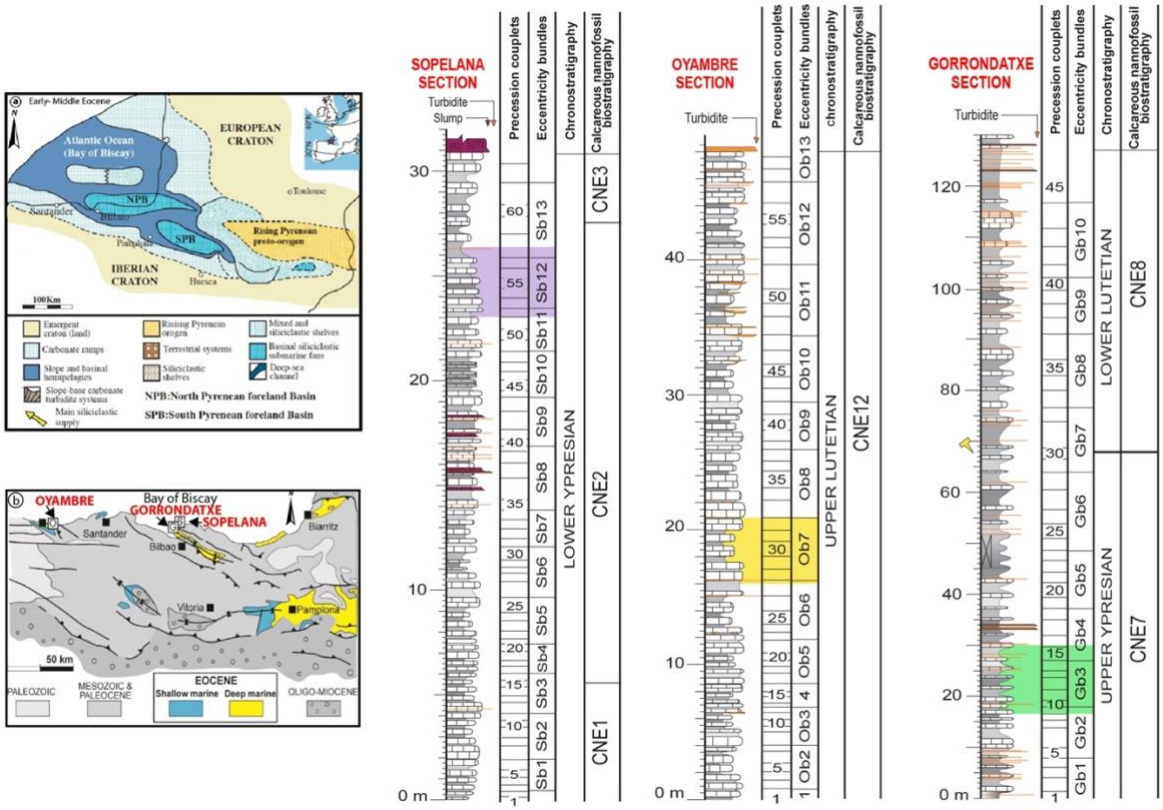

Fig. 3.2: (a) Pyrenean and Basque-Cantabrian paleogeographic setting during Early-Middle Eocene times (modified from Pujalte et al., 2002). (b) Simplified geological map showing the location of the studied sections in Sopelana (S), Gorrondatxe (G) and Oyambre (O). The lithostratigraphic logs, cyclostratigraphy and biochronostratigraphy of the three studied sections are shown on the right. The sampled intervals are highlighted in color (modified from Martinez-Braceras et al., 2017).

3.3 Methods

3.3.1 Preparation of calcareous nannofossils and statistical data treatment

A total of 271 samples were collected and prepared for calcareous nannofossil analysis. Smear slides for coccolithophore analysis were prepared according to Flores and Sierro (1997) for the measurement of absolute coccolith abundance. The absolute abundances were reported as number of calcareous nannofossils per gram of sediment, nanno/g. All the slides were analyzed under a Zeiss Axioplan 2 transmitted light microscope at 1250x magnification. In order to characterize the calcareous nannofossil assemblage, approximately 500 autochthonous

specimens were counted on each slide. Minor reworking was observed in the Sopelana and Oyambre sections, but where present, as in the Gorrondatxe section, reworked specimens were counted separately. The taxonomy mainly follows Perch-Nielsen (1985) and Bown (2005). Fornaciari et al. (2010) and Agnini et al. (2014) were followed for *Dictyococcites* taxonomy, so that this genus has been subdivided into two species: *Dictyococcites bisectus* consists of specimens >10µm and *D. scrippsae* is represented by specimens <10 µm. Species diversity (Shannon index; H) was calculated using the free paleontological statistical software (PAST) (Hammer et al., 2001). Principal Component Analysis (PCA) and Cluster analysis were performed using PAST (PAleontology STatistic) software (Hammer et al., 2001). The PCA and Cluster analysis were performed using the log-ratio transformation of the species percentage as variables in the input matrix. Subsequently, the factors with maximum variance (PC1 and PC2) were evaluated and the patterns of key taxa in the cluster analyses were interpreted in terms of paleoclimate and ecological changes through the investigated intervals. Only the species with continuous abundance higher than 3% were taken into account for statistical analysis.

3.3.2 Palaeoecological affinities of key taxa

The assignment of specific the ecological affinities to extinct calcareous nannofossils taxa can be problematic due to the connection between environmental factors such as temperature and nutrient supply (Agnini et al., 2007). In addition, some fossil species are inferred to have undergone an evolutionary shift in their ecological preference over time (Haq & Lohmann, 1976). Despite these problems, there is general agreement that certain species reflect specific ecological/environmental conditions (e.g. Wei & Wise, 1990a; Wei et al., 1992; Bralower, 2002; Raffi et al., 2005; Gibbs et al., 2006; Villa et al., 2008, Toffanin et al., 2011; Agnini et al., 2016). Here, we report the ecological preferences of key taxa used in this study based on literature data.

Discoasters are considered K-specialist, with preference for warm, oligotrophic, open ocean environment and stable environments (Bukry, 1973; Wei & Wise, 1990a; Aubry 1992; Bralower, 2002; Gibbs et al., 2006; Agnini et al, 2007, 2016), being rare or absent in high fertility equatorial area (Chepstow-Lusty et al., 1989, Chapman and Chepstow-Lusty, 1997, Wade and Bown, 2006) and in marginal seas (Perch-Nielsen, 1985).

Sphenolithus spp. is a dominant component of assemblages at equatorial sites and its abundance declines in mid-high latitudes. Diversity follows an analogous pattern, with high diversity at low latitudes but decreasing at mid- to high latitudes. This evidence, joined with its close relation with *Discoaster*, are interpreted as a preference for oligotrophic, warm-water conditions (Wei & Wise, 1990a; Bralower, 2002; Gibbs et al., 2006; Agnini et al, 2006; Schneider et al., 2013) even though Wade and Bown (2006) and Dunkley Jones et al., (2008) have questioned this interpretation inferring this species to strongly eutrophic conditions.

Ericsonia is generally considered a warm-water and oligotrophic taxon (Wei et al., 1992; Bralower 2002; Tremolada and Bralower 2004; Villa et al., 2008), however, Schneider et al. (2013), suggested that it was adapted to tolerate a wide nutrient range.

The ecological preference of *C. pelagicus* appears to have suffered a shift in temperature preference through time (Haq & Lohman, 1976). The modern species has a preference for cool-water and high nutrient environments (McIntyre & Bé, 1967; Cachão & Moita 2000; Balestra et al., 2004; Parente et al., 2004, Narciso et al., 2006; Silva et al., 2008; Dylmer et al., 2015) but the Paleogene fossil species is inferred to have had a preference for temperate-and mesotrophic waters (Wei & Wise, 1990; Monechi et al., 2000; Persico & Villa, 2004; Villa et al., 2008; Agnini et al., 2007). During a cooling period the *C. pelagicus* changed the size of the body of coccolits as well as other placolith forms (Mita, 2001). In our samples from the Oyambre and Gorrondatxe studied intervals, there were the largest abundance of the forms with 5-10 μm size of the body, and secondary by species with >10 μm size of the body. *Coccolithus pelagicus* with dimensions

of 5–10 µm is characteristic of cooler water, actually this form lives in arctic waters with temperatures less than 10 °C (Parente et al., 2004), whereas *C. pelagicus* >10 µm lives in slightly warm waters in the oceans, and nowadays is recorded near coasts of Iberia and it is influenced by the position of coastal upwelling of Iberia.

Chiasmolithus spp. have generally been considered cool-water taxa (Bukry, 1973a; Bralower, 2002; Persico & Villa, 2004; Villa, et al., 2008). However, Wei & Wise (1990a) suggested that an increase in chiasmoliths towards higher latitudes during the middle Eocene–Oligocene only applies to the group as a whole, but some of the larger species, such as *C. gigas* and *C. grandis*, are rare to absent at higher latitudes. Aubry (1998) proposed that this group was adapted to mesotrophic or eutrophic environments.

Cyclicargolithus floridanus is considered an indicator of high productivity environments, (Aubry, 1992; Monechi et al., 2000; Dunkley Jones et al., 2008, Fioroni et al., 2015). Other authors interpret it as cosmopolitan R-type taxon (Aubry, 1998; Bown et al., 2004; Honjo, 1976; Okada and Honjo, 1973).

Toweius was interpreted by Bralower (2002) to be mesotrophic because of its ability to tolerate a large variations in nutrient supply and temperature variations. Other authors have interpreted it to have a preference for cooler, mesotrophic to eutrophic conditions (Bralower, 2002; Bown et al., 2004; Gibbs et al., 2006; Agnini et al., 2007). In our samples only *T. eminens* is recorded. This species is interpreted by Self-Trail et al. (2012) as dominant in cool and mesotrophic conditions.

Zygrhablithus bijugatus is a K-strategist taxon and is considered to be adapted to oligotrophic conditions (Wei & Wise, 1990, Agnini et al., 2007, Agnini et al., 2016; Aubry, 1998; Bralower, 2002), being common in middle to outer neritic settings (Self-Trail, 2012). However, Kalb and Bralower (2012), Tremolada and Bralower (2004) and Villa et al., (2008) proposed it to have been affinity for cooler and eutrophic conditions.

Braarudosphaera is a long range taxon, associated to surface water salinity, environmental stress (Gran and Braarud, 1935; Bybell and Gartner, 1972; Bown, 2005) and neritic settings (Martini, 1967; Takayama, 1972; Tanaka, 1991, Hagino et al., 2016). Liebrand et al., (2018) consider *Braarudosphaera* as an hyperstratification indicator.

Small placoliths are often considered opportunistic r-strategist taxa (Okada, 1971), cool-water favoring eutrophic environments (Wade and Bown 2006).

Tribrachiatus is considered a warm-water and oligotrophic environment taxon, and it is often interpreted as K specialist (Haq and Lohmann, 1976; Wei and Wise, 1990; Agnini et al., 2007; Agnini et al., 2017).

Reticulofenestra dictyoda is interpreted as a mesotrophic to eutrophic indicator (Schneider et al. 2011, Shamrock and Watkins 2012; Newsam et al., 2017).

Helicosphaera is a nutrient-rich water indicator (Perch-Nielsen, 1985a; De Kaenel and Villa, 1996; Guerreiro et al., 2014, 2015) commonly associated with shallow and low salinity water (Wei and Wise, 1990; Nagymarosy, 2000).

Blackites are widespread on continental platforms, more abundant into low-medium latitudes, and seem to be tolerant to hyposaline waters (Baldi-Beke, 1984). Its acme is found in the lower Oligocene in many southern high latitude locations (Marino and Flores, 2002; Mc Gonigal and Di Stefano, 2002; Wei and Wise, 1990) suggesting its preference for cold waters. Nevertheless in literature there are still uncertainties concerning paleoecological affinity for this genus.

Dictyococcites spp. is either considered a warm (Monechi et al., 2000), warm-temperate (Wei and Wise, 1990a) or temperate genus (Villa et al., 2008; Villa and Persico, 2006; Wei et al., 1992).

Thoracosphaera spp. have been considered warm water taxa and appear to have tolerance to mesotrophic up to oligotrophic conditions (Wei and Wise, 1990).

3.4 Results

3.4.1 Calcareous nannofossil assemblage changes in the Sopelana section

The calcareous nannofossil abundance is generally high, with an average of 45 species, and the preservation varies from poor to moderate. The lowest values of richness are recorded in the 0-1 m interval, with only 41 species at the 38 cm level. The Shannon diversity index (H), varies between 3.1 to 3.6, and it shows lower values in the marls than in limestone beds. The calcareous nannofossil content consists mainly of *Coccolithus pelagicus* (15%), *Toweius eminens* (10%) and *Chiasmolithus* (10%). Among nannoliths *Discoaster* (15-20%), pentaliths (10%), and *Sphenolithus* (10%) are the most prominent. Reworked nannofossils are present in few samples and consist of rare specimens of Cretaceous and Paleocene taxa.

A variation in abundance of the whole assemblage is recorded at 1.20m, coinciding with the base of limestone bed L3 (Fig. 3.3). *Coccolithus pelagicus* shows a decrease from 15% to 8% in the interval 1.20-2 m, subsequently increasing upwards. *Chiasmolithus* shows a decrease (from 10% to 5%) in the interval 1.20-1.80 m. Pentaliths increase from 2% to 10% at 1.20 m, whereas *E. formosa* decreases from 8% to 3%. *Toweius* shows a general decreasing trend from the base to the top of the studied section, with 3 discrete intervals of abundance variation: an abrupt decrease (from 6% to 4%) at 1.20 m, a stable trend up to 2.40 m, with a further decrease (to 3%) in the last 50 cm of the studied interval. *Discoaster* shows a decreasing trend up to 1.20 m (from 17% to 10%), but subsequently increases upwards. Small placoliths, increase in abundance between 0.75-1.5m. A visible decrease of relative and absolute abundance of *Discoaster* at the eccentricity maxima (1.2m) appears correlated with the increase in small placoliths (Fig. 3.3). *Sphenolithus, Z. bijugatus, Thoracosphaera* and *Tribrachiatus* do not show a peculiar trend across the studied interval.

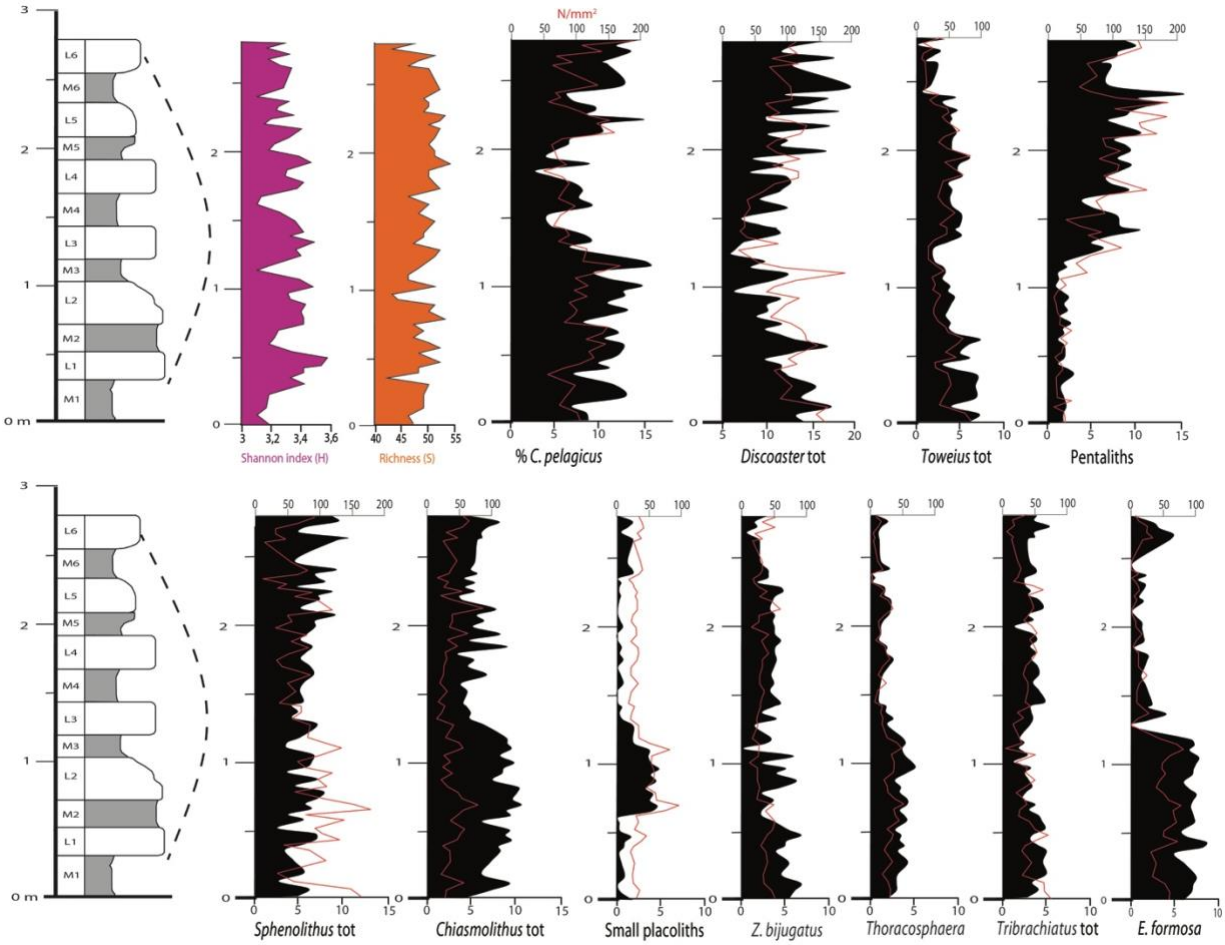

Fig. 3.3: Shannon diversity index (H), richness (S), absolute nannofossil concentration per gram (g) of sediment (red line) and relative (black curves) abundances of selected calcareous nannofossils across the eccentricity bundle 'Sb12' in the Sopelana section.

3.4.2 Calcareous nannofossils and $CaCO_3$ variations in the Sopelana section

Potential relationships between calcareous nannofossil abundances and $CaCO_3$ content were investigated along the Sopelana marl-limestone alternation (Fig. 3.4). As far as the *Discoaster* and *Toweius* are concerned, their general abundance trend vary in opposition (r^2=-0.85) to $CaCO_3$ content, which are well expressed in the whole investigated interval. *Coccolitus pelagicus* appear to be in opposition (r^2=-0.32) to $CaCO_3$ variation's pattern in the interval 1.2-2m (corresponding to maximum eccentricity, Martinez-Braceras et al., 2017). As far as pentaliths are concerned, in the interval 0-1.2m it is not possible to observe an evident correlation (r^2=0.02) with $CaCO_3$

content, maybe due to their scarce abundance, whereas in the upper portion (except for the marl beds M5 and M6) a moderate positive correlation (r^2=0.45) is observable.

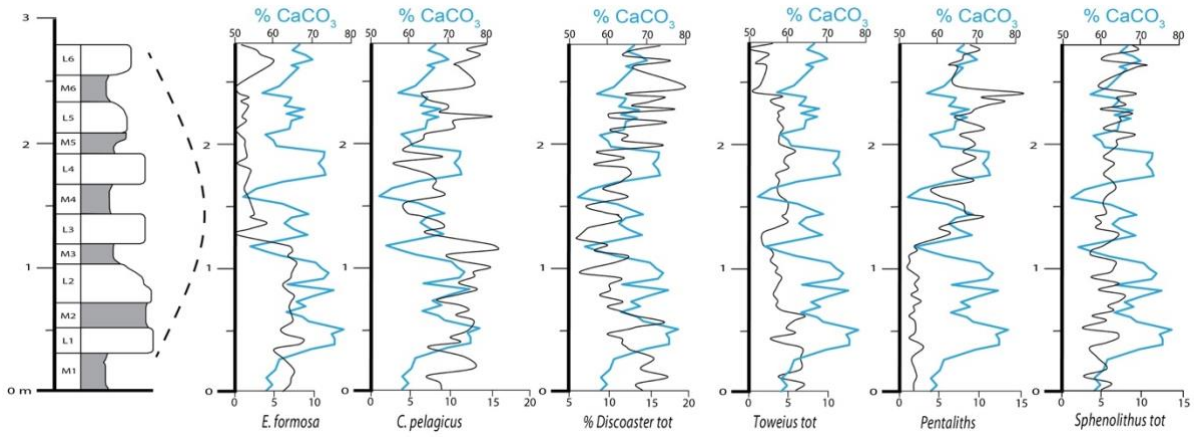

Fig. 3.4: $CaCO_3$ content (blue line) and relative abundance (black line) of selected calcareous nannofossil taxa across the eccentricity bundle 'Sb12' of the Sopelana section.

3.4.3 Calcareous nannofossils and $\delta^{13}C$ variations in the Sopelana section

A comparison between calcareous nannofossil abundance variations and isotopic $\delta^{13}C$ value (from Martinez-Braceras et al., 2017) was performed in order to deduce possible changes in the primary productivity. Few taxa correlate (either positively or negatively) with $\delta^{13}C$. *Chiasmolithus, C. pelagicus, Toweius* and pentaliths show a positive (r^2=0.75; 0.52; 0.45; 0.68 respectively) correlation with $\delta^{13}C$, well expressed in the interval 1.20-2 m (maximum eccentricity). These taxa are interpreted as meso-eutrophic (e.g., Wei & Wise, 1990a; Aubry 1998; Agnini et al, 2007; Villa et al., 2008; Self-Trail et al., 2012; Agnini et al., 2017). High values of $\delta^{13}C$ correspond to high productivity. In correspondence of the maximum eccentricity there is an increase in nutrients, as confirmed by increase in eutrophic taxa, that are also interpreted as r-selective. An increase in r-selective forms might imply an increase in productivity as highlighted by $\delta^{13}C$ value. This hypothesis seems to be sustained also by a decrease in oligotrophic taxa (*Ericsonia, Discoster* and *Sphenolithus)*, that show a negative correlation with respect to $\delta^{13}C$ across the entire studied interval (r^2=-0.54) (Fig. 3.5).

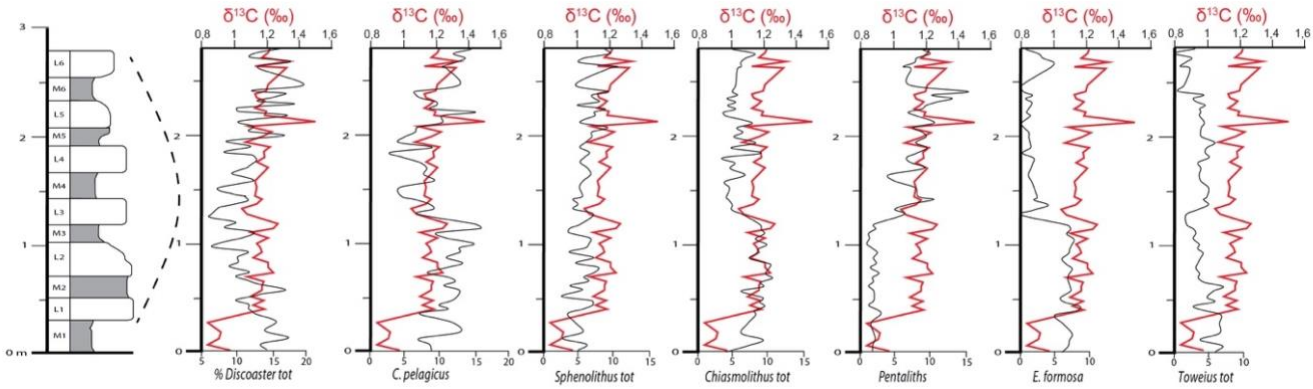

Fig. 3.5: δ ^{13}C values (red line) and relative abundance (black line) of selected calcareous nannofossil taxa across the eccentricity bundle 'Sb12' of the Sopelana section.

3.4.4 Calcareous nannofossil assemblage changes in the Oyambre section

Calcareous nannofossils are generally abundant, while preservation varies through the studied interval from medium to poor. Thirty species were identified, the lowest richness values occurring at the interval 2-4 m with a minimum value of 26 species at 3.75 m.

The Shannon diversity index varies from 2.9 to 3.2, showing the highest values in the limestone lithology; the lowest values (2.9) are recorded at 2 and 3 m in marly layers, as observed in the Sopelana section. The nannofloral content is mainly dominated by placoliths belonging to *C. pelagicus* (15%), *Cyclicargolithus floridanus* (10%) and *Reticulofenestra* (13%) are mainly composed by *R. dictyoda and R. scripssae.* Nannoliths as *B. bigelowi* (10%), *Pemma (3%), Micrantholitus (1%)* and *Zygrablithus bijugatus* (3%) are present throughout the section. *Discoaster* (6-8%) is represented mostly by *D. barbadiensis. Sphenolithus* (17%) are mainly composed by *S. moriformis* and *S. radians*. Reworking is rare and it mainly consists of Cretaceous taxa (*Micula*, *Watznaueria* and *Prediscosphaera)*.

Calcareous nannofossil assemblages show few changes throughout the studied interval (Fig. 3.6). In the interval between 1.60 and 3 meters *Ericsonia formosa* and *Discoaster* total show a decrease, whereas, *Sphenolithus* tot increase up to 18%. The absolute abundance of *E. formosa*

shows a stable pattern across the interval. A slight increase in abundance of *Chiasmolihtus* and pentaliths correlate with the maximum abundance of sphenoliths at 2m. *Reticulofenestra dictyoda* shows an increase in the interval 2.6-4m, whereas a decrease to a minimum value (3%) is recorded at 4.80m. *Coccolithus pelagicus* shows a stable abundance trend across the interval, with a slight decrease in absolute abundance at 3 m.

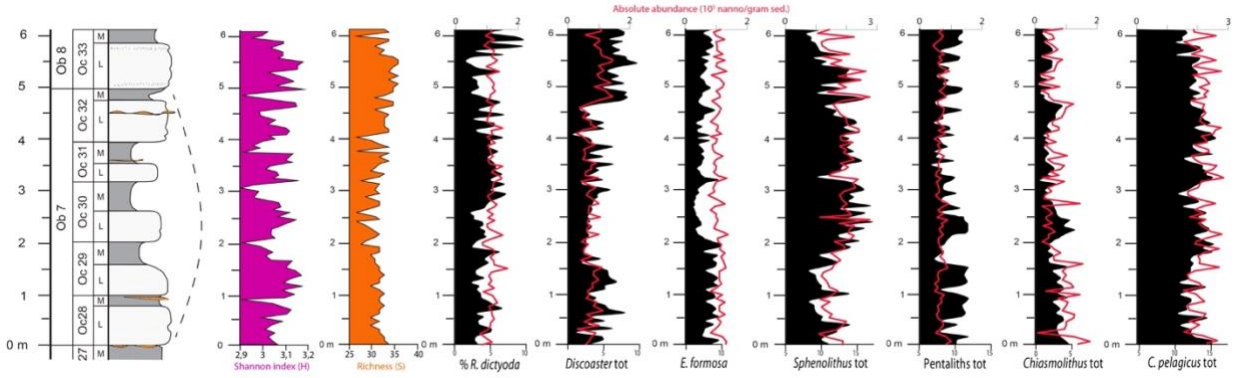

Fig. 3.6: Shannon diversity index (H), richness (S), absolute nannofossil concentration per gram (g) of sediment (red line) and relative (black plot) abundances of selected calcareous nannofossils across the eccentricity bundle 'Ob7' of the Oyambre section.

3.4.5 Calcareous nannofossils and $CaCO_3$ variations of the Oyambre section

In the studied interval of the Oyambre section, few genera show a correlation (positive or negative) with calcium carbonate content (Fig. 3.7). *Discoaster* seems to vary independently from $CaCO_3$ content, in the interval 2-2.5 m shows a decrease where $CaCO_3$ increases. *Sphenolithus*, up to 2,80 m seems to have a positively (r^2=0.39) matching trend with $CaCO_3$ content, but from 2,80 to 4 m the relationship reverses (r^2=-0.24). *Reticulofenestra dictyoda* anticorrelates with $CaCO_3$ content (r^2=-0.58), best expressed in the interval 4-6 m.

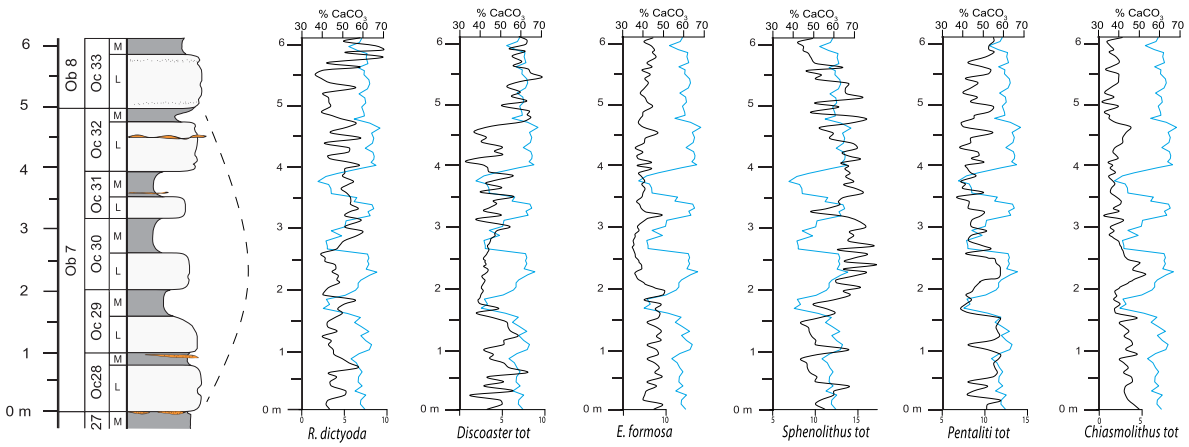

Fig. 3.7: $CaCO_3$ content (blue line) and relative abundance (black line) of selected calcareous nannofossil taxa across the eccentricity bundle 'Ob7' of the Oyambre section.

3.4.6 Calcareous nannofossils and $\delta^{13}C$ variations in the Oyambre section

A moderate negative correlation (r^2=-0.47) between *Discoaster*, *E. formosa* and $\delta^{13}C$, and a strongly positive correlation (r^2=0.82) between $\delta^{13}C$ and *Sphenolithus* and *Chiasmolithus* can be observed in the limestone at 2 m (Oc30L), and the minimum in $\delta^{13}C$ is likely correlated with the increase in the spenoliths abundance between 1.5 m and 4 m. In the marl bed at 2.5 m (Oc30M), low $\delta^{13}C$ values occur along with an increase in abundance of *Discoaster* and *R. dictyoda*. *Coccolithus pelagicus* shows an opposite trend (r^2=-0.43) with respect to $\delta^{13}C$ across the entire analyzed bundle (Fig. 3.8).

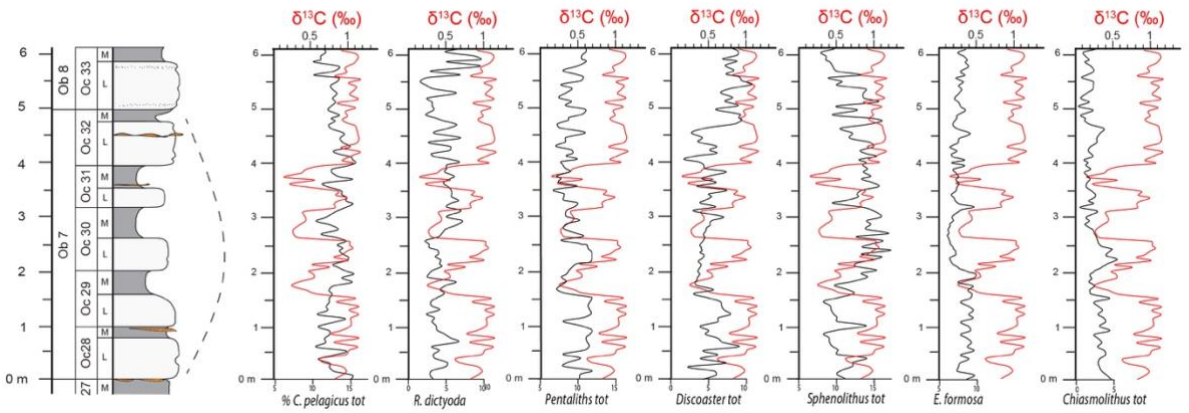

Fig. 3.8: $\delta^{13}C$ values (red line) and relative abundance (black line) of selected calcareous nannofossil taxa across the eccentricity bundle 'Ob7' of the Oyambre section.

3.4.7 Calcareous nannofossil assemblage changes in the Gorrondatxe section

Calcareous nannofossil assemblages are generally rich and preservation varies from medium to poor. An average of 39 species was observed, the highest richness value (44 species) being recorded at 2.6 m and the lowest value (34 species) at 5.2 m. The Shannon diversity index shows highly variable pattern through the studied interval, ranging between 2.7-3.1; lowest values are recorded in the interval 2-3 m in marly lithology (Fig. 3.9)..

The assemblages are dominated by *Discoaster tot* (20%), *Sphenolithus* total (10%), *Chiasmolithus tot* (10%), mainly crepresentd by *C. grandis* and *C. solitus, Girgisia gammation* (12%), *Coccolithus pelagicus* 7-10 μm (12%) and *Helicosphaera* (5%). Reworked Cretaceous and Paleogene nannofossils (5-8%) occur throughout the studied interval.

The most significant variations in the nannoflora abundance occur in the interval 1.5-3 m. *Sphenolithus tot., E. formosa* and *G. gammation* show a decrease in abundance, whereas, pentaliths, *Chiasmolithus* and *Blackites* increase (Fig. 3.9). *Discoaster* tot show a decrease from the lower part of the studied interval (23%) to a minimum value at 1.80m (12%), an increase in the interval 2.20-3.9 m (maximum value 19%), whereas in the upper part of the studied interval it shows a high frequency variation in abundance. *Chiasmolithus* shows a roughly stable abundance from the base up to 5 m where an abrupt decrease has been observed (minimum value at 6.3 m of 3%). *Coccolithus pelagicus* (7-10μm) does not vary significantly throughout the studied interval. *Sphenolithus* displays a stable distribution attested at 10% on average in the interval 0-6 m, with an increase in abundance up to 20% in the interval 6-7 m.

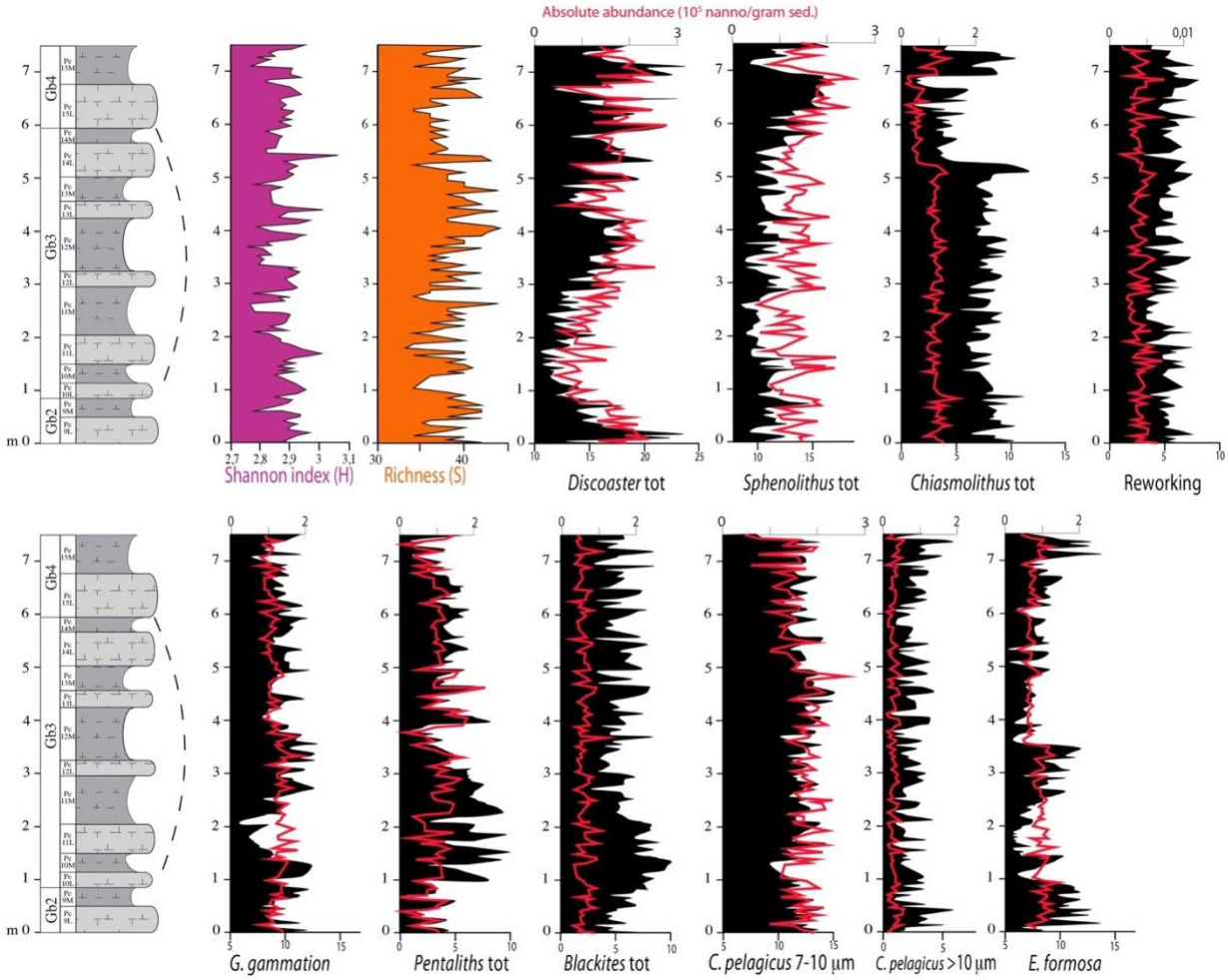

Fig. 3.9: Shannon diversity index (H), richness (S), absolute nannofossil concentration per gram (g) of sediment (red line) and relative (black plot) abundances of selected calcareous nannofossils across the eccentricity bundle 'Gb3' of the Gorrondatxe section.

3.4.8 Calcareous nannofossils and $CaCO_3$ variations in the Gorrondatxe section

A positive correlation (r^2=0.73) between *Discaster* abundance and $CaCO_3$ content characterizes the interval 0-6m, whereas a negative correlation (r^2=-0.49) can be observed from 6 m up to the top of the section. *Sphenolithus* and *Blackites* show a strongly positive correlation (r^2=0.95) with $CaCO_3$ content. *Ericsonia* shows a moderate positive correlation (r^2=0.53) with $CaCO_3$ content up to 2 m, but above this level it shows a strongly negative correlation (r^2=-0.86). *Chiasmolithus* and pentaliths have a moderate negative correlation (r^2=-0.58) with $CaCO_3$ content (Fig. 3.10).

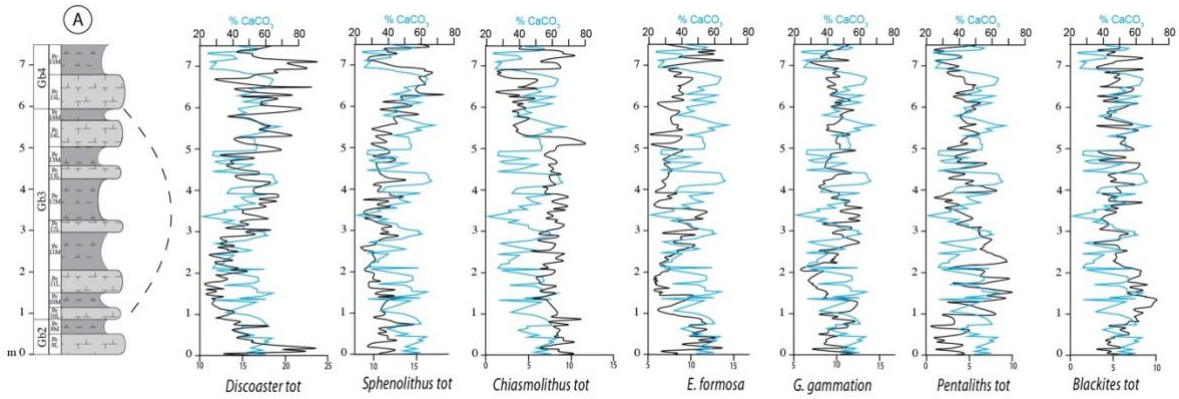

Fig. 3.10: $CaCO_3$ content (blue line) and relative abundance (black line) of selected calcareous nannofossil taxa across the eccentricity bundle 'Gb7' of the Gorrondatxe section.

3.4.9 Calcareous nannofossils and δ ^{13}C variations in the Gorrondatxe section

No clear correlation between $\delta^{13}C$ and nannofossil abundances was observed. However, some taxa (*Discoaster, E. formosa, G. gammation)* seem to have a negative correlation (r^2=-0.41; -0.53; -0.29) with the carbon isotope record (Fig. 3.11).

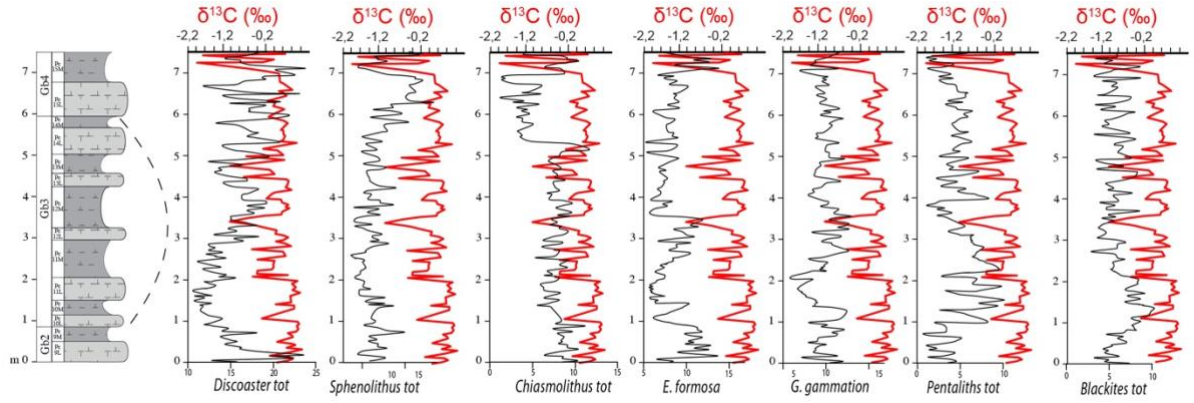

Fig. 3.11: δ ^{13}C results (red line) and relative abundance (black line) of selected calcareous nannofossil taxa across the eccentricity bundle 'Gb3' of the Gorrondatxe section.

3.5 Interpretation and Discussion

3.5.1 Cluster analysis in the Sopelana section

Cluster analysis was applied to the 11 selected species, namely *Ericsonia*, pentaliths, C*. pelagicus, Discoaster, Sphenolithus, Tribrachiatus, Chiasmolithus,* Small placoliths*, Toweius,*

Thoracosphaera, Z. bijugatus. In order to define ecological assemblages, cluster analysis was performed using paired group as algorithm and Rho as similarity measure. It was used to define the ecological assemblages. Three groups of taxa can be identified at different levels (Fig. 3.12).

Group A (*Discoaster, Sphenolithus, Ericsonia, Tribrachiatus* and *Z. bijugatus*) is composed of species with ecological preference for warm water and oligotrophic conditions.

Group B (pentaliths, *Thoracosphaera, C. pelagicus* and *Toweius*) is characterized by species that are considered to be adapted to temperate water and meso-eutrophic conditions.

Group C (Small placoliths and *Chiasmolithus)* is composed of taxa living into cooler waters with affinity for more eutrophic conditions.

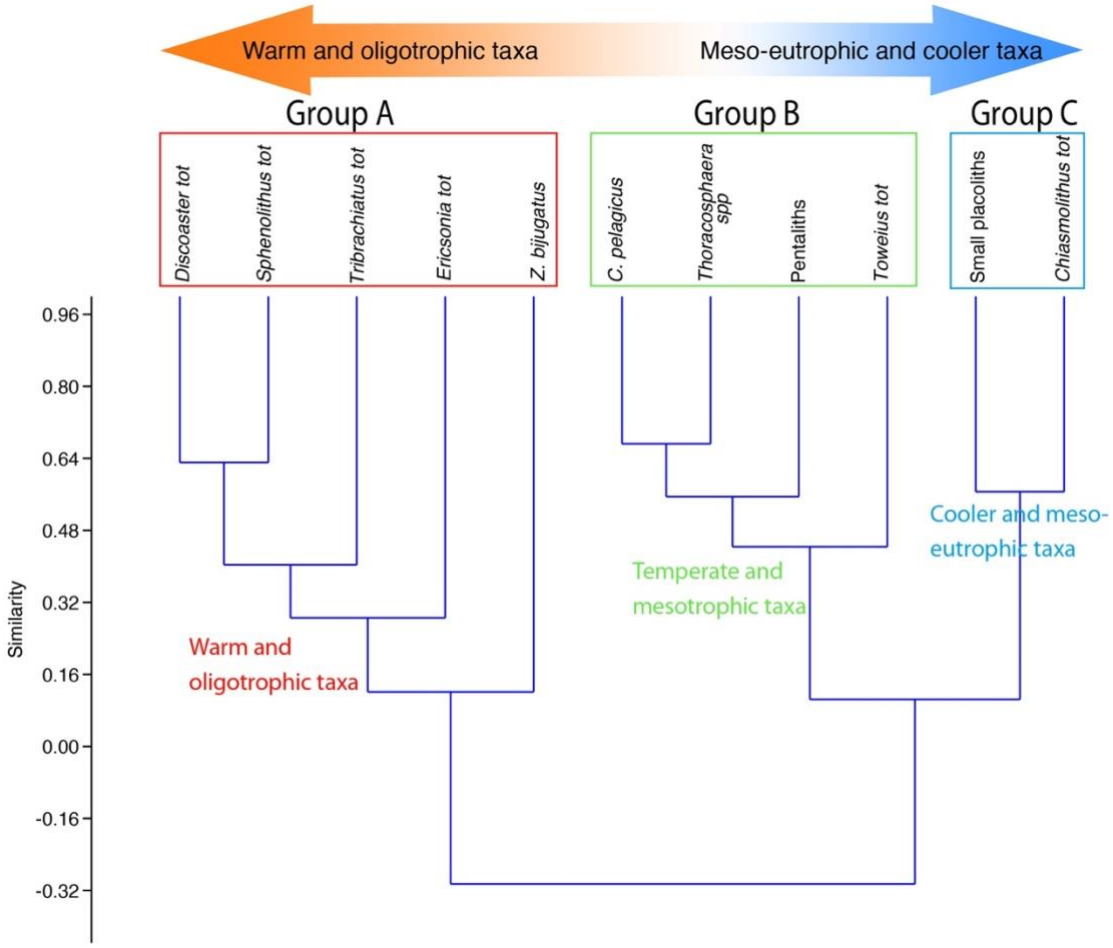

Fig. 3.12: Ecological clusters of nannofossil assemblages from the studied interval in the Sopelana section. A cluster analysis (paired group as algorithm, Rho as similarity measure) was used to define ecological assemblages. The potential affinity of each cluster, from warm to the cool water environments, is indicated.

3.5.2 Principal Component Analysis (PCA) in the Sopelana section

The PCA analysis was performed on the same data-set used for cluster analysis. This indicates that PC1 (65.4 %) and PC2 (14.1 %) together account for 79.5% of the variance in the data set. The PCA graph shows that nannofossil assemblages can be subdivided into three subgroups (Fig. 3.13a). The three populations of taxa are distinguished because of their different positions along the x axis (PC1) and y axis (PC2). Each of these three populations would suggests a homogeneous group in term of ecological-trophic characteristics. The first population, placed on positive values of PC2 and positive value of PC1 is composed of taxa with affinity for temperate water and mesotrophic condition (*Toweius*, pentaliths and *Thoracosphaera*). The second cluster placed in negative values of PC1 and positive values of PC2, is composed of taxa with affinity for cooler water and eutrophic conditions (small placoliths and *Chiasmolithus*). The third population, placed on positive values of PC1 and negative values of PC2, is composed of taxa with affinity for warm water and oligotrophic environments (*Discoaster, Ericsonia, Sphenolithus* and *Tribrachiatus*). Thus, the PCA factor analysis, according to the ecological affinities of the taxa, suggests that the main factors controlling the nannofossil assemblages of the Sopelana section were temperature (PC1) and nutrient availability (PC2). According to our interpretation of PC1 and PC2, *C. pelagicus* is considered a mesotrophic and temperate taxon. This ecological attribution appears to be in agreement with literature data for the Eocene period at middle latitudes (Wei & Wise, 1990a; Monechi et al., 2000; Agnini et al., 2007).

The PCA analysis was also performed on R-mode (Fig. 3.13b). A distinct subdivision of 2 groups reflecting the cluster of sample arrangement is noticeable. One group, including samples collected in limestone beds, is mainly located in the fourth quadrant, few samples extending onto the y axis and the first quadrant. The other group, composed of samples from marl beds, is mainly constrained to the second quadrant. This means that marls were formed at high nutrient and low

temperature conditions, whereas limestones were deposited under warmer and meso-oligotrophic conditions.

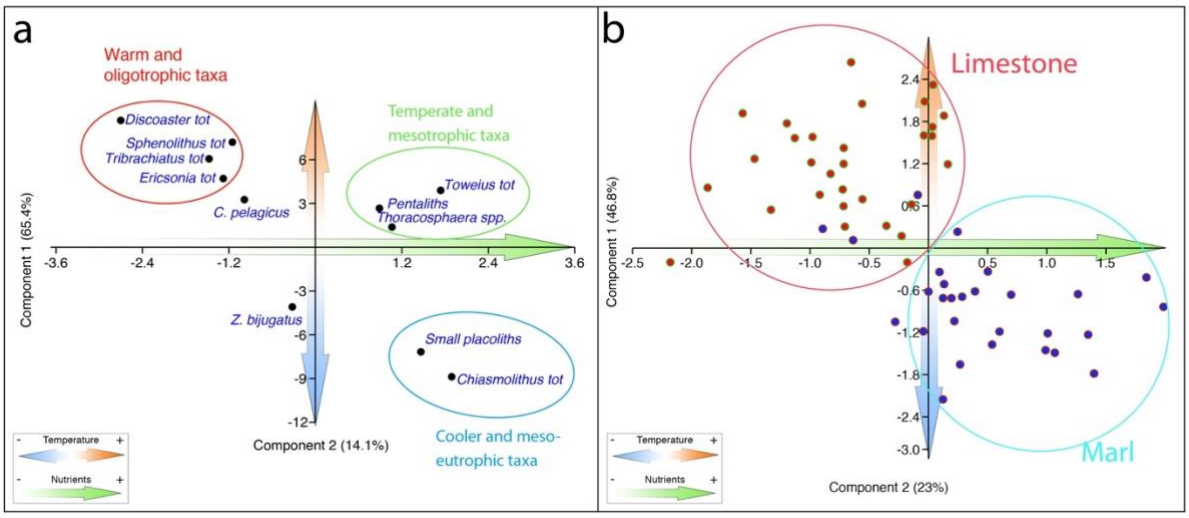

Fig. 3.13: Principal component analysis (PCA) scatter plot of log-centered data of calcareous nannofossil taxa (a) and samples (marl in blue, limestone in red) (b) from the Sopelana eccentricity bundle 'Sb12' in terms of the first and second components. (Lithological sample identification is based on Martinez-Braceras et al., 2017)

In summary, the calcareous nannofossil assemblages of the Sopelana section seem to correlate with $CaCO_3$ content and some taxa (*Chiasmolithus, C. pelagicus, Toweius* and pentaliths) seem that may furnish information about productivity. Maximum eccentricity conditions can be recognized correspond to couplets where sharp contrast in $CaCO_3$ content occurs (Martinez-Braceras et al., 2017). At maximum eccentricity seasonality reaches both maximum values (during half of a precession cycle, when summer occurs at perihelion) and minimum values (during the other half of the precession cycle, when summer occurs at aphelion). Maximum seasonality increases terrestrial runoff during half of a precession cycle, but minimum seasonality would lead to stable conditions during the other half of the precession cycle. These changes are supported by a decrease of *Discoaster, Ericsonia,* warm temperate and oligotrophic taxa and an increase of *Toweius* and pentaliths adapted to mesotrophic conditions.

The depositional model proposed by Martìnez-Braceras et al. (2017) for this section suggests that limestones were formed during period of high pelagic carbonate productivity during warm water conditions and slow circulation, linked to periods of low seasonality (summers at aphelion); conversely, marls accumulated when pelagic carbonate productivity decreased during periods with cooler waters and active circulation, linked to high seasonality (summers at perihelion). *Toweius*, a meso-eutrophic and cooler water taxa, shows an increase in limestone semi-couplets during the maximum eccentricity, whereas *Discoaster, (*warm and oligotrophic taxa), has a decrease in limestone semi-couplets at the maximum eccentricity. The differentiation of taxa in the two lithologies, recorded at the maximum of eccentricity, supports the model indicating that marls deposited during maximum eccentricity reflect periods of eutrophication, while limestones reflect oligotrophic phases.

This interpretation seems to be confirmed by the PCA analysis (Fig. 3.13b), which shows that marls were deposited during periods with higher nutrients (meso-eutrophic) and with lower temperature, whereas limestones were formed in periods with higher temperatures and with a lower nutrients supply.

3.5.3 Cluster analysis in the Oyambre section

The cluster analysis was applied to 14 selected species namely *C. floridanus*, *E. formosa,* pentaliths*, C. pelagicus* <7 μm, 7-10μm and >10μm (these distinctions were done following the literature and considering that *C. pelagicus* changes its paleoecology according to different body-size; see section 3.3.2), *D. scrippsae, R. dictyoda, Discoaster, Sphenolithus, Blackites*. To this end, different methodologies and distance measures among variables can be used. In order to define ecological assemblages, the cluster analysis was performed using paired group as algorithm and Rho as similarity measure. As a result, different groups of taxa at different similarity levels could be identified (Fig. 3.14).

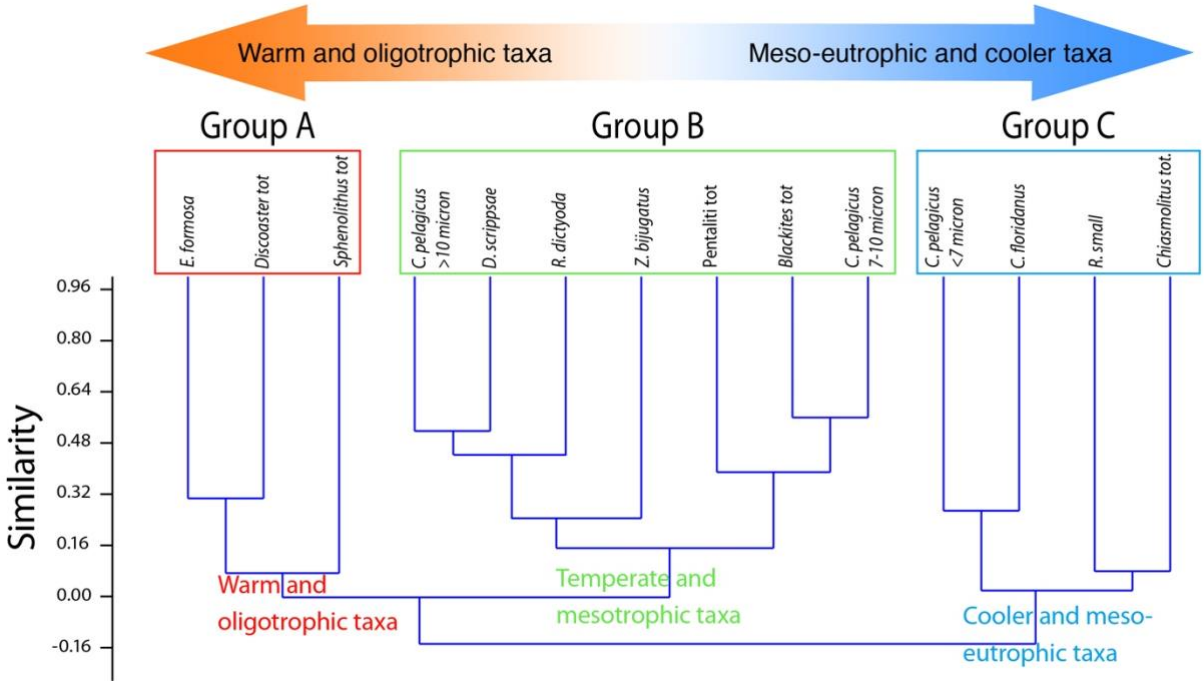

Fig. 3.14: Ecological clusters of nannofossil assemblages from the studied interval in the Oyambre section. A cluster analysis (paired groups as algorithm, Rho as similarity measure) was used to define the ecological assemblages. The potential affinity of each cluster, from the water warm to the cool water environments, is indicated.

Group A (*Discoaster* total*, E. formosa* and *Sphenolithus* total*)* is composed of species with ecological preference for warm water and oligotrophic environment.

Group B (*D. scrippsae, R. dictyoda,* pentaliths*, C. pelagicus* >10μm and 7-10μm, *Blackites* and *Z. bijugatus*) is characterized by species that are the main component of the nannoflora at the Oyambre section, which are considered to be adapted to mesotrophic environments under temperate water conditions.

Group C (*C. floridanus, C. pelagicus* <7 μm, *Reticulofenestra* small and *Chiasmolithus*) is composed of taxa living into cooler waters and high nutrient conditions.

3.5.4 Principal Component Analysis (PCA) in the Oyambre section

The PCA analysis was performed with the same data-set used for cluster analysis. This indicates that PC1 (87.1%) and PC2 (4.3%) together account for 91.4% of the variance in the data set. The PCA graph shows that nannofossil assemblages can be subdivided into three clusters (Fig. 3.15a). Each of the three populations constitutes a homogeneous group in terms of ecological-trophic characteristics. The first population, placed at high values of PC1 and in the range between -1 and -0.6 in PC2, is composed of taxa with affinity for warm water and oligotrophic conditions (*Discoaster* and *E. formosa*). The second population is the largest; it is composed of temperate and meso-oligotrophic taxa (*D. scrippsae, R. dictyoda,* pentaliths*, C. pelagicus >10 μm and 7-10 μm, Blackites* and *Z. bijugatus*). The third population, with high values of PC2 and negative values of PC1, is composed of eutrophic taxa living in cooler waters (*C. floridanus, C. pelagicus* <7 μm, R. small and *Chiasmolithus*). Thus, the PCA analysis strongly suggests that the main factors controlling the upper Lutetian calcareous nannofossil assemblages of the Oyambre section were temperature (PC1) and nutrient availability (PC2). Based on the interpretation of PC1 and PC2, *Sphenolithus* turns out to be a taxon of warm waters but with a greater availability of nutrients.

The PCA analysis was also performed on R-mode (Fig. 3.15b). A distinct subdivision of 2 groups reflecting the cluster of sample arrangement is noticeable. One group, including samples collected in limestone layers, is located in the fourth quadrant, few samples extending onto the y axis and into the first quadrant. The other group, composed of samples from marl beds, is largely restricted to the second quadrant. The distribution pattern of the limestone and marls samples with respect to PC1 and PC2 suggests that marl deposition was related to periods with high nutrient input and cooler water, whereas deposition of limestones occurred under warmer and mesotrophic conditions.

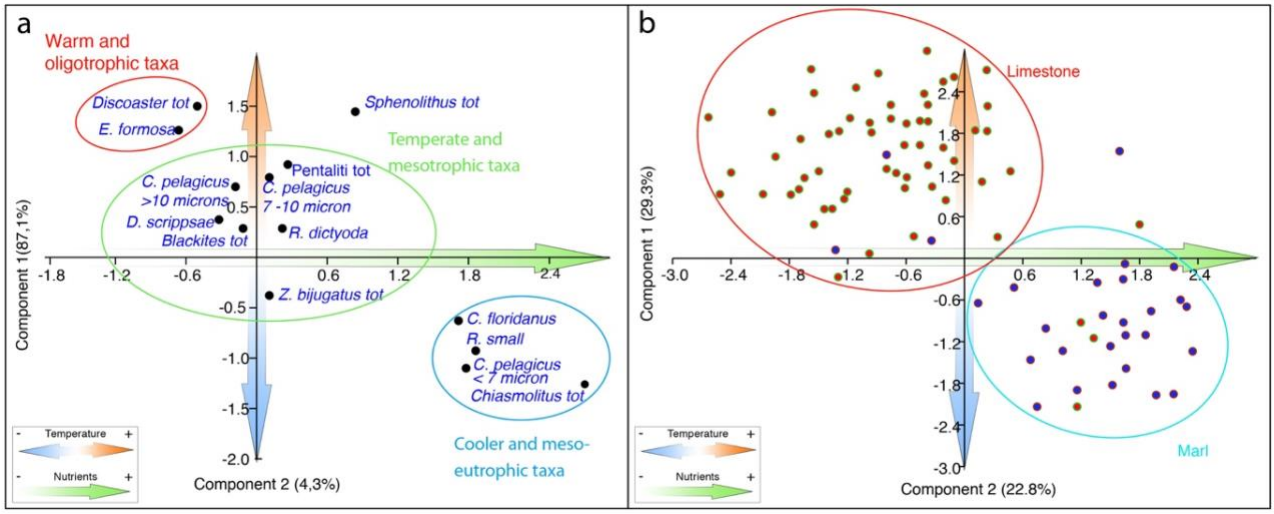

Fig. 3.15: Principal component analysis (PCA) scatter plot of log-centered data of calcareous nannofossil taxa (a) and samples (b) from the Oyambre eccentricity bundle Ob7 in terms of the first and second components.

In summary, for the Oyambre section the major calcareous nannofossil changes seem to be related to couplets 'Oc29', 'Oc30' and 'Oc31' (1-4 m), which are considered to represent maximum eccentricity conditions (Martinez-Braceras et al., 2017). This interval is characterized by a decrease in warm-temperate oligotrophic (stratified water) taxa, such as *Discoaster* and *Ericsonia* and *R. dictyoda*, and a slight increase in pentalits and *Chiasmolitus*, respectively low salinity and cool-eutrophic taxa. The abundance of *Sphenolithus* also increases at maximum of eccentricity, together with eutrophic taxa; this supports the results of the PCA analysis, which suggest that *Sphenolithus* probably has an affinity for warm and meso-eutrophic environments. The ecological attribution of *Sphenolithus* has been extensively discussed in the literature, Wade and Bown (2006) and Dunkley Jones et al. (2008) supporting the Oyambre interpretation. In agreement with this interpretation, the comparison between $\delta^{13}C$ values and calcareous nannofossil abundance indicates a positive correlation between isotopic values and *Sphenolithus* abundance. Considering that high $\delta^{13}C$ values may indicate high productivity, this correlation implies that *Sphenolithus* might be a meso-eutrophic taxon.

The model proposed by Martínez-Braceras et al. (2017) suggested that limestones were formed during periods of high carbonate production whereas marls were formed when carbonate production decreased as a consequence of increased continental run-off and reduced seawater salinity. However, the PCA analysis of the calcareous nannofossil assemblages imply that, even in an environmental setting close to the coast, such as Oyambre, nutrients and temperature are the main parameters that influence nannoflora assemblages and the deposition of marls and limestones.

3.5.5 Cluster analysis in the Gorrondatxe section

The cluster analysis was performed on 13 groups of taxa, namely *Chiasmolithus* tot*, C. pelagicus* (7-10 μm and >10 μm), *R. dictyoda, Blackites, Helicosphaera,* pentalits*, Ericsonia, Discoaster, Sphenolithus, G. gammation, Z. bijugatus.* Reworked taxa were also taken into account due to their abundances in all samples. Three distinctive clusters of taxa at different similarity levels were recognized (Fig. 3.16).

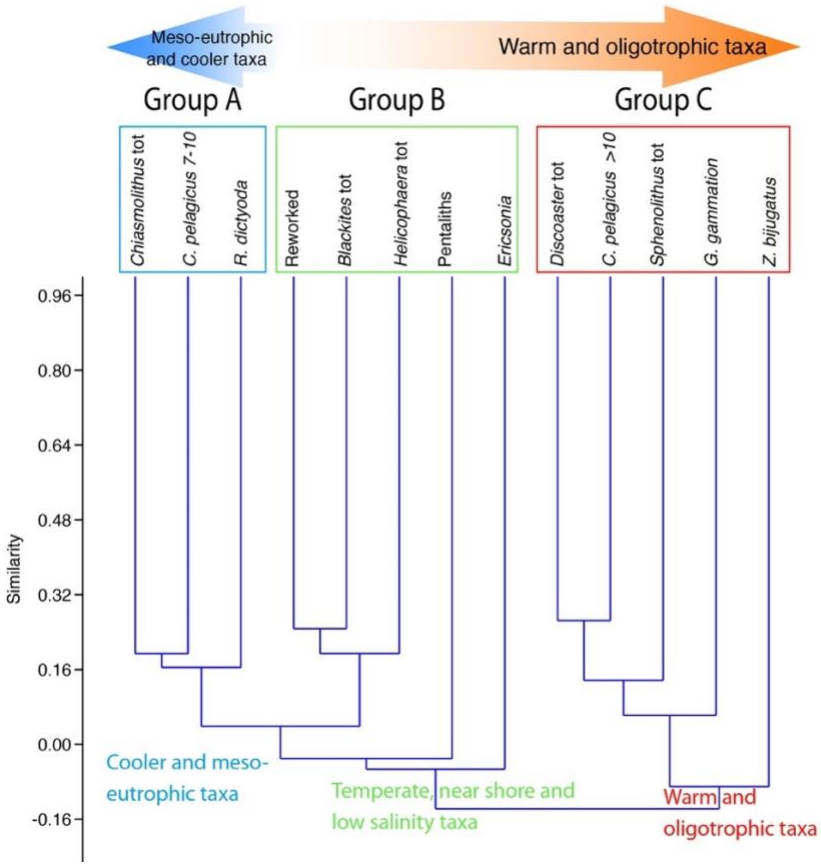

Fig. 3.15: Cluster analysis from the log-ratio transformation data of the Gorrondatxe calcareous nannofossil data. A cluster analysis (paired groups as algorithm, Rho as similarity measure) was used to define the ecological assemblages.

Group A (*Chiasmolithus, C. pelagicus* 7-10 μm and *R. dictyoda*) group species thriving in cooler and meso-eutrophic environments.

Group B (*Blackites, Helicosphaera*, pentaliths, *Ericsonia* and reworked taxa*)* includes taxa with affinity to low salinity, near shore environments and mesotrophic environments. Interesting is the presence of reworking in the group with near shore taxa that may suggest that reworking is more abundant in an environment closer to the continent. It is interesting the presence of *Ericsonia* within this group. No information about affinity to low salinity are reported in literature for this taxon. It presence in group B might be tentatively explained considering the nutrients. It is possible that *Ericsonia* has an affinity to slightly higher nutrient values than group C, leading the cluster analysis to include it with taxa belonging to group B.

Groups C (*Discoaster, C. pelagicus* >10 μm, *Sphenolithus, G. gammation, Z. bijugatus*) is composed of species with ecological preference for warm waters and oligotrophic conditions.

3.5.6 Principal Component Analysis (PCA) in the Gorrondatxe section

The PCA analysis shows that PC1 contains 83.7% of the information about the examined calcareous nannofossil assemblages, whereas PC2 accounts for 5%. The PCA graph shows that the calcareous nannofossil assemblages can be subdivided into three clusters (Fig. 3.17).

Each of these three populations is composed of an homogeneous group in terms of ecological and trophic affinities. The first population, placed on positive values of PC1 and negative values of PC2, is composed of taxa with affinity for cool waters and meso-eutrophic conditions (*Chiasmolithus, C. pelagicus* 7-10 and *R. dictyoda*). The second cluster, placed in very negative values of PC2 and positive values of PC1, is composed by near shore taxa with affinity to hyposaline and cooler water (*Helicosphaera, Blackites* and pentaliths). Also the Reworking is within the cluster, thus suggesting that it has affinity with near-coast environment. Reworked taxa are also grouped within this cluster, thus suggesting their affinity for coastal environments. The third population has negative values of PC1 and the values of PC2 range from -4 up to 2, being composed of taxa with affinity for warm and oligotrophic waters (*Discoaster, C. pelagicus* >10, *Sphenolithus, Ericsonia, G. gammation* and *Z. bijugatus).* Thus, the PCA factor analysis suggests that the main factors controlling the upper Ypresian nannofossil assemblages of the Gorrondatxe section might be the nutrients (PC1) and the temperature (PC2).

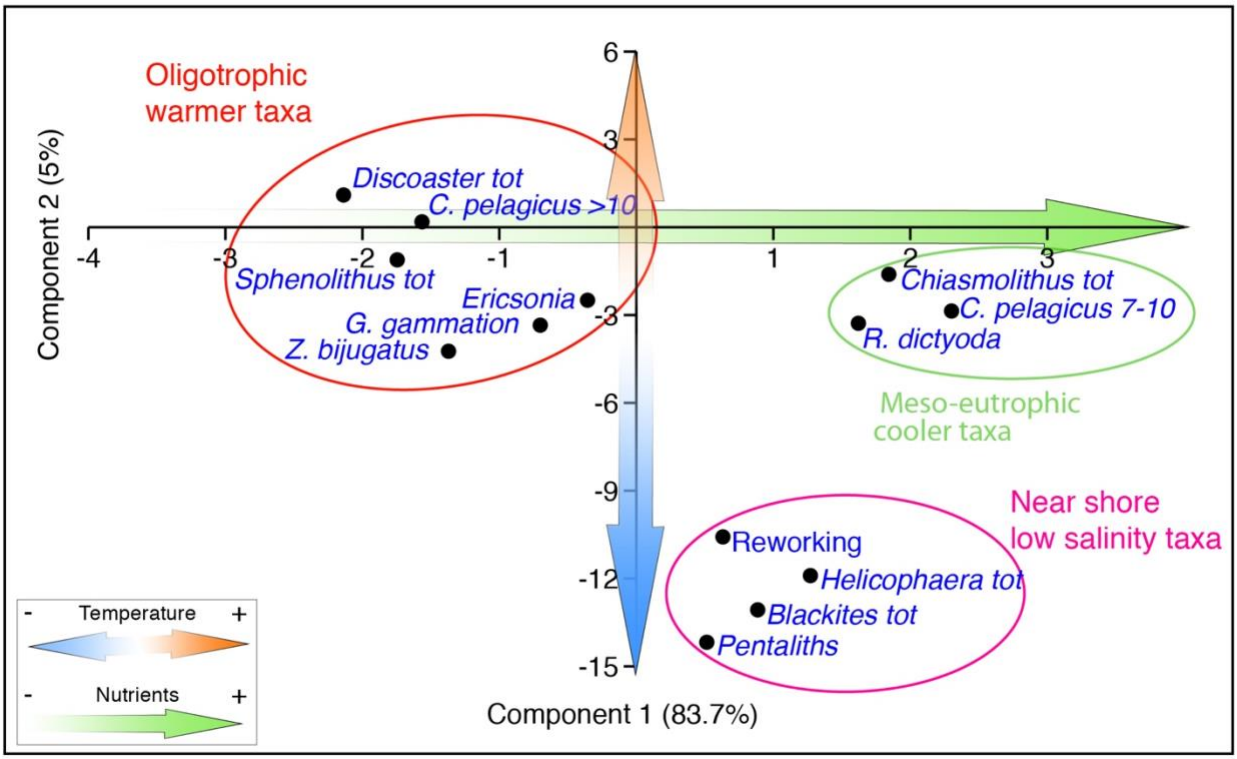

Fig. 3.17: Principal component analysis (PCA) scatter plot of log-centered data of calcareous nannofossil taxa from the Gorrondatxe eccentricity bundle 'Eb3' in terms of the first and second components.

The PCA analysis was also presented on R-mode (Fig. 3.18a/b). PC1 accounts for 27.4% of the information and PC2 for 21.6%. Given that the combination of PC1 and PC2 accounts for only 49%, PC3 with 15.2% of the information was also considered, thus obtaining 76% of the information regarding the Gorrondatxe dataset. Considering PC1 and PC2 (Fig. 3.18a), two separate clusters can be observed. The samples of marl beds are separated from limestone samples, implying that dominant environmental parameters reversed during the sedimentation of marl and limestones beds. Marls beds, according to the sedimentation model proposed by Martinez-Braceras et al. (2017) reflect an increase of continental sediment input (i.e involving an increase in nutrient and fresh water input). Consequently, it can be assumed that PC1 is regulated by nutrients and PC2 by temperature. Our interpretation, based on distribution of calcareous nannofossil assemblages into the two lithologies (marls and limestones), indicate that marls

formed under meso-eutrophic conditions with low temperature water. On the other hand, limestones, placed on a negative values of PC1, reflect a decrease in nutrients (oligotrophic environments). No clear interpretation can be inferred from the PC2 component (temperature) for the formation of limestones beds. In order to have more information on the ecological factors that controlled the environment during the deposition of limestones and marls, PC1 was plotted versus PC3 (Fig. 3.18b). In this case, the limestone and marl samples are clearly separated. Marl beds were formed in periods of higher nutrient availability and lower value of PC3 than in limestones beds. Therefore, PC3 component might reflect salinity variations. According to this interpretation, the marl beds of the Gorrondatxe section were formed in periods with lower temperatures, higher nutrient supply and lower salinity

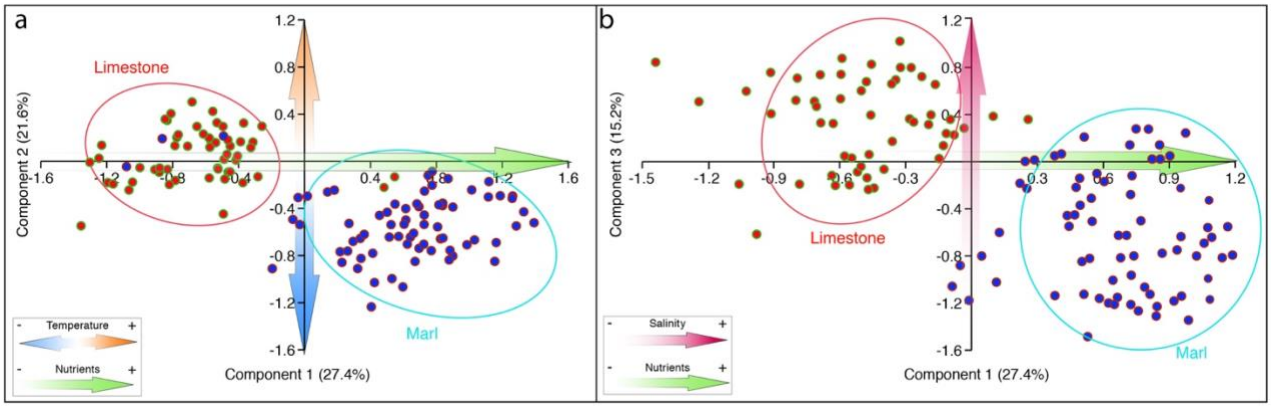

Fig. 3.18: Principal component analysis (PCA) scatter plots (R mode) of samples from the Gorrondatxe eccentricity bundle 'Eb3' in terms of PC1 versus PC2 (a) and PC1 versus PC3 (b).

Interpretation of the calcareous nannofossil changes in the Gorrondatxe section is not straightforward. This section contains a large number of turbidites intercalated in the hemipelagic succession, which may have distorted and sometimes obscured the primary pelagic sedimentary signal. The sedimentological model proposed by Martinez-Braceras et al. (2017) indicates that the mid-bundle couplets were related to high-amplitude oscillations in geochemical parameters reflect maximum eccentricity. In a few species, a link between calcareous nannofossils and maximum or minimum of eccentricity (couplets 'Gc11' and 'Gc12')

has been observed. *Ericsonia* and *Sphenolithus*, interpreted as meso-oligotrophic and warm-water taxa, decrease at maximum eccentricity. This aspect is confirmed by the correlation between $\delta^{13}C$ values and calcareous nannofossil abundance, which shows a decrease of oligotrophic taxa with high $\delta^{13}C$ values. High values of this proxy (associated with high productivity) are recorded at maximum eccentricity, in correspondence of which oligotrophic taxa decrease, implying therefore high productivity. Pentaliths, usually associated with low salinity, near-shore and highly stressed environments (Thierstein, 1981; Thomas et al., 2018) show a slight increase at maximum eccentricity.

Overall, the Gorrondatxe data suggest that the main parameters influencing calcareous nannofossil assemblages were nutrients, salinity and temperature. Our analyses confirm the model proposed by Martinez-Braceras et al., (2017), although they suggested that, in a section where turbiditic supplies were high, the impact of orbitally driven palaeoenvironmental changes on nannoflora may have be partially obscured.

3.6 Conclusions

The analysis of calcareous nannofossil abundance in the Sopelana, Oyambre and Gorrondatxe sections, implemented with statistical analysis (Principal Component Analysis and Cluster), generally confirms the previous sedimentological models proposed by Martinez-Braceras et al. (2017), but adds new palaeoenvironmental information on the processes affecting deep-sea sedimentary environments of the Basque Cantabrian Basin in Eocene times.

Larger $\%CaCO_3$ oscillations in the central couplets of bundle 'Sb12'in the Sopelana section, starved deep-sea basin, referred to as maximum eccentricity by Martinez-Braceras et al. (2017), correspond to the largest calcareous nannofossil assemblage variations. Maximum eccentricity caused a decrease in oligotrophic and stable environment taxa (E. *formosa* and *Discoaster*) in correspondence along with it is possible to observe an increase in eutrophic (*Toweius*) and low

salinity taxa (pentaliths). These observations confirm that maximum eccentricity produced maximum seasonality, which regulated the mixing of seawater layers and determined the presence of more eutrophic waters.

In the Oyambre sections, upper slope, the proposed model indicates that at maximum eccentricity, during maximum seasonality, salinity decreased and nutrient input increased as a consequence of increased continental runoff. This model is confirmed by a decrease, in limy hemicouplets in taxa that thrived in oligotrophic, stable and warm-water environments *(Discoaster* and *E. formosa)* and an increase, in marly hemicouplets, in eutrophic (*Chiasmolithus*) and low salinity (pentaliths) taxa at maximum eccentricity.

In the Gorrondatxe section, submarine fan fringe, the calcareous nannofossils data suggest a more complex environment controlled by three parameters. Marls testify to lower salinity, lower temperatures and higher nutrient availability, whereas limestones beds were formed when temperatures were higher, nutrient availability reduced and water had normal marine salinity. The previously proposed model (Martinez-Braceras et al., 2017) for this section indicated that the main control on sedimentation was related to terrigenous input linked to the intensity of continental rainfall and runoff, which were amplified at maximum eccentricity in the marly hemicouplets. The increase in continental supplies induced eutrophication and lower salinity of marine water. This is confirmed by the calcareous nannoflora results, which show an increase in eutrophic, low salinity and near shore taxa (*Chiasmolithus* and pentaliths, *Blackites*) in correspondence with maximum eccentricity. A decrease in taxa attributed to meso-oligotrophic (*Sphenolithus, E. formosa* and *G. gammati*on) and adapted to stable environments (*Discoaster*) is also recorded at maximum eccentricity. Overall, the present study demonstrates that orbitally driven climate and environmental change was recorded by calcareous nannofossil communities, during early-middle Eocene times, in different ways according to different paleoenvironmental settings.

Acknowledgements

This study is part of the PhD thesis of the first author (GF), who is funded by a doctoral grant of the University of Florence and by the Erasmus+ programme of the European Commission. The participation of NMB, AP, GB and SM was funded by the Spanish Government project CGL2015-65404-R (MINECO/FEDER, EU) and by the Basque Government project IT-930-16. NM-B received pre-doctoral grants from the Basque Government.

References

Ábalos, B. (2016). Geologic map of the Basque-Cantabrian Basin and a new tectonic interpretation of the Basque Arc. International Journal of Earth Sciences, 105(8), 2327-2354.

Agnini, C., Fornaciari, E., Raffi, I., Catanzariti, R., Pälike, H., Backman, J., Rio, D., (2014). Biozonation and biochronology of Paleogene calcareous nannofossils from low and middle latitudes. Newsletters on Stratigraphy, 47 (2), 131-181.

Agnini, C., Fornaciari, E., Rio, D., Tateo, F., Backman, J., & Giusberti, L. (2007). Responses of calcareous nannofossil assemblages, mineralogy and geochemistry to the environmental perturbations across the Paleocene/Eocene boundary in the Venetian Pre-Alps. Marine Micropaleontology, 63(1–2), 19–38, doi: 10.1016/j.marmicro.2006.10.002.

Aubry, M.P., (1992). Paleogene Calcareous nannofossils from the Kerguesen Plateau, Leg 120. In: Wise Jr., S.W., Schlich, R., et al. (Eds.), Proc. ODP. Sci. Results, vol. 120, pp. 471–491.

Baldi-Beke, M., (1984), The nannoplankton of the Transdanubian Paleogene formations. Geologica Hungarica, Palaeontologica, Budapest. v. 43, 307 pp.

Balestra, B., Ziveri, P., Monechi, S., & Troelstra, S. (2004). Coccolithophores from the Southeast Greenland Margin (Northern North Atlantic): Production, ecology and the surface sediment record. Micropaleontology, 50(1), 23–34.

Berrocoso, Á. J., Elorza, J., & MacLeod, K. G. (2013). Proximate environmental forcing in fine scale geochemical records of calcareous couplets (Upper Cretaceous and Palaeocene of the Basque-Cantabrian Basin, eastern North Atlantic). Sedimentary Geology, 284, 76-90.

Boulila, S., De Rafaelis, M., Hinnov, L. A., Gardin, S., Galdrun, B., Collin, P. (2010): Orbitally forced climate and sea-level changes in the Paleoceanic Tethyan domain (marl-limestone alternations, Lower Kimmerifgian, SE FRance). Palaeogeogr. Palaeoclimatol. Palaeoecol., 292, 57–70.

Bown, P. R. (2005), Paleogene calcareous nannfossils from the Kliwa and Lindi areas of coastal Tanzania (Tanzania Drilling Project 2003–4),J. Nannoplankton Res., 27,21–95.

Bown, P. R., Lees, J. A., & Young, J. R. (2004). Calcareous nannoplankton evolution and diversity through time. In Thierstein, H. R., & Young, J. R. (Eds.), Coccolithophores: From Molecular Processes to Global Impact (pp. 481–508). Berlin: Springer-Verlag.

Bralower, T. J. (2002). Evidence of surface water oligotrophy during the Paleocene-Eocene thermal maximum: Nannofossil assemblage data from Ocean Drilling Program Site 690, Maud Rise, Weddell Sea. Paleoceanography, 17(2), 13-1–13-12, doi: 10.1029/2001pa000662.

Bukry, D. (1973). Coccolith and silicoflagellate biostratigraphy, Tasman Sea and southwest Pacific Ocean, Deep Sea Drilling Project Leg 21. In Burns, R. E., Andrews, J. E., et al., Initial Reports of the Deep Sea Drilling Project (Vol. 21, pp. 885–893). Washington, DC: US Government Printing Office.

Bybell, L.M., Gartner, S., 1972. Provincialism among mid-Eocene calcareous nannofossils. Micropaleontology 18, 319–336. http://dx.doi.org/10.2307/1485011

Cachão, M. & Moita, M.T. (2000). Coccolithus pelagicus, a productivity proxy related to moderate fronts off Western Iberia. Marine Micropaleontology, 39: 131-155.

Chapman, M. R., & Chepstow-Lusty, A. J. (1997). Late Pliocene climatic change and the global extinction of the discoasters: an independent assessment using oxygen isotope records. Palaeogeography, Palaeoclimatology, Palaeoecology, 134(1), 109-125.

Chepstow-Lusty, A., Backman, J., & Shackleton, N. J. (1989). Comparison of upper Pliocene Discoaster abundance variations from North Atlantic Sites 552, 607, 658, 659 and 662: further evidence for marine plankton responding to orbital forcing. In Ruddiman, WF, Sarnthein, M., et al., Proc. ODP, Sci. Results (Vol. 108, pp. 121-141).

Cramer, B. S., J. D. Wright, D. V. Kent, M.-P. Aubry, (2003), Orbital climate forcing of d13C excursions in the late Paleocene–early Eocene (chrons C24n–C25n), Paleoceanography, 18, doi:10.1029/2003PA000909.

Dinarès-Turell, J., Baceta, J.I., Pujalte, V., Orue-Etxebarria, X., Bernaola, G., Lorito, S.,(2003). Untangling the Palaeocene climatic rhythm; an astronomically calibrated early Palaeocene magnetostratigraphy and biostratigraphy at Zumaia (Basque Basin, northern Spain). Earth and Planetary Science Letters 216, 483–500.

Dinarès-Turell, J., Payros, A., Monechi, S., Orue-Etxebarria, X., Ortiz, S., Apellaniz, E., Bernaola, G., (2014). In Search of the Bartonian (Middle Eocene) GSSP (II): Preliminary Results From the Oyambre Section (N Spain). In: Rocha, R., et al. (Eds.), Springer International Publishing, Switzerland, pp. 79–83 (Strati 2013).

Dinarès-Turell, J., Stoykova, K., Baceta, J.I., Ivanov, M., Pujalte, V., (2010). High resolution intra and interbasinal correlation of the Danian–Selandian transition (Early Paleocene): the Bjala section (Bulgaria) and the Selandian GSSP at Zumaia (Spain). Palaeogeography, Palaeoclimatology, Palaeoecology 297, 511–533.

Dinarès-Turell, J., Martínez-Braceras, N., & Payros, A. (2018). High-Resolution Integrated Cyclostratigraphy From the Oyambre Section (Cantabria, N Iberian Peninsula): Constraints for Orbital Tuning and Correlation of Middle Eocene Atlantic Deep-Sea Records. Geochemistry, Geophysics, Geosystems, 19(3), 787-806.

De Kaenel, E., & Villa, G. (1996). Oligocene-Miocene calcareous nannofossil biostratigraphy and paleoecology from the Iberia Abyssal Plain. In PROCEEDINGS-OCEAN DRILLING PROGRAM SCIENTIFIC RESULTS (pp. 79-146). NATIONAL SCIENCE FOUNDATION.

Dunkley-Jones, T., Bown, P. R., Pearson, P. N., Wade, B. S., Coxall, H. K., & Lear, C. H. (2008). Major shifts in calcareous phytoplankton assemblages through the Eocene-Oligocene transition of Tanzania and their implications for low-latitude primary production. Paleoceanography, 23(4)

Elder, W.P., Gustason, E.R., Sageman, B.B., (1994). Correlation of basinal carbonate cycles to nearshore parasequences in the Late Cretaceous Greenhorn seaway, Western Interior U.S.A. GSA Bulletin 106, 892–902.

Elorza, J.J., Orue-Etxebarria, X. and Lamolda, M.A. (1984) Existencia de una fracturacion intensa en el area de Sopelana-Meñakoz. I Congreso Español de Geologia, 3, 177-188.

Erba, E., Castradori, D., Guasti, G., Ripepe, M., 1992. Calcareous nannofossils and Milankovitch cycles: the example of the Albian Gault Clay Formation (Southern England). Palaeogeogr. Palaeoclimatol. Palaeoecol. 93, 47–69.

Fioroni, C., Villa, G., Persico, D., & Jovane, L. (2015). Middle Eocene-Lower Oligocene calcareous nannofossil biostratigraphy and paleoceanographic implications from Site 711 (equatorial Indian Ocean). Marine Micropaleontology, 118, 50-62.

Flores, J.A., Marino, M., Sierro, F.J., Hodell, D.A. and Char- les, C.D. (2003). Calcareous plankton dissolution pattern and coccolithophore assemblages during the last 600 kyr at ODP Site 1089 (Cape Basin,South Atlantic): paleocea- nographic implications. Palaeogeography, Palaeoclima- tology, Palaeoecology, 196, 409-426

Flores, J.A., Sierro, F.J., 1997. Revised technique for calculation of calcareous nannofossil accumulation rates. Micropaleontology, 43, 321-324. http://dx.doi.org/10.2307/1485832

Fornaciari, E., Agnini, C., Catanzariti, R., Rio, D., Bolla, E. M., & Valvasoni, E. (2010). Mid-latitude calcareous nannofossil biostratigraphy and biochronology across the middle to late Eocene transition. Stratigraphy, 7(4), 229.

Gibbs, S. J., Bralower, T. J., Bown, P. R., Zachos, J. C., & Bybell, L. M. (2006). Shelf and open- ocean calcareous phytoplankton assemblages across the Paleocene–Eocene Thermal Maximum. Earth and Planetary Science Letters, 295, 583–592.

Gibbs, S., Shackleton, N.J., Young, J., (2004). Orbitally forced climate signals in mid-Pliocene nannofossil assemblages. Mar. Micropaleontol. 51, 39–56. doi:10.1016/j.marmicro.2003.09.002.

Giorgioni, M., Tiraboschi, D., Erba, E., Hamann, Y., & Weissert, H. (2017). Sedimentary patterns and palaeoceanography of the Albian Marne a Fucoidi Formation (Central Italy) revealed by high-resolution geochemical and nannofossil data. Sedimentology, 64(1), 111-126.

Guerreiro, C., Sá, C., de Stigter, H., Oliveira, A., Cachão, M., Cros, L., ... & Rodrigues, A. (2014). Influence of the Nazaré Canyon, central Portuguese margin, on late winter coccolithophore assemblages. Deep Sea Research Part II: Topical Studies in Oceanography, 104, 335-358.

Guerreiro, C., Cachão, M., Pawlowsky-Glahn, V., Oliveira, A., & Rodrigues, A. (2015). Compositional Data Analysis (CoDA) as a tool to study the (paleo) ecology of coccolithophores from coastal-neritic settings off central Portugal. Sedimentary Geology, 319, 134-146.

Gran, H. H., & Braarud, T. (1935). A quantitative study of the phytoplankton in the Bay of Fundy and the Gulf of Maine (including observations on hydrography, chemistry and turbidity). Journal of the Biological Board of Canada, 1(5), 279-467.

Hagino, K., Tomioka, N., Young, J. R., Takano, Y., Onuma, R., & Horiguchi, T. (2016). Extracellular calcification of Braarudosphaera bigelowii deduced from electron microscopic observations of cell surface structure and elemental composition of pentaliths. Marine Micropaleontology, 125, 85-94.

Hammer et al., (2001). Ø. Hammer, D.A.T. Harper, P.D. Ryan PAST: paleontological statistics software package for education and data analysis Palaeontol. Electron., 4 (1).

Haq, B.U., Lohmann, G.P., (1976). Early Cenozoic calcareous nannoplankton biogeography of the Atlantic Ocean. Mar. Micropaleontol. 1, 119–194. doi:10.1016/0377-8398(76)90008-6.

Herrle, J.O., Pross, J., Friedrich, O., Hemleben, C., (2003b). Short- term environmental changes in the Cretaceous Tethyan Ocean: micropalaeontological evidence from the Early Albian Oceanic Anoxic Event 1b. Terra Nova 15, 14–19.

Herrle, J.O., Pross, J., Friedrich, O., Ko¨hler, P., Hemleben, C., (2003a). Forcing mechanisms for mid-Cretaceous black shale for- mation: evidence from the upper Aptian and lower Albian of the Vocontian Basin (SE France). Palaeogeogr. Palaeoclimatol. Pa- laeoecol. 190, 399–426.

Hilgen, F.J., (1991). Astronomical calibration of Gauss to Matuyama sapropels in the Mediterranean and implication for the Geomagnetic Polarity Timescale. Earth Planet. Sci. Lett., 104: 226-224.

House, M.R., Gale, A.S. (Eds.), 1995. Orbital Forcing Timescales and Cyclostratigraphy. Spec. Publ.-Geol. Soc. Lond., vol. 85. 204 pp.

Intxauspe-Zubiaurre, B., Martínez-Braceras, N., Payros, A., Ortiz, S., Dinarès-Turell, J., & Flores, J. A. (2018). The last Eocene hyperthermal (Chron C19r event,~ 41.5 Ma): Chronological and paleoenvironmental insights from a continental margin (Cape Oyambre, N Spain). Palaeogeography, Palaeoclimatology, Palaeoecology.

Jiang, S., & Wise Jr, S. W. (2006). Surface-water chemistry and fertility variations in the tropical Atlantic across the Paleocene/Eocene Thermal Maximum as evidenced by calcareous nannoplankton from ODP Leg 207, Hole 1259B. Revue de micropaléontologie, 49(4), 227-244.

Kalb, A. L., and T. J. Bralower. (2012). Nannoplankton origination events and environmental changes in the late Paleocene and early Eocene. Marine Micropaleontology 92–93:1–15.

Kelly, D.C., Bralower, T.J., Zachos, J., Premoli Silva, I., Thomas, E., (1996). Rapid diversification of planktonic foraminifera in the tropical Pacific (ODP Site 865) during the late Paleocene thermal maximum. Geology 24, 423–426.

Liebrand, D., Raffi, I., Fraguas, Á., Laxenaire, R., Bosmans, J. H., Hilgen, F. J., ... & Bown, P. R. (2018). Orbitally forced hyperstratification of the Oligocene South Atlantic Ocean. Paleoceanography and Paleoclimatology.

Marino, M., Girone, A., Maiorano, P., Di Renzo, R., Piscitelli, A., & Flores, J. A. (2018). Calcareous plankton and the mid-Brunhes climate variability in the Alboran Sea (ODP Site 977). Palaeogeography, Palaeoclimatology, Palaeoecology, 508, 91-106.

Marino, M., Maiorano, P. and Flower, B.P. (2011). Calcareous nannofossil changes during the Mid-Pleistocene Revo- lution: Paleoecologic and paleoceanographic evidence from North Atlantic Site 980/981. Palaeogeography, Pa- laeoclimatology, Palaeoecology, 306, 58-69.

Marino, M., Maiorano, P., Lirer, F. and Pelosi, N. (2009). Response of calcareous nannofossil assemblages to pa- leoenvironmental changes through the mid-Pleistocene revolution at Site 1090 (Southern Ocean). Palaeogeogra- phy, Palaeoclimatology, Palaeoecology, 280, 333-349.

Martínez-Braceras, N., Payros, A., Miniati, F., Arostegi, J., Franceschetti, G., (2017). Contrasting environmental effects of astronomically driven climate change on three Eocene hemipelagic successions from the Basque–Cantabrian Basin. Sedimentology 64 (4), 960-986. http://dx.doi.org/10.1111/sed.12334

Martini, E. (1967). Nannoplankton und Umlagerungserscheinungen im Persischen Golf und im nördlichen Arabischen Meer.Neues Jahrbuchfür Geologie und Paläontologie,10, 597–607.

Mattioli, E. (1997). Nannoplankton productivity and diagenesis in the rhythmically bedded Toarcian–Aalenian Fiuminata sequence (Umbria–Marche Apennine, Central Italy).

McIntyre, A., & Bé, A. W. H. (1967). Modern Coccolithophoridae of the Atlantic Ocean - I. Placoliths and cyrtoliths. Deep-Sea Research, 14, 561–597.

Mita, I., 2001: Data Report: Early to late Eocene calcareous nannofossil assemblages of Sites 1051 and 1052, Blake Nose, northwestern Atlantic Ocean. In: Kroon, D., Norris, R. D. & Klaus, A. (eds.): Proceedings of the Ocean Drilling Program, Scientific Results, College Station, TX (Ocean Drilling Program), 171B, 1 – 28, doi:10.2973/171B.122.2001

Monechi, S., Angori, E., & von Salis, K. (2000). Calcareous nannofossil turnover around the Paleocene/Eocene transition at Alamedilla (southern Spain). Bulletin Societe Géologie France, 171, 477–489.

Nagymarosy A (2000) Lower Oligocene nannoplankton in anoxic deposits of the central paratethys. 8th International Nannoplankton Association Conference, Bremen (Germany). J Nannoplankton Res 22:128–129

Narciso, A., Cachao, M., & de Abreu, L. (2006). Coccolithus pelagicus subsp. pelagicus versus Coccolithus pelagicus subsp. braarudii (Coccolithophore, Haptophyta): A proxy for surface subarctic Atlantic waters off Iberia during the last 200 kyr. Marine Micropaleontology, 59(1), 15-34.

Newsam, C., Bown, P. R., Wade, B. S., & Jones, H. L. (2017). Muted calcareous nannoplankton response at the Middle/Late Eocene Turnover event in the western North Atlantic Ocean. Newsletters on Stratigraphy, 50(3), 297-309.

Ortiz,S., Alegret,L. Baceta,J.I., Kaminski,M.A., and Payros,A., (2012).Cretaceous to Paleogene hemipelagic and Flysch Successions in Western Pyrenees,Northern Spain. Ninth International Workshop on Agglutinated Formainifera, Field trip guide.Zaragoza, 82 p.

Okada, H., 1971.Modern Coccolithophorid in the Pacific Ocean. [Dissertation]. HokksidoUniversity, Sapporo.

Parente, A., Cachão, M., Baumann, K. H., de Abreu, L., & Ferreira, J. (2004). Morphometry of Coccolithus pelagicus sl (Coccolithophore, Haptophyta) from offshore Portugal, during the last 200 kyr. Micropaleontology, 50(Suppl_1), 107-120.

Payros, A., Dinares-Turell, J., Bernaola, G., Orue-Etxebarria, X., Apellaniz, E. and Tosquella, J. (2011) On the age of the Early/Middle Eocene boundary and other related events: cyclostratigraphic refinements from the Pyrenean Otsakar section and the Lutetian GSSP. Geol. Mag., 148, 442–460.

Payros, A., Orue-Etxebarria, X., Bernaola, G., Apellaniz, E., Dinares-Turell,J.,Tosquella,J.andCaballero,F.(2009) Characterization and astronomically calibrated age of the first occurrence of Turborotalia frontosa in the Gorrondatxe section, a prospective Lutetian GSSP: implications for the Eocene time scale. Lethaia, 42, 255– 264.

Payros, A., Ortiz, S., Alegret, L., Orue-Etxebarria, X., Apellaniz, E. and Molina, E. (2012) An early Lutetian carbon-cycle perturbation: insights from the Gorrondatxe section (western Pyrenees, Bay of Biscay). Paleoceanography, 27, PA2213.

Payros, A. and Martínez-Braceras, N. (2014) Orbital forcing in turbidite accumulation during the Eocene greenhouse interval. Sedimentology, 61, 1411-1432.

Payros, A., Bernaola, G., Orue-Etxebarria, X., Dinarès-Turell, J., Tosquella, J. and Apellaniz, E. (2007) Reassessment of the Early–Middle Eocene biomagnetochronology based on evidence from the Gorrondatxe section (Basque Country, western Pyrenees). Lethaia, 40, 183-195.

Payros, A., Dinarès-Turell, J., Monechi, S., Orue-Etxebarria, X., Ortiz, S., Apellaniz, E., Martínez-Braceras, N., (2015). The Lutetian/Bartonian transition (middle Eocene) at the Oyambre section (northern Spain): Implications for standard chronostratigraphy. Palaeogeography, Palaeoclimatology, Palaeoecology 440, 234-248. http://dx.doi.org/10.1016/j.palaeo.2015.09.015

Payros, A., Dinarès-Turell, J., Orue-Etxebarria, X., Monechi, S., Ortiz, S., Apellaniz, E., Bernaola, G., (2014). In Search of the Bartonian (Middle Eocene) GSSP (I): Potential in the Basque–Cantabrian and Aquitanian Basins (W Pyrenees). In: Rocha, R., et al. (Eds.), Springer International Publishing, Switzerland, pp. 79–83 (Strati 2013).

Payros, A., Orue-Etxebarria, X., Bernaola, G., Apellaniz, E., Dinarès-Turell, J., Tosquella, J. and Caballero, F. (2009) Characterization and astronomically calibrated age of the first occurrence of Turborotalia frontosa in the Gorrondatxe section, a prospective Lutetian GSSP: implications for the Eocene time scale. Lethaia, 42, 255-264.

Perch-Nielsen, K., (1985). Cenozoic calcareous nannofossils, in: Bolli, H.M., Saunders, J. B., Perch-Nielsen, K. (Eds.), Plankton Stratigraphy. Cambridge University Press, Cambridge, pp. 427-554.

Persico, D., & Villa, G. (2004). Eocene–Oligocene calcareous nannofossils from Maud Rise and Kerguelen Plateau (Antarctica): paleoecological and paleoceanographic implications. Marine Micropaleontology, 52(1–4), 153–179, doi: 10.1016/j.marmicro.2004.05.002.

Pujalte, V., Baceta, J.I. and Payros, A. (2002) Chapter 13: Tertiary: Western Pyrenees and Basque–Cantabrian region. In: The Geology of Spain (Eds W. Gibbons and T. Moreno), pp. 293–301. Geol. Soc., London.

Raffi, I., Backman, J., Zachos, J. C., & Sluijs, A. (2009). The response of calcareous nannofossil assemblages to the Paleocene Eocene Thermal Maximum at the Walvis Ridge in the South Atlantic. Marine Micropaleontology, 70(3), 201-212.

Roca, E., J. A. Muñoz, O. Ferrer,and N. Ellouz., (2011). The role of the Bay of Biscay Mesozoic extensional structure in the configuration of the Pyrenean orogeny Constraints from the MARCONI deep seismic reflection survey, Tectonics, 30, TC2001, doi:10.1029/2010TC002735.

Röhl, U, Ogg, J., Geib, T., and G. Wefer, (2001), Astronomical calibration of the Danian time scale in Norris et al., Special Publication of the Geological Society of London, v. 183, p. 163-183.

Röhl, U., Norris, R. D. Ogg, J. G., (2003). Astronomical forcing and cyclostratigraphy of Late Paleocene and Early Eocene sediments drilled at Blake Nose Site 1051 (western North Atlantic). GSA Spec.Publ. 369, p. 567-588.

Schneider, L. J., Bralower, T. J., Kump, L. R., & Patzkowsky, M. E. (2013). Calcareous nannoplankton ecology and community change across the Paleocene-Eocene Thermal Maximum. Paleobiology, 39(4), 628-647.

Shackleton, N J; Crowhurst, S; Hagelberg, T; Pisias, N G; Schneider, D A., (1995), A new late Neogene time scale; application to Leg 138 sites, Proceedings of the Ocean Drilling Program, Scientific Results, vol.138, pp.73-101.

Shamrock, J.L., Watkins, D.K., 2012. Eocene calcareous nannofossil biostratigraphy and community structure from Exmouth Plateau, Eastern Indian Ocean (ODP Site 762). Stratigraphy 9, 1, 1–54.

Silva, A., Palma, S., & Moita, M. T. (2008). Coccolithophores in the upwelling waters of Portugal: Four years of weekly distribution in Lisbon bay. Continental Shelf Research, 28(18), 2601-2613.

Takayama, T. (1972). A note on the distribution ofBraarudosphaera bigelowi(Gran and Braarud) Deflandre in the bottom sediments ofSenday Bay, Japan.Transactions and Proceedings. Paleontological Society of Japan,87, 429–435.

Tanaka, Y. (1991). Calcareous nannoplankton thanatocoenoses in surface sediments from seas around Japan Rep (pp.127–198).Tohoky University.

Thierstein, H. (1981). Late Cretaceous nannoplankton and the change at the Cretaceous-Tertiary boundary. Society of Economic Paleontologists and Mineralogists, Special Publication, 32, 355–394.

Thomas, E., Boscolo-Galazzo, F., Balestra, B., Monechi, S., Donner, B., & Röhl, U. (2018). Early Eocene Thermal Maximum 3: Biotic response at Walvis Ridge (SE Atlantic Ocean). Paleoceanography and Paleoclimatology, 33(8), 862-883

Tremolada, F., & Bralower, T. J. (2004). Nannofossil assemblage fluctuations during the Paleocene–Eocene thermal maximum at Sites 213 (Indian Ocean) and 401 (North Atlantic Ocean): palaeoceanographic implications. Marine Micropaleontology, 52(1-4), 107-116.

Villa, G., Fioroni, C., Pea, L., Bohaty, S., & Persico, D. (2008). Middle Eocene–late Oligocene climate variability: Calcareous nannofossil response at Kerguelen Plateau, Site 748. Marine Micropaleontology, 69(2), 173–192, doi: 10.1016/j.marmicro.2008.07.006.

Wade, B. S., & Bown, P. R. (2006). Calcareous nannofossils in extreme environments: the Messinian salinity crisis, Polemi Basin, Cyprus. Palaeogeography, Palaeoclimatology, Palaeoecology, 233(3-4), 271-286.

Weber, M.E., Fenner, J., Thies, A., Cepek, P., 2001. Biological response to Milankovitch forcing during the late Albian (Kir- chrode I borehole, northwestern Germany). Palaeogeogr. Palae- oclimatol. Palaeoecol. 174, 269–286.

Weber, M.E., Fenner, J., Thies, A., Cepek, P., 2001. Biological response to Milankovitch forcing during the late Albian (Kir- chrode I borehole, northwestern Germany). Palaeogeogr. Palae- oclimatol. Palaeoecol. 174, 269–286.

Wei, W., Wise Jr., S.W., (1990). Biogeographic gradients of middle Eocene– Oligocene calcareous nannoplankton in the South Atlantic Ocean. Palaeogeogr. Palaeoclimatol. Palaeoecol. 79, 29–61. doi:10.1016/0031- 0182(90)90104-F

Westphal, H., Bohm, F. and Bornholdt, S. (2004). Orbital frequencies in the carbonate sedimentary record: distorted by diagenesis? Facies, 50, 3–11.

Zachos, J., Pagani, M., Sloan, L., Thomas, E. and Billups, K. (2001). Trends, rhythms, and aberrations in global climate 65 Ma to present. Science, 292, 686–693.

Chapter 4

Reassessing the Bartonian unit stratotypes: an integrated approach*

Abstract

The Global boundary Stratotype Section and Point (GSSP) for the base of the Bartonian, currently remains undefined. The Bartonian unit stratotype is located at the Barton coastal section in the Hampshire Basin, on the South Coast of the UK. Moreover the bases of the chronostratigraphic and lithostratigraphic units do not coincide. The parastratotype section is located at Alum Bay, 7 km away, on the Isle of Wight. Despite a number of studies carried out in 1970s and '80s on both sections, global correlation remains problematic. Here we present an integrated (micropaleontological, stratigraphic, paleomagnetic) study of the Lutetian-Bartonian transition at Alum Bay, and aim at improving the stratigraphy of this section to better define the base of the Bartonian and contribute towards a decision on the GSSP.

4.1 Introduction

The Eocene period is a dynamic period of Earth's history and has been the focus of numerous (palaeontological) biostratigraphical, geochemical, magnetostratigraphical, and palaeoclimatic studies, however two of the Eocene stage boundaries remain formally undefined, the Bartonian and the Priabonian.

***** This chapter is based on a manuscript in preparation for submission to *Newsletter on Stratigraphy*

LAURA J. COTTON[1], LUCÍA RIVERO-CUESTA[2], GLORIA FRANCESCHETTI[3], ALINA IAKOVLEVA[4], JERRY J. HOOKER[5], LAIA ALEGRET[2], JAUME DINARÈS-TURELL[6], STACY L. YAGER[7], RICHARD H. FLUEGEMAN[7], SIMONETTA MONECHI[3]

[1]University of Florida, [3]Università degli Studi di Firenze, Italy; [2]Universidad de Zaragoza, Spain; USA; [4]Geological Institute RAS, Russia; [5]Natural History Museum, London; [6]Istituto Nazionale di Geofisica e Vulcanologia, Italy; [7]Ball State University, USA

At present the base of the Bartonian stage has no designated Global boundary Stratotype Section and Point (GSSP). Traditionally the Bartonian has been defined by the Bartonian unit stratotype at Barton, within the Hampshire Basin in the south of the UK, which contains well-preserved Paleogene sedimentary sequences. However, within the section at Barton the bases of the chronostratigraphic and lithostratigraphic units do not coincide, and the section itself is somewhat obscured by slumping. The base itself was defined by Curry (1981) on the *Nummulites prestwichianus* bed at this locality. The parastratigraphic section for the Bartonian is located 7 km away at Alum bay on the Isle of Wight and is better exposed, although beds are steeply dipping. Although numerous studies have been carried out since the 70s (Martini 1971; Murray and Wright 1974; Bujak 1980; Curry 1981; Aubry 1983, 1985, 1986; Dawber at al., 2011; King 2016; Hooker and King, 2018) , correlation of the sites to global stratigraphy has been challenging due to a lack of studies combining stratigraphic methods, and a lack of clear global overturning events around this level.

The boundary has frequently been placed on the basal beds of *Nummulites prestwichianus*, however, this species not widely correlatable outside of the Hampshire basin. The species only extends as far as France, and large benthic foraminifera (LBF) are well known to be restricted to shallow platform environments, therefore this is not a reliable marker. In addition to this, King (2016) showed a series of *N. prestwichianus*-like forms found around the level, further clouding correlations, whose taxonomy will be addressed in detail in a later publication. Only a single, long-ranged, planktonic foraminifer has been identified, *Dipsidripella danvillensis*, and so correlation of this bed with planktonic foraminiferal biostratigraphy has not been possible. The dinoflagellates do show a taxonomic turnover with *Rhombodinium draco* occurring a few centimeters above the level of the *N. prestwichianus* bed at several localities in the Hampshire basin, however, this is not consistent outside of this region. Calcareous nannofossils from the site were relatively impoverished, with NP zones being largely recognized by secondary markers.

However, Aubry (1983, 1986) recognized *Reticulofenestra umbilicus*, which is a primary marker of CP14a, within the CP zonation (Okada & Bukry, 1980) suggesting further correlation potential for calcareous nannoplankton. Palaeomagnetic studies have also been carried out at the Alum bay section; Dawber et al., (2011) identified C18n with the NP16-17 boundary and the *Nummulites prestwichianus* bed as being within the underlying reversed interval, but there are problems with their interpretation of the nannofossil record. More recently, Jovane et al. (2010) and Flugeman (2007) suggested the top and base, respectively, of Chron C19n as boundary markers –although the GSSP proposal has not been submitted and, no decision has yet been made.

In order to resolve this issue, we re-examine the Alum bay section using integrated nannofossil, dinoflagellate, LBF, small benthic foraminifera and magnetostratigraphy to assess potential correlations and placements for boundaries. In particular, we aim to address the occurrences of new nannofossil zonal indicators of the Agnini et al. (2014) mid-latitude zonation and the occurrence of key taxa of dinocysts as *A. sentosa, A. tauloma* and *Rhombodinium prorosum* against the sequencestratigraphy and palaeomagnetism of King (2016). The base of *Distatodinium paradoxum* is re-examined for its correlation with the *N. sub- prestwichianus* bed within the Barton clay as shown in Eaton (1976), as an additional potential biostratigraphic marker. Likewise the range of *R. draco* is examined to determine where the base falls within the C19n interval 2-5 m above the base of the Barton Clay as recorded in SW Siberia. Improvement in the stratigraphy is essential to better define this interval and contribute towards a decision for the GSSP.

4.2 Geological Setting

Alum bay is situated within the Hampshire basin, which consists of an asymmetric syncline within the larger Anglo – Paris – Belgium basin (Fig. 4.1). The sediments were deposited in a series of regressive and transgressive cycles during the Paleogene, and consist of various continental shelf sediments. The Barton Clay formation spans the late Lutetian to late Bartonian, and is overlain by the Barton Sand formation, in the late Bartonian. The Lutetian–Bartonian transition therefore lies within this unit. At Alum bay the Barton clay succession comprises of a series of glauconitic clays and sandstones, with the basal beds showing a clear abundance of larger benthic foraminifera.

There are two models for the deposition of this formation (see King and Hooker for detailed discussion), the first indicates the base of the Barton Clay is a timeline onlapping in a westwards direction over the underlying Boscombe Sand Formation. Alternatively a number of authors (Hooker 1986; Plint 1988; Keen, 1993; Huggett & Gale, 1997) interpret the succession as three cycles that transgress progressively westwards, with the Boscombe Sands being the more proximal shoreline facies and the Barton Clay the more distal offshore facies. The larger benthic foraminifera at the base of the Barton Clay however do indicate that these lower most beds were deposited within the photic zone and therefore not deeper than ~ 100 m water depth. The south of the UK also represents the most northerly extent of the range of *Nummulites* (LBF) during the Paleogene at a paleolatitude of ~ 40 degrees North and temperatures in keeping with this.

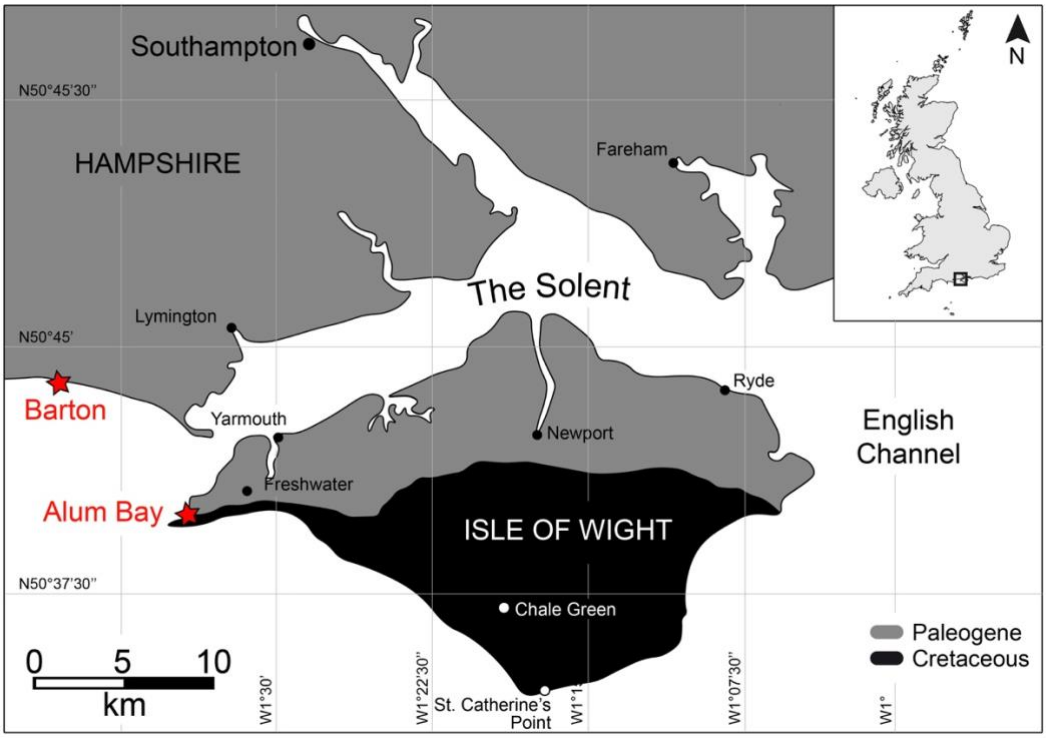

Fig. 4.1: Map of the Hampshire Basin, showing the location of the Alum Bay and the Barton sections. In grey are reported the Paleogene outcrops and in black the Cretaceous deposits.

4.3 Methods

The Alum Bay section was visited in 2015 by members of the Bartonian working group, part of the Subcommision of Paleogene Stratigraphy, as part of an effort to formally constrain the base of the Bartonian stage. The Alum Bay section comprises of a 100 m coastal outcrop with near vertical bedding, although the part of the base is obscured by a chair lift, the section is largely accessible. A total of 32 levels were collected for the study across an almost 100 m transect section, with samples taken approximately from 50 to 6m, through the middle to upper Eocene and therefore including the base of the Bartonian stage.

4.3.1 Small benthic foraminifera

A set of twenty-five samples was collected to study small benthic foraminiferal assemblages. Samples were soaked in water for 24 hours to help disaggregation; wet sieved over a 63 µm sieve

and the collected residue was oven-dried at 50ºC for 24 hours. Quantitative analyses of benthic foraminiferal assemblages were based on representative splits of 300 individuals per sample. Picked specimens were identified to species level whenever possible; when the preservation was poor or the test was fragmented, determination was at the genus or higher level. The relative abundance (given as percentage) of each species, the percentage of agglutinated and calcareous-walled taxa, diversity (Fisher-α index), heterogeneity (Shannon-Weaver index) of the assemblages and the planktic/benthic (P/B) ratio were calculated. Additionally, specimens were assigned to infaunal or epifaunal microhabitats based on Murray (1991). The sediment from which the 300 specimens were picked was weighed, and used as an approximate estimation of the concentration of foraminifera per gram of sediment.

Only 6 samples out of 25 (AB12 to AB17, lower part of the section) contain enough specimens of small benthic foraminifera to perform quantitative analyses (300 specimens) of the assemblages. In order to show a longer record, samples with low concentration of foraminiferal tests (AB10, AB19, AB22d and AB22f) were also studied. As samples below AB10 and above AB22f were barren of small benthic foraminifera, the interpretation given here refers to the lower half of the log. The overall preservation of the tests is good and there are no signs of dissolution, although fragmented tests make up ~ 20% of the assemblages.

4.3.2 Larger benthic foraminifera

Seven of the twenty-five small benthic foraminiferal samples contained larger benthic foraminifera (LBF). Samples were picked up to a maximum of 300 specimens. Representative examples of LBF were examined in oriented section, and natural split sections, and traditional measurements of proloculus and deuteroconch size along with successive whorl radii were taken. A total of 18 equatorial sections were used and 2 axial sections.

4.3.3 Calcareous nannofossil

Twenty-seven samples were collected in the Alum Bay section to study calcareous nannofossil assemblages. Smear slides were prepared from raw material using the technique described by Bown and Young (1998). Qualitative and semi-quantitative analyses were conducted on the light microscope Zeiss Axiophot, at a magnification of 1250x. Two random long traverses were analysed to detect rare key species (i.e. *Chiasmolithus solitus, Sphenolithus furcatolithoides* morphotype *B, S. spiniger, S. obtusus and Discoaster distinctus*). Taxonomy follows Perch-Nielsen (1985), Fornaciari et al. (2010) for *Dictyococcites* and Agnini et al. (2014) for *Sphenolithus.* The biostratigraphic schemes adopted are those of Agnini et al. (2014), codified CNE, and Martini (1971) codified NP.

4.3.4 Palynology

Seventeen samples from the Alum Bay section were analyzed palynologically. Palynomorphs were prepared using the standard palynological techniques of the British Geological Survey (Riding & Kyffin-Hughes, 2004) consisting of four main steps: (1) dissolution of carbonates and silicates by HCl and HF acid digestion; (2) sieving between 106 and 10 µm; (3) neutralization with distilled water and centrifugation; (4) staining with Safranin-O. The palynological preparations are stored within the collections of Zaragoza University (Spain).

Once prepared a quantitative analysis of the samples was carried out. Firstly a minimum 200 palynomorphs were counted and grouped into 6 broad categories as dinocysts, reworked dinocysts (mostly Mesozoic), acritarchs, prasinophytes, conifers and foraminiferal linings, but finally prasinophytes, conifers and foraminiferal linings were represented only by few specimens and did not achieve 1%. Secondly, a minimum of 200 dinocysts were counted; the remaining material was scanned for rare dinocyst taxa. For paleoenvironmental reconstructions we followed the approach of Sluijs & Brinkhuis (2009) in using a grouping of

morphologically/ecologically related dinocyst taxa and assigned dinocysts to 12 groups: *Wetzelielloids; Phthanoperidinium*; other peridinioids; Homotryblium-group (mostly *Homotryblium*, plus *Lingulodinium, Heteraulacacysta, Polysphaeridium*); *Areoligera*-group (*Areoligera, Glaphyrocysta, Adnatosphaeridium, Membranophoridium*); Enneadocysta/Areosphaeridium; Distatodinium; *Cordosphaeridium*-group (*Cordosphaeridium, Fibrocysta, Araneosphaera araneosa*); *Hystrichokolpoma*; *Spiniferite*s-group (*Spiniferites, Achomosphaera, Hystrichosphaeropsis, Hystrichostrogylon, Rottnestia borussica*); other g*onyaulacoids*; *gonyaulacoids* indet.

4.5 Paleomagnetism

The paleomagnetic sampling at Alum Bay was conducted along about 85 m of a Barton Clay Fm stratigraphic section with the meter 0 stablished at the base of the Formation. A total of 15 stratigraphic levels were sampled corresponding to equivalent biostratigraphic samples. The lower 20 m of the studied section was sampled in more detail (average sampling of about 2 m) whereas a loose sampling was performed along the upper part in this pilot study. Samples consisted in either hand-samples or cubic plastic cubes (2 x 2 x 2 cm) that were pressed on a soft clay cut surface on the outcrop. Both sample types were oriented in-situ with a magnetic compass. The hand-samples were cut in regular standard block samples in the laboratory before paleomagnetic measurements. Natural remanent magnetization (NRM) and remanence through demagnetization were measured on a 2G Enterprises DC SQUID high-resolution pass-through cryogenic magnetometer (manufacturer noise level of 10^{-12} Am^2) operated in a shielded room at the Istituto Nazionale di Geofisica e Vulcanologia in Rome, Italy. A Pyrox oven in the shielded room was used for thermal demagnetizations and alternating field (AF) demagnetization was performed with three orthogonal coils installed in line with the cryogenic magnetometer. Progressive stepwise AF demagnetization was routinely used and applied after a single heating

step to 150°C. AF demagnetization included 14 steps (4, 8, 13, 17, 21, 25, 30, 35, 40, 45, 50, 60, 80, 100 mT). Characteristic remanent magnetizations (ChRM) were computed by least-squares fitting (Kirschvink, 1980) on the orthogonal demagnetization plots (Zijderveld, 1967). The ChRM declination and inclination were used to derive the latitude of the virtual geomagnetic pole (VGP) of each sample. This parameter was taken as an indicator of the original magnetic polarity, normal polarity being indicated by positive VGP latitudes and reverse polarity by negative VGP latitudes.

4.4 Results

4.4.1 Palaeoenvironmental changes, the response of small benthic foraminiferal assemblage

Richness of the small benthic foraminiferal assemblages is low, with an average of 20 species per sample. The Fisher-α diversity index ranges from 2.8 to 6.8, and the Shannon-Weaver H (S) heterogeneity index ranges from 1.31 to 2.13. Both indices show their highest values between meters 14 and 22 (samples AB 10 to AB 17), and subsequently decrease and remain relatively constant towards the uppermost sample containing benthic foraminifera at 48 m. The P/B ratio yields percentages below 5%, possibly indicating a shallow setting close to the coastline. It is noticeable that there is a positive correlation between the P/B ratio and the number of foraminifera- per gram.

Calcareous taxa dominate the benthic assemblages, and only one agglutinated and two miliolid taxa were identified. Epifaunal morphogroups clearly dominate over infaunal ones (<10%). The genus *Cibicides* is the most abundant epifaunal taxon, making up to >70% of the assemblages in all samples. Less abundant but commonly occurring genera include *Bolivina, Brizalina, Buccella, Buliminella, Discorbis, Globulina, Melonis, Nonion*, *Pullenia*, *Quinqueloculina, Robertina* and *Rosalina.*

The quantitative analysis of the assemblages allowed us to differentiate three intervals (Fig. 4.2):

Interval A: 14 to 20.5 m (samples AB 10 to AB 16). The genus *Cibicides* strongly dominates the assemblages, with the species *Cibicides pygmeus* and *Cibicides ungerianus* together making up ~ 50% of the assemblages. Species that are present but make up less than 10% of the assemblages include *Anomalinoides ypresiensis, Bolivina cookei, Cibicides fortunatus, Discorbis perplexa, Globulina gibba* and *Protelphidium* sp. The highest diversity values (Fisher-α = 6.8 and H(S) = 2.13) and the highest percentage of infaunal morphogroups (up to 9.28 %) across the whole studied succession have been recorded across this interval. Sample AB 16 yields the highest diversity, and a x100 fold in foraminifera per gram, likely related to a condensed horizon.

Interval B: 20.5 to 40.5 m (samples AB 17 to AB 19). Within the genus *Cibicides*, the species *C. pygmeus* dominates over *C. ungerianus*. The relative decrease in % *C. ungerianus* is coupled with a decrease in the percentage of *Buccella propingua* and *Protelphidium* sp. and a small increase in the percentage of *Rosalina* sp. Diversity and the percentage of infaunal morphogroups are lower than in interval A. There is no data available from the middle part of this interval as sample AB18 is barren of foraminifera, however assemblages from its lower and upper parts are very similar, and slightly differ in the lower number of fragments of *Cibicides* sp. and higher percentage of *Rosalina* sp. towards the upper part of interval B.

Interval C: 40.5 to 48 m (samples AB 22d to AB 22e). The genus *Cibicides* reaches its maximum abundance (90% of the assemblages) with a strong dominance of *C. ungerianus* (> 50%) over *C. pygmeus*. The percentages of *Buccella propingua, Cibicides fortunatus, Globulina gibba* and *Nonion leave* are higher than in the previous interval B. Diversity of the assemblages (Fisher α = 2.8, H(S) = 1.31) and the percentage of infaunal morphogroups (2%) show the lowermost values of the studied section.

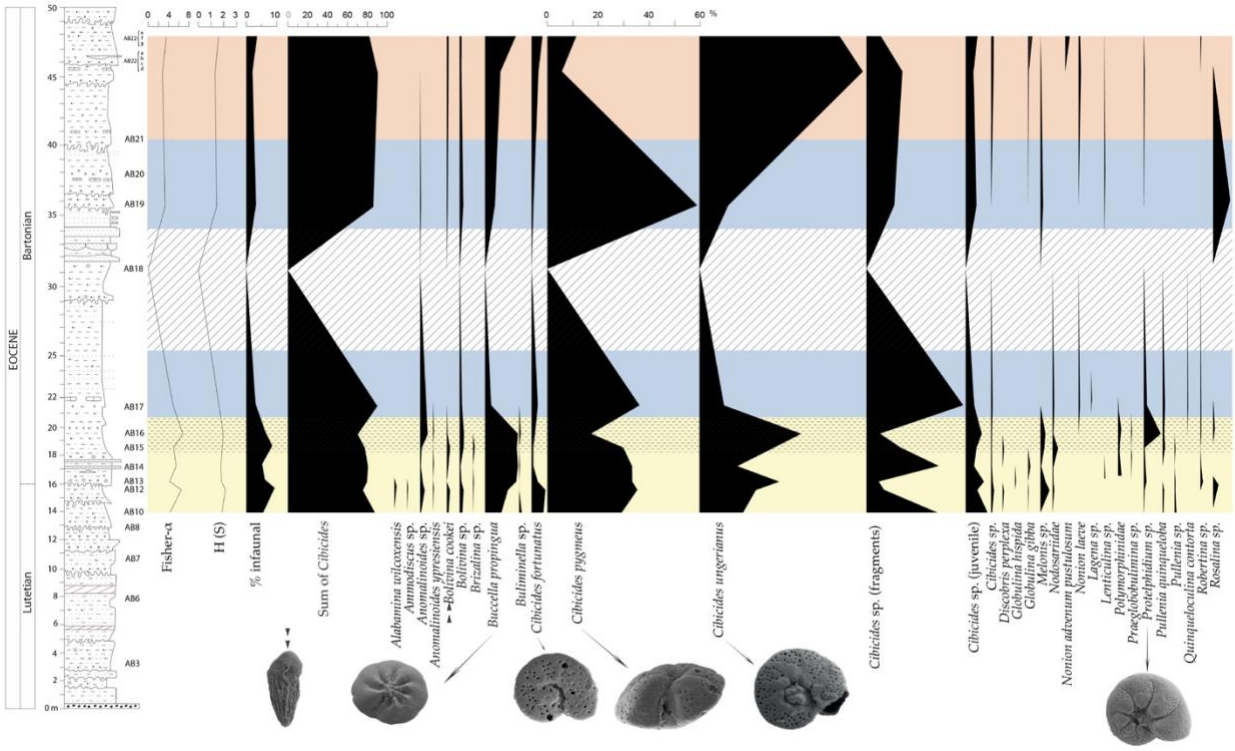

Fig. 4.2: Quantitative analysis of the small benthic foraminifera assemblages across the Alum Bay section. The colored rectangles indicate the three different identified intervals. From the base to the top, the interval A corresponds to the yellow rectangle, the interval B is marked by light blue rectangle at the interval C is represented by the pink rectangle. The white rectangle (25-34m) contains one barren sample of small benthic foraminifera.

4.4.2 Larger benthic foraminifera

Larger benthic foraminifera, where present, were low diversity but high in abundance in specific levels. Preservation of the tests is generally good to excellent although there is some pyritisation. The exception to this is sample AB17 where all specimens are poorly preserved and heavily pyritised. Two taxa were identified, *Nummulites prestwichianus* and *Nummulites rectus,* although assemblages appear monospecific and *N. prestwichianus* was the more abundant of the two taxa. *Nummulites prestwichianus* is characterized by a flattened test with sigmoidal sutures, and loose spiral, following Blondeau (1966), whilst *N. rectus* is more lenticular, with a comparatively tight spiral. Measured specimens of *N. prestwichianus* had a mean proloculus diameter of 93 microns, and range of 65 - 145 microns. It should be noted that the range of proloculus diameters in

sample AB12 was larger than in AB14 and may be linked to taxonomic issues within *N. prestwichianus* which we outline in the discussion. *Nummulites prestwichianus* was abundant in samples AB12 – AB14, with ~ 200 specimens picked from AB12 and > 500 in each of AB13 and AB14. Thereby indicating the *N. Prestwichianus* beds utilized in previous studies as the base of the Bartonian. Samples AB15 and AB16 contain far fewer specimens. Preservation in sample AB17 was poor and specimens could not be accurately identified to species level. *Nummulites rectus* is comparatively more lenticular, with a tight spiral. Only two specimens of *N. rectus* were identified and both were within AB18, the uppermost sample containing LBF.

4.4.3 Calcareous nannofossil biostratigraphy

The nannofossil assemblages consist mainly of *Reticulofenestra umbilicus*, *R. samodurovii*, *Cyclicargolithus floridanus, Coccolithus pelagicu*s and *Blackites inflatus. Discoaster* are rare. However, among discoasterids *D. barbadiensis* is the most frequent. Nannoliths such as *Braarudosphaera bigelowi, Lanternithus minutus*, and *Zygrablithus bijugatus* are always present. Few reworked upper Cretaceous taxa (*Micula murus, Watznaueria* and *Prediscosphaera)* are present throughout the section. *Blackites inflatus,* in agreement with Aubry (1983), has been considered reworked since its stratigraphic range is limited to lower Lutetian (NP14-NP15, Perch-Nielsen 1985).

The total abundance of calcareous nannofossils varies from rare to common and the preservation from poor to moderate along the section. Generally, the calcareous nannofossil assemblages are moderately diversified throughout the Alum Bay section. Ten samples of twenty-seven are barren of coccoliths, the majority located in the lower part of the section up to 13 m (3 samples) and in the interval between 47 to 72m (7 samples). Only the sample collected at 72,5m shows a good preservation and the highest total abundance among the studied samples.

The first sample with calcareous nannofossils is at 13m (AB8). The total abundance is common, but the richness is low, in fact, only 4 species (*Cribrocentrum reticulatum, R. umbilicus, B. inflatus, B. spinosus*) have been recognized. The co-occurrence of *R. umbilicus* and *C. reticulatum* markers of the base of CP14a and CNE14 respectively, recognized in sample AB8 suggest, following Agnini et al. 2014, for the lower part of Alum Bay section Zones CNE14 (CP14 and middle-upper part of Zone NP16) (Fig. 4.3).

In the interval from 14 m to 22 m (AB10 to AB17) abundance increases and the preservation is moderate. The assemblages are comprised of *R. umbilicus*, *Neococcolithus dubius, C. pelagicus and B. bigelowi* and secondary by *D. barbadiensis, D. distinctus, D. saipanensis, L. minutus, C. floridanus, C. reticulatum, S. furcatolithoides* morphotype B, and *R. samodurovii*. *Chiasmolithus* are very rare. Only a single specimen of *C. solitus*, marker of the base of NP17 Zone (Martini 1971), has been identified at 13.80m. *Chiasmolithus solitus* is rare or absent in low latitude sediments, difficult to recognize in poorly preserved material and strongly diachronous at different latitudes (Perch-Nielsen 1985; Wei and Wise 1989; Aubry 1992; Berggren et al. 1995; Marino and Flores 2002; b; Villa et al. 2008; Fornaciari et al, 2010; Agnini et al., 2014). Due to the sporadic distribution of this species Perch-Nielsen (1985) suggested to use the Top of *S. furcatolithoides* as an alternative event to the Top of *C. solitus*. Agnini et al. (2014) recognized two different morphotypes of *S. furcatolithoides* A and B. The differences between morphotype A and B are in the extinction patterns and in the stratigraphic distribution. *Sphenolithus furcatolithoides* morphotype A has its stratigraphic range limited to CNE10 up to lower part of CNE11 Zone, and it corresponds to the middle- upper part of NP15 Zone. On the contrary, *S. furcatolithoides* morphotype B has a younger stratigraphic distribution from CNE12 to CNE14 Zones (the upper part of NP15 to the upper part of NP16 Zones). Furthermore, Agnini et al. (2011) in the Alano section and in ODP Site 1051 and 1052 have correlated the Top of *S. furcatolithoides* B to the upper part of C18r. In the Alum Bay section only morphotype B of *S. furcatolithoides* has

been recognized and the top has been identified at 22 m (AB17). According to Martini (1971) also the Top of *D. distinctus* could be used, in this area, to approximate the NP16/NP17 boundary. *Discoaster distinctus* is continuously present from 14 m up to 22 m (sample AB17) where its Top has been observed. Unfortunately, the identification of *D. distinctus* is not very easy in not well preserved material, and according to Dunkley Jones et al. (2009) its range is diachronous and he reported the highest occurrence up to NP23. Within the interval from 36 m up to 46 m the calcareous nannofossil assemblages are lesser abundant and the nannofloral content is similar to the previous interval. The Base of *Dictyococcites bisectus* >10 µm, marker of the base of CNE15 Zone has been identified at 40.5m (AB21). From this level this form is continuously present. In agreement with Fornaciari et al. (2010) we define as *D. bisectus* all specimens larger than 10 µm while *D. scrippsae* specimens <10 µm.

In the upper part of the section only two samples (AB22 and AB23b), of the seven studied, contain calcareous nannofossils. The co-occurrence of *S. obtusus, S. spiniger* (rare) and *D. bisectus* allow to assign the sample (AB22) to the lower part of CNE15 Zone (Agnini et al. 2014). The last sample with calcareous nannofossil content has been collected at 73 m (AB23b). This sample shows the highest abundance and an assemblage similar to previous sample AB22, without the presence of *S. spiniger*. The Top of *S. spiniger* occurs in the lower part of CNE15 Zone slightly above of the Base of *S. obtusus* confirming CNE15 Zone for the upper part of the section (Fig. 4.3).

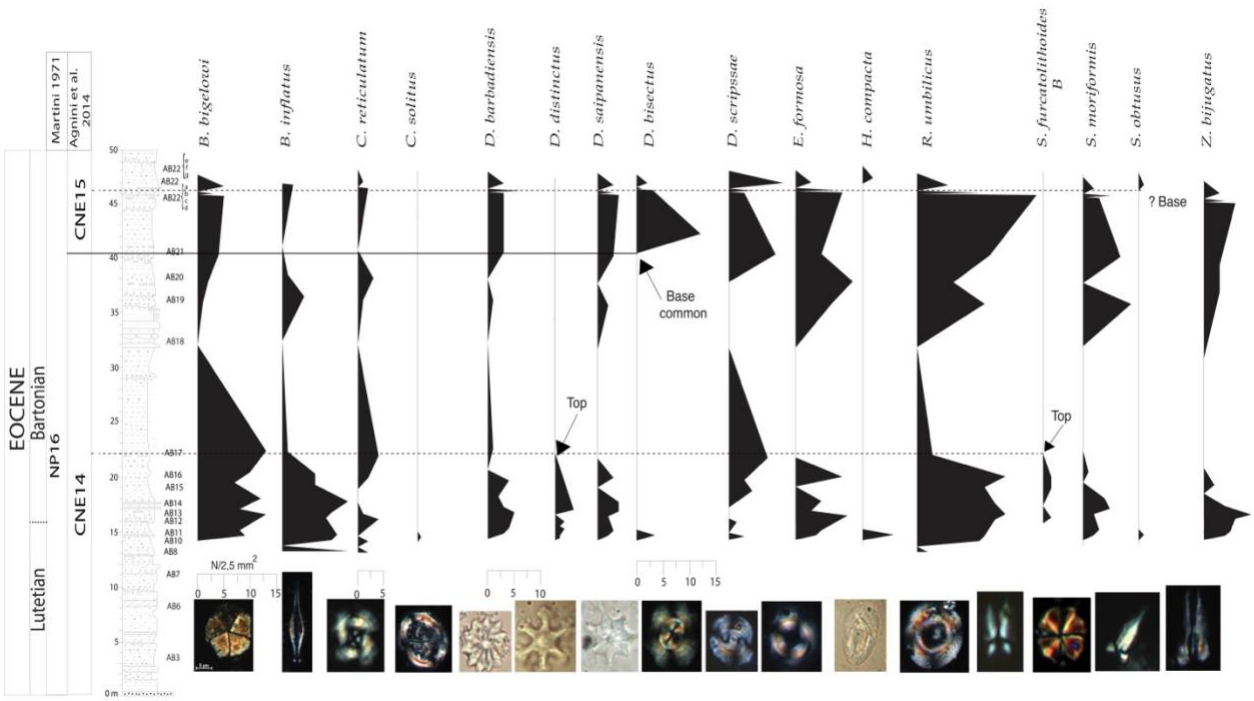

Fig. 4.3 : Abundance pattern of selected nannofossil taxa across the Alum Bay section, expressed as number of specimens per mm^2. Biostratigraphic events are indicated with arrows. The Tops of *D. distinctus* and *S. furcatolithoides* are at 22 m, The Bases of *D. bisectus* and *S. obtusus* are at 40.5 m at 47 m respectively. The biozonation schemes by Agnini et al. (2014) and Martini (1971) are also reported.

4.4.4 Dinocyst biostratigraphy

In general, all 17 palynological samples revealed quantitatively rich palynomorph assemblages with the absolute (80-100%) dominance of dinocysts; acritarchs do not exceed 15%. The lower part of the studied interval is marked by the presence (up to 9%) of reworked Mesozoic dinocysts. Prasinophytes (*Pterospermella*, *Pediastrum*) and pollen grains of conifers represent less than 1% of the total assemblage. Dinoflagellate cyst assemblages from studied samples are diversified with moderately well preserved dinocysts: in total, ca. 96 dinocyst taxa were recognized in the studied part of the Alum Bay.

The distribution of stratigraphically significant species as well as the major changes in relative abundance of different dinocyst eco-group fluctuations allowed to recognize five dinocyst intervals (Fig. 4.4).

The lowermost part of the section (samples AB03-AB07) is characterized by the presence from the base of stratigraphically important Lutetian species *Corodsphaeridium cantharellus*, *Enneadocysta arcuata* and *Enneadocysta multicornuta*; species *Distatodinium craterum*, *Selenophemphix nephroides*, *S. selenoides*, *S. armata* and *Glaphyrocysta laciniiforme* are also present. Therefore, this part of the Alum Bay section corresponds to the part of the *Areosphaeridium arcuatum-Cyclonephelium intricatum* zones interval in southern England (Bujak et al., 1980), the part of the *Enneadocysta arcuata* zone in Denmark (Heilmann-Clausen, 1988), part of the *E. arcuata-E. multicornuta* subzones in Ukraine (Andreeva-Grigorovich et al., 2010) and the part of the Costacysta bucina zone in eastern Peri-Tethys (Shcherbinina et al., 2017). The dinocyst assemblage from this part of the section is characterized by the dominance (20-50%) of *Areoligera*-group; *Homotryblium*- and *Spiniferites*-groups are very common and attain up to 25% and 20% respectively. This may be interpreted as a part of transgressive phase in the inner neritic environments.

The second interval (samples AB07-AB08) revealed the first occurrence of stratigraphically important *Enneadocysta pectiniformis* at ~10.5 m (sample AB07). The highest occurrence of *Areoligera tauloma* is noted at ~13.0 m. Consequently, this part of the Alum Bay may be correlated with the *E. pectiniformis* zone in eastern Peri-Tethys (Iakovleva 2017). Dinocyst assemblage from this interval is characterized by the dominance of *Areoligera* (up to 36%) and *Homotryblium* (up to 35%) groups; *Spiniferites*-group attains 10%. This may be interpreted as a continuation of the transgressive phase in inner neritic environments.

The third dinocyst interval (samples AB10-AB12) is characterized by the lowermost occurrences of *Thalassiphora fenestrata* and *Phthanoperidinium geminatum* at ~14.0 m and of *Heteraulacacysta porosa* at ~15.5 m. It should be noted that previously the Base of *Th. fenestrata* was often recognized only from the Priabonian (Liengjarern et al., 1980; Bujak & Mudge, 1994; Köthe, 2012). Now the Base of typical *Th. fenestrata* is known from the Rhombodinium draco

zone interval in Denmark (Heilmann-Clausen & Van Simaeys, 2005) and eastern Peri-Tethys (Iakovleva 2017), while the Base of specimens recognized as cf. *Th. fenestrata* were noted by Heilmann-Clausen and Van Simaeys (2005) from the uppermost Lutetian part of the *E. arcuata* zone. In the present study the Base of *Rhombodinium draco* is recognized only from ~17.1 m. Due to the unfavorable facies characteristics (sandy units with glauconite, pebbles and shells), we cannot exclude that the true lowermost occurrence of *Rh. draco* was omitted. In this case, this part of the Alum Bay should be tentatively attributed to the part of the *Rh. draco* zone. Palynological assemblage from the sample AB10 revealed a relative influx of acritarchs and reworked dinocysts, indicating a new possible transgressive impulse, while the dinocyst assemblage from the sample AB12 demonstrates a decrease in open-marine *Spiniferites*-group (only 7%), still common *Homotryblium*-group (7%) and an increase in *Enneadocysta*-group (33%); peridinioid taxa attain up to 10%. This may indicate a more restricted inner-neritic environments. The fourth dinocyst interval (Samples AB14-AB17) revealed the successive occurrences of *Rhombodinium draco* and *Distatodinium paradoxum* at ~ 17.1 m, *Enneadocysta partridgei* at ~18.5 m, *Enneadocysta fenestrata* at ~19.9 m, *Membranophoridium aspinatum* and *Hemiplacophora semilunifera* at ~21.8 m. The Top of *Areoligera undulata* is recognized at ~17.1 m, the Base of *Axiodinium prearticulatum* is noted at ~19.9 m, and the Top of *Charlesdowniea coleothrypta* – at ~21.8 m. Based on the occurrence of stratigraphically important *Rhombodinium draco*, this part of the Alum Bay may be attributed to the Rh. draco zone from the West European zonation of Powell (1992), Ukrainian zonation of Andreeva-Grigorovich et al. (2010), W Siberian zonation of Iakovleva & Aleksandrova (2013) and Peri-Tethyan zonation of Iakovleva (in press). According to nannoplankton data, the recognized LO of *Rh. draco* in the Alum Bay corresponds to the topmost part of the NP16 zone. Taking into account the questionable attribution of the 3rd dinocyst interval to the *Rh. draco* zone, the stratigraphical level of the Base of *Rh. draco* correlates well with the data from eastern Peri-Tethys, where the Base of *Rh. draco* is directly

calibrated to calcareous nannoplankton and corresponds to the upper part of NP15-NP16 zone interval (Iakovleva 2017). Dinocyst assemblage from this interval is characterized by the dominance of open-marine *Spiniferites*-group (up to 30%), taking turns to the increase in low-salinity tolerant *Homotryblium*-group (42%), indicating a possible transition to the restricted shallow-water environments with reduced salinity.

The fifth dinocyst interval represents ~ a half of width of studied section (samples AB18-AB23) and revealed the lowermost occurrences of species *Homotryblium floripes* and *Glaphyrocysta intircata* at ~32.4 m, the Base of *Distatodinium craterum-biffii* (transitional form to *D. biffii*) at ~46.5 m and the Base of *Hemisphaeridium fenestratum* at ~47.2 m. Based on the virtual absence of *Rhombodinium porosum* and any other stratigraphically younger taxa, the upper part of the section is attributed to the *Rh. draco* zone interval. Dinocyst assemblage again is characterized in the lowermost part of the interval by an increase in *Spiniferites*-group (28%) and a relative decrease (21%) in *Homotryblium*-group, while the most part of this interval is marked by a significant increase and dominance of *Homotryblium*-group, which varies between 49 and 65%. Such dominance of *Homotryblium*-group may indicate restricted shallow environments with reduced salinity. A slight influx in *Areoligera*- and *Enneadocysta*-groups at ~48.0 m may probably reflect a short transgressive pulse.

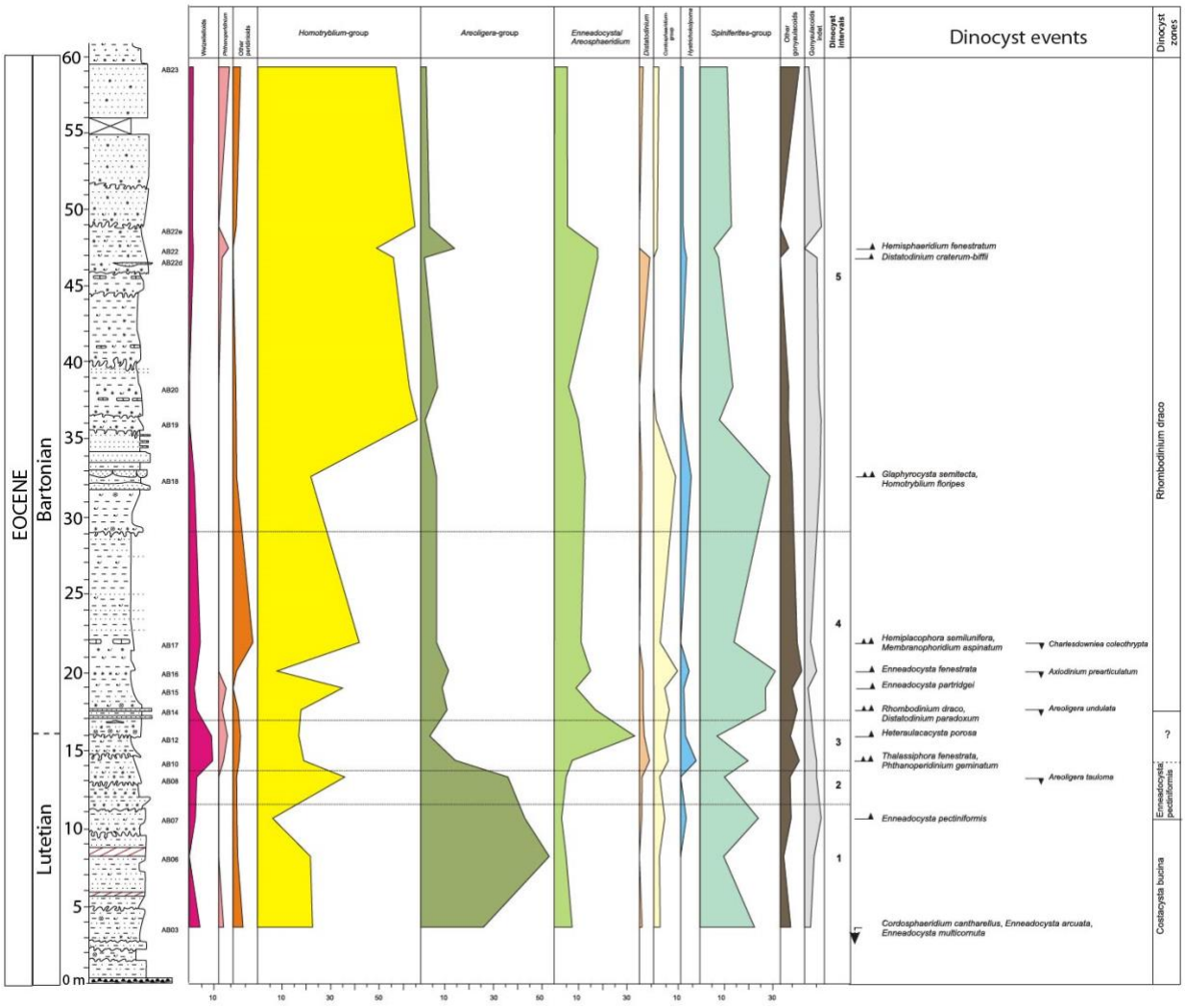

Fig. 4.4: Relative abundance variation patters of selected dinocyst groups at the Alum Bay section. Five dinocyst intervals are recognized. On the right the main recognized dinocyst events are reported with their relative biozones.

4.4.5 Magnetostratigraphy

A total of 15 samples have been demagnetized stepwise following the combined thermal and alternating field (AF) protocol outlined above. The NRM intensity generally ranges from 0.2 x10-3 to 0.6 x 10-3 A/m. with the exception of sample AB2-1A at 2 m that corresponds to a reddish lithology which has an intensity value of 4 x 10-3 A/m. Samples from 11 stratigraphic levels have provided moderate good quality demagnetization data. Samples from 4 stratigraphic levels display scattered demagnetization data preventing the computation of any magnetization

components. These later samples are qualified as “class C” samples. Normally, intensity of the samples drops noticeably after the first heating step at 150ºC and proceeds up to about 25-30 mT demagnetizing a component which is usually northerly oriented and steep in *in-situ* (geographic) coordinates (Fig. 4.5). Above those demagnetizing fields an up to about 80-100mT demagnetization trajectories trending toward the origin define the characteristic remanent magnetization (ChRM). The ChRM components is either northerly and moderately steeply downward (Fig. 5a) or southerly and upwards (Fig. 4.5b and c) oriented in bedding corrected coordinates. The fact that strata is subvertical along the studied sections assures that this component is of pre-tilt origin and likely represents a primary magnetization with dual polarity. The firstly removed low-field component conforms to a recent viscous geomagnetic field direction in geographic coordinates and, thus, represents a secondary overprint. We classify as “class A“ samples those where a clear ChRM trajectory including several demagnetization steps trending towards the demagnetization diagram can be retrieved (Fig. 4.5a-c) or “class AB” when this trajectory is no so well defined.

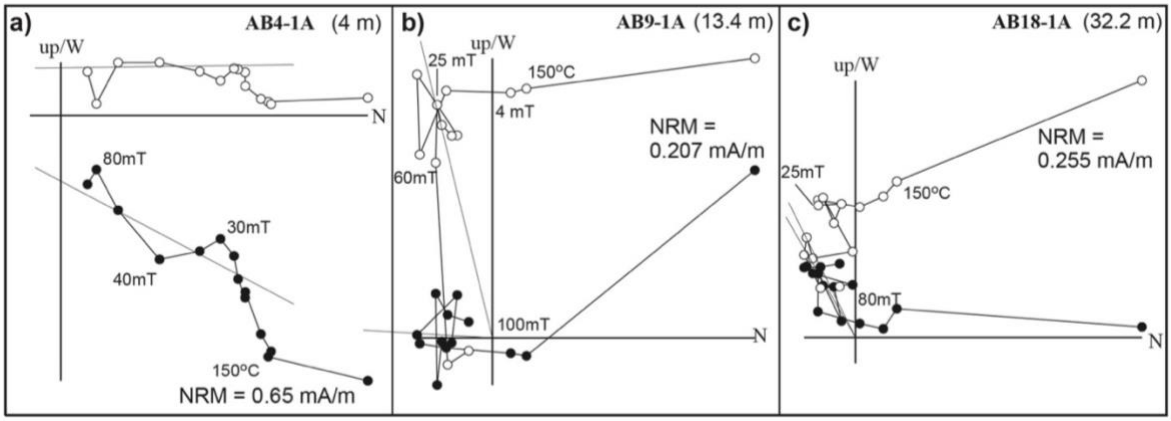

Fig. 4.5 : Representative “class A” normal (a) and reverse (b and c) tilt-corrected (TC) orthogonal demagnetization diagrams from the studied Alum Bay section. The stratigraphic position in meters, the natural remanent magnetization (NRM) intensity and some demagnetization steps are indicated. Open and closed symbols indicate projections onto the upper and lower hemisphere respectively. The computed ChRM direction is shown by a solid grey thick line.

The magnetostratigraphy (Fig. 4.6) indicates a clear reversal boundary located within the 4-5.4 m interval defining a lower normal polarity chron represented by three sample levels and an upper reverse chron that extends up to about 19 m and probably up to 33 m although there is a sampling gap of about 10 m. The interval from 32.2 m up to 86.8 m contains only two sampled stratigraphic levels with “Class C samples” and therefore the polarity of this interval cannot be interpreted with the present dataset. A sample level at the top of the section (86.8 m) presents normal polarity.

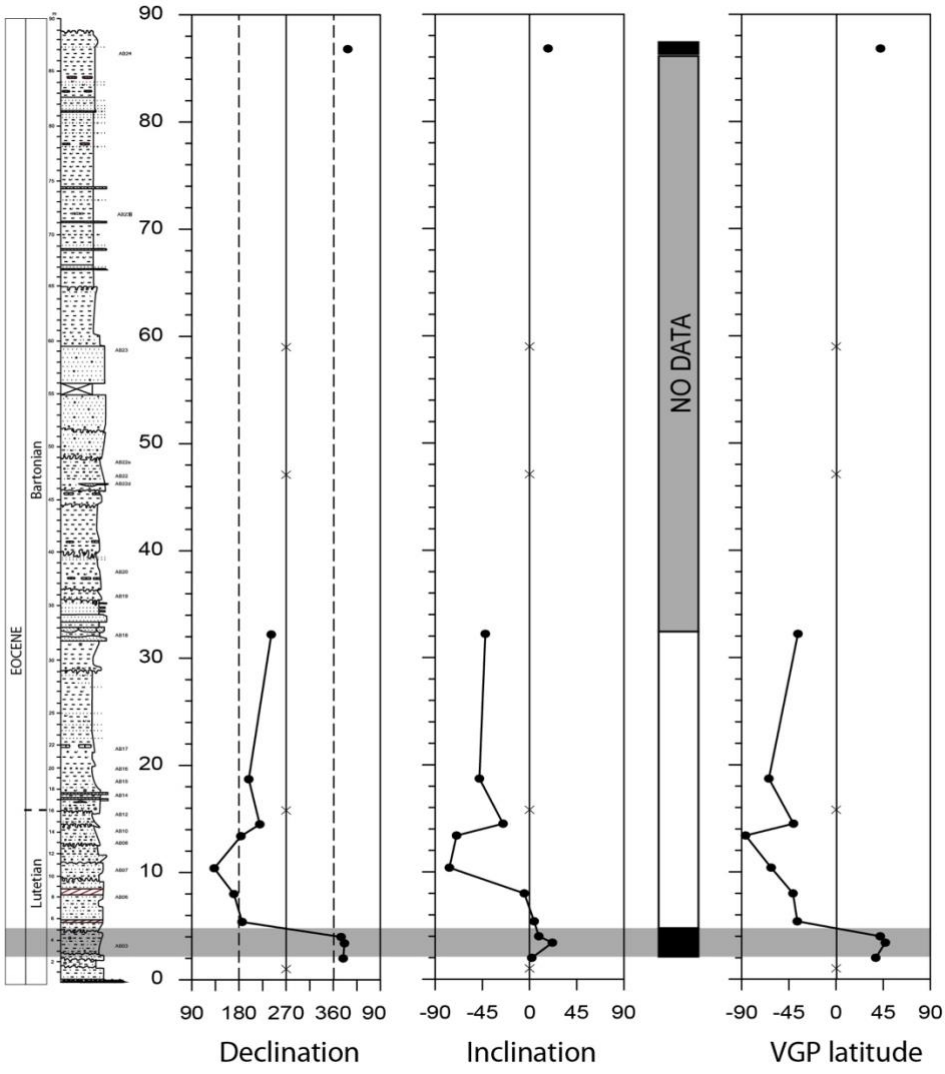

Fig. 4.6: Magnetic polarity stratigraphy of the Alum Bay section. Crosses indicate “class C” specimens (no data), and closed circles mark “class A and AB” specimens (reliable directions). Magnetostratigraphic interpretation includes normal polarity (black), reverse polarity (white) and undefined polarity (grey) bands.

4.5 Interpretation and discussion

Overall the biostratigraphic records are in general agreement with each other and show that the Lutetian-Bartonian transition certainly occurs within the section as it is currently defined. In the absence of a formal Bartonian GSSP, following GTS (2004,2012), the base of the Bartonian could be approximate at the C19n/C18r boundary. In the nannofossil zonation the Alum Bay section falls largely into CNE14 and the upper part within CNE15. Following Agnini et al., 2014, the Lutetian/Bartonian boundary is generally considered to occur in the middle part of CNE14, from nanno-data alone, it's presence is therefore uncertain. However, the palaeomagnetic data indicates it is present. In the scheme of Agnini et al., 2014 the Lutetian - Bartonian boundary is placed at the top of C19n (Fig. 4.7).

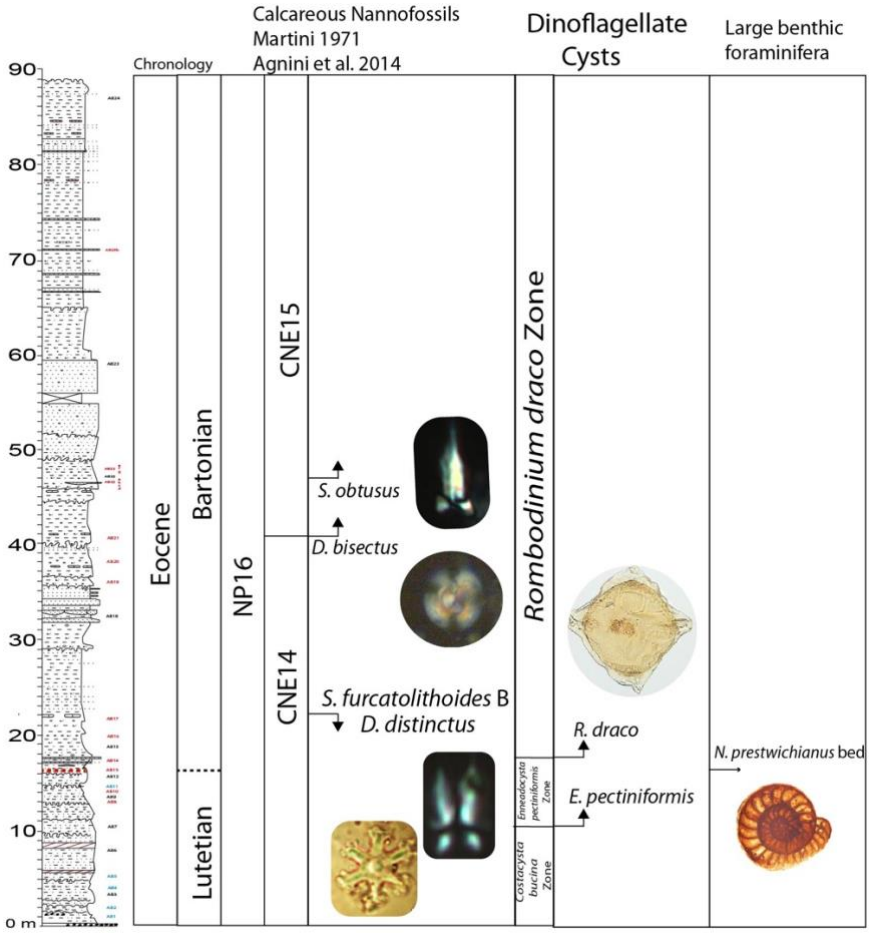

Fig. 4.7: Biostratigraphic data for the Alum Bay section, showing the correlation between calcareous nannofossils, Dynoflagellate cysts and larger benthic foraminifera. In this figure, the Lutetian/Bartonian boundary is still approximated by the *N. prestwichianus* bed.

The palaeomagnetic data from Alum bay indicates that in the lowermost part of the section - 0-5 m C19n and the C19n/C18r occur, indicating that the Bartonian/Lutetian boundary occurs approximately between 4.5m and 5m. The C18r and C18n have been recognized, but at present, it is not possible to determine the C18r/C18n boundary, because in the interval from 32.2 m up to 86.8 m the polarity cannot be interpreted. However, the nannofossil data (Top *S. furcatolithoides B, D. bisectus* and *S. obtusus* Base) suggest (as reported by Agnini et al.,2014) that the C18r/C18n would be between 40.5m and 47 m. Therefore, an additional palaeomagetic sampling would be required to resolve this further (Fig. 4.8).

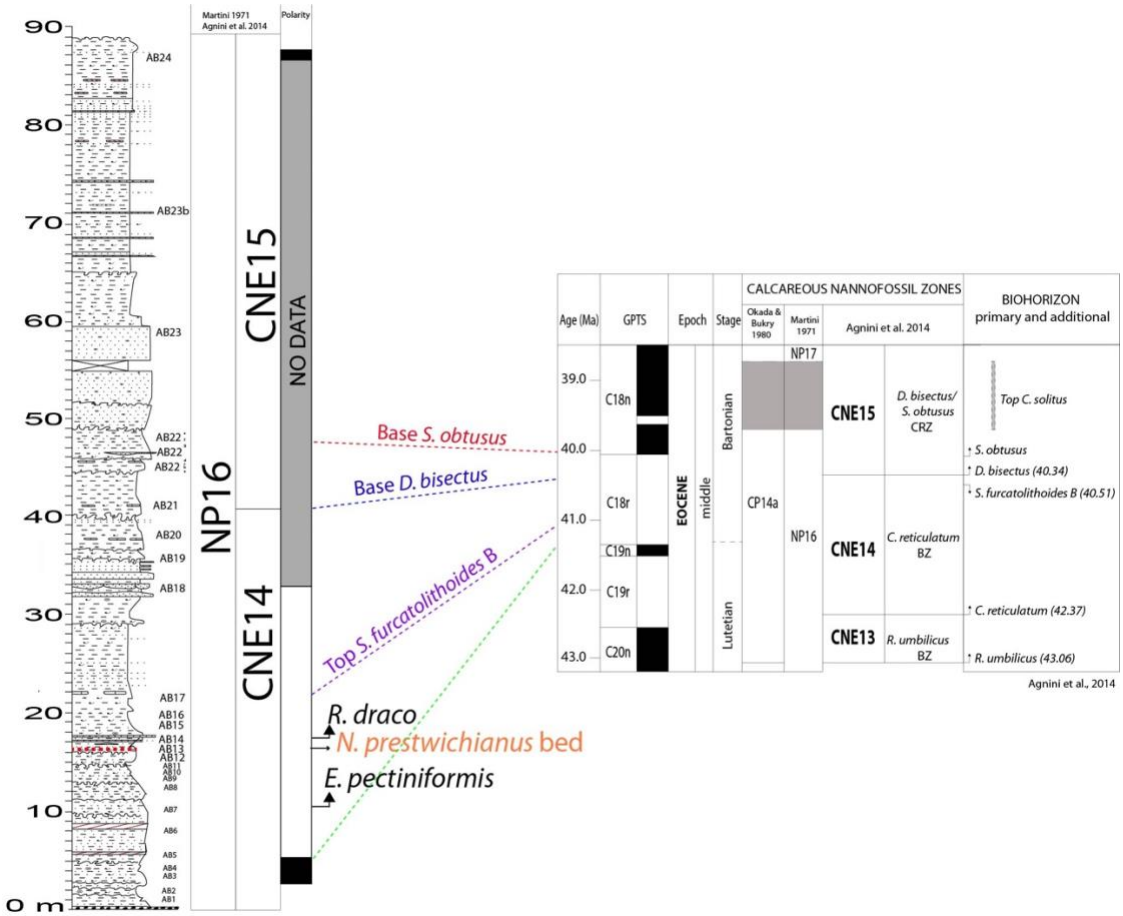

Fig. 4.8: Calcareous nannofossil biostratigraphic data from the Alum Bay section (left) correlated with Agnini et al. 2014 zonation scheme (right) allowing to assign the normal chron recorded at the base of the section to C19n (5 m) and approximating the Lutetian/Bartonian boundary in the absence of a formal GSSP.

When nannofossil indicators are compared with Aubry 1983, 1986 and Dawber et al., 2011 using the *Nummulites prestwichianus* beds as a marker, sample 2165 (12.30 m) of Aubry approximately seems to correlate with AB8 at 13 m. The Tops of *S. furcatolithoides* B and *D. distinctus* were recognised by Aubry at 18 m, which correlates with 18.75 m in this study. In our results the Tops of *S. furcatolithoides B* and *D. distinctus* are at 22 m (AB17), extending their range slightly. In Aubry 1983, 1986 these are used to denote the NP16-NP17 boundary, however more recent work has shown this correlation to be incorrect. Agnini et al 2014 place the Top of *S. furcatolithoides* B in the middle part of NP16 Zone (upper C18r) and following Dunkley Jones et al 2009 the range of *D. distinctus* extends to NP23. Additionally Aubry (1983, 1986) reports the occurrence of *S. obtusus* approximately at 27.2 m, whilst in our results it is at 47 m (AB22). The nannofossil data and dinoflagellate (*R. draco*) levels appears to be the same in our study as that reported in Dawber et al., 2011 (from Bujack et al., 1980). Within the palynological data *R. draco* is one of the most biostratigraphically important occurrences. The recognised Base of *R. draco* in Alum bay corresponds to the topmost part of the NP16 zone (CNE14) and lower part of C18r. When the questionable attribution of the third dinocyst interval to the *R. draco* zone, the stratigraphic occurrence of the Base of *R. draco* correlates well with data from the Eastern Peri-Tethys, where the Base of *R. draco* is directly calibrated to the calcareous nannoplankton and corresponds to the upper part of the NP16 zone interval (Iakovleva 2017), and Chron 18r. It also co-incides with the acme of *Nummulites prestwichianus*. *Nummulites prestwichianus* has previously been suggested to have an upper NP16, lower NP17 range (King 2016) and thus further supports (in our study the *N. preststwichianus* falls only in NP16 Zone, NP17 Zone has not been recognized) the dinoflagellate and nannoplankton results. King (2016) correlated this with the SBZ17, however given the challenges of larger benthic foraminiferal stratigraphy (see Cotton and Pearson 2011; Papazzoni et al., 2017) and applying it to a monospecific assemblage this correlation is tentative. In addition *N. rectus* which occurs in samples AB17 and AB18 is correlated

to NP 17 (for us is not NP17 but NP16) and SBZ17 in King 2016. This gives a younger age than other analyses in this study, and is more likely a problem with the understanding of ranges of NW European *Nummulites*, particularly as *N. rectus* occurs in very low numbers. Suggesting the *Nummulites* of this region need to be restudied in detail.

The larger benthic foraminifera are comprised of a largely monospecific assemblage, with *Nummulites rectus* only being found in very low numbers at the top of the *N. prestwichianus* beds. Such assemblages of *Nummulites* are not uncommon and may be linked to the area being at the limits of their range and not a typical oligotrophic shallow carbonate environment. Previous studies have suggested that the *N. prestwichianus* from this region consisted of several morphotypes (King 2016). There is some variation in the proloculus size between the beds, however, a full morphological comparison, including other material from the south of the UK is needed to clarify this. All however, closely fit the descriptions of *N. prestwichianus* following Blondeau 1966, and therefore for the purpose of this study we keep them as *N. prestwichianus*. Whilst the beds are certainly distinctive, they have limited use as biostratigraphic marker beds as due to the lateral discontinuity and potential for diachroneity. Larger benthic foraminifera are well known to be restricted to the photic zone, and thus my follow transgressions and regressions.

This shallow water environmental interpretation is supported by the small benthic foraminifera assemblages.. Murray and Wright (1974) inferred the paleodepth at Alum Bay based on benthic foraminifera, and they interpreted a near shore shelf depositional setting, with fine substrate and turbid water for this part of the sequence. Our new study corroborates this interpretation, as in addition to *Cibicides,* the rest of the genera identified at Alum Bay (*Bolivina, Brizalina, Buccella, Buliminella, Discobris, Nonion*, *Quinqueloculina* and *Rosalina*) are common in inner shelf environments (0-100 m; Murray, 1991).

The dominance of a single genus (*Cibicides*) is the most remarkable feature of the small benthic foraminifera assemblages at Alum Bay. This genus is commonly associated with cold waters (Murray 1991). The upper half of the studied section is not only dominated by this one genus, but it also has a strong dominance of one species (>50% of *C. pygmeus* in interval B, and *C. ungerianus* in interval C), which accounts for the low diversity of the assemblages.

Interval A (14 – 20.5 m) represents a near shore, shallow and stable shelf setting, possibly partially restricted and/or slightly hyposaline due its low diversity values (Murray, 2006). This hypothesis is supported by the occurrence of *Protelphidium*, as this genus is associated with low salinity environments (Murray and Wright, 1974). Dinoflagellate assemblages also point towards a restricted-inner neritic environment (sample AB12). The maximum values of diversity, P/B ratio and foraminifera per gram in sample AB16 (19.5 m) of this interval may reflect a condensed horizon, possibly caused by reduced sedimentation rates and/or changes in sea level.

Interval B (20.5 – 40.5 m) is dominated by *C. pygmeus*, and it contains one sample barren of foraminifera. Murray and Wright (1974) interpreted barren samples from this part of the log as reflecting intertidal conditions, which might point to variations in sea level and unstable conditions. We argue that *C. pygmeus* may have adapted to environmental instability related to rapidly changing sea level, becoming more abundant in this interval. *Rosalina* spp. has been argued to have a clinging mode of life (attached with organic 'glue' to the seaweeds or hard substrates), indicative of a high energy environment (Kitazato, 1988), supporting a near-shore setting with episodes of intertidal settings.

The interval C (40.5 – 48 m) is characterised by a strong dominance of *C. ungerianus,* and by a small increase in percentage of species present in interval A such as *Buccella propingua, Cibicides fortunatus and Globulina gibba*. These results point to a return to conditions similar to those inferred from the lower part of the section. However, diversity and the percentage of infaunal morphogroups are lower, possibly due to the proliferation of opportunistic species (*C.*

ungerianus and *Buccella propingua*). After the instability recorded in interval B, the assemblages seem to recover and reflect environmental conditions similar to those from interval A.

Our results agree with the interpretation and intervals defined by Murray and Wright (1974) for this part of the section, corresponding to the Upper Bracklesham beds and lower Barton beds. However, the interpretation given by Dawber et al. (2011) for the same section slightly differs from our results. They infer a shallowing-upward trend from the lower part of the section (70-120 m paleodepth, equivalent to our interval A) to 30-70 m paleodepth towards our interval B, and 0-30 m towards our interval C. Diversity values are also slightly lower, with Fisher-α ranging from 0 to 5 and H (S) from 0 to 1.5. Neither of these trends fit our observations. We do not know the source of these discrepancies, and we cannot evaluate the results in that publication as it does not provide information regarding the methodology followed in the study of benthic foraminifera (e.g., number of specimens counted per sample, permanent record of the picked specimens, taxonomic criteria used in the identification of taxa, etc.), and a table with the benthic foraminiferal counts is missing

A difference in the preservation of calcareous nannofossils was noted when compared to that previously reported by Aubry. With our observations indicating a poor/average preservation compared to Aubry, 1983, 1986 in the calcareous nannofossil content. The exception to this is the larger benthic foraminifera in the *N. prestwichianus* bed. Though pyrite is common the preservation of the LBF is often exceptional, due to their preservation in clay, rather than carbonate as is more common. This exceptional preservation has led to their inclusion in studies of *Nummulites* mineralogy (Cotton et al. in prep) and will be included in future clumped isotope work.

4.6 Conclusion

Integrated stratigraphy combining nannofossils, small and large benthic foraminifera, dinoflagellate and palaeomagnetic studies has been carried out for the first time from Alum bay, to reassess its potential to define the Lutetian/Bartonian boundary. The Alum bay section is within nannoplankton Zones CNE14 and CNE15, the base of *Rh. draco* is recognised within the section, which also coincides with the acme of *N. prestwichianus*, both of which are correlated with nannoplankton Zone NP16 which spans the late Lutetian and early Bartonian. The palaeomagnetic correlation with calcareous nannofossil data allows to assign the normal Chron at the base of the section to C19n. The remaining part of the section correlates to C18n and C18r. All analyses therefore support that the section is largely early Bartonian in age, with the palaeomagnetic data indicating the first 5 m of the section also contains the late Lutetian and that the boundary is therefore within the section. These results largely confirm those from previous individual stratigraphic studies (e.g. Eaton 1976, Aubry 1983, 1986, Dawber et al., 2011) although notable differences were found in the quality of preservation in the nannoplankton, it has also highlighted the potential of LBF from this site for future geochemical work. Higher resolution palaeomagnetic sampling would be needed to further refine the biostratigraphy. It appears unlikely that Alum Bay alone will be able to resolve the placement of the Lutetian-Bartonian boundary, however, it still remains an important section in understanding the biostratigraphy across this interval.

References

Agnini, C., Fornaciari, E., Giusberti, L., Grandesso, P., Lanci, L., Luciani, V., ... & Stefani, C. (2011). Integrated biomagnetostratigraphy of the Alano section (NE Italy): A proposal for defining the middle-late Eocene boundary. Bulletin, 123(5-6), 841-872.

Agnini, C., Fornaciari, E., Raffi, I., Catanzariti, R., Pälike, H., Backman, J., & Rio, D. (2014). Biozonation and biochronology of Paleogene calcareous nannofossils from low and middle latitudes. Newsletters on Stratigraphy, 47(2), 131-181.

Andreeva-Grigorovich, A.S., Waga, D.D., (2010). Nannofossil biostratigraphy of the Paleogene sediments of the Crimea-Caucasus region (southern Ukraine and Russia). Abstracts of 4th French Congress on Stratigraphy “Strati 2010”, 6–8.

Aubry, M.-P., (1983). Biostratigraphie du Paléogène épicontinental de l’Europe du nord-ouest. Étude fondée sur les nannofossiles calcaires. Documents des Laboratoires de Géologie de la Faculté des Sciences de Lyon 89, 1–317.

Aubry, M.-P., (1985). Northwestern European Paleogene magnetostratigraphy, biostratigraphy, and paleogeography: calcareous nannofossil evidence. Geology 13, 198–202.

Aubry, M.-P., (1986). Paleogene calcareous nannoplankton biostratigraphy of northwestern Europe. Palaeogeography, Palaeoclimatology, Palaeoecology 55, 267–334.

Berggren, W. A., Kent, D. V., Swisher III, C. C., & Aubry, M. P. (1995). A revised Cenozoic geochronology and chronostratigraphy.

Blondeau, A. (1966). Les nummulites de l'Eocene de Belgique. Bulletin de la Société géologique de France, 7(6), 908-919.

Bown, P. R. and Young, J. R. (1998). Techniques, in: Calcareous Nanno- fossil Biostratigraphy, Chapman & Hall, London, 16–28.

Bujak, J., & Mudge, D. (1994). A high-resolution North Sea Eocene dinocyst zonation. Journal of the Geological Society, 151(3), 449-462.

Bujak, J.P., Downie, C., Eaton, G.L., Williams, G.L., (1970). Dinoflagellate cysts and acritarchs from the Eocene of southern England. Special Papers in Palaeontology 24, 1–100.

Cotton, L. J., & Pearson, P. N. (2011). Extinction of larger benthic foraminifera at the Eocene/Oligocene boundary. Palaeogeography, Palaeoclimatology, Palaeoecology, 311(3-4), 281-296.

Curry, D., (1981). In: Pomerol, C. (Ed.), Stratotypes of Paleogene stages. Bulletin d’Information des Géologues du Bassin de Paris (Mém. hors série), vol. 2. , pp. 23–36.

Dawber, C.F., Tripati, A.K., Gale, A.S., MacNiocaill, C., Hesselbo, S.P., (2011). Glacioeustacy during the middle Eocene? Insights from the stratigraphy of the Hampshire Basin, UK. Palaeogeography, Palaeoclimatology, Palaeoecology 300, 84–100.

Dunkley Jones, T., Bown, P. R., & Pearson, P. N. (2009). Exceptionally well preserved upper Eocene to lower Oligocene calcareous nannofossils (Prymnesiophyceae) from the Pande Formation (Kilwa Group), Tanzania. Journal of Systematic Palaeontology, 7(4), 359-411.

Eaton, G.L., (1976). Dinoflagellate cysts from the Bracklesham Beds (Eocene) of the Isle of Wight, southern England. Bulletin of the British Museum (Natural History) (Geology) 26, 227–332 21 pls.

Fluegeman, R. H. (2007). Unresolved issues in Cenozoic chronostratigraphy. Stratigraphy, 4(2-3), 109-116.

Fornaciari, E., Agnini, C., Catanzariti, R., Rio, D., Bolla, E. M., & Valvasoni, E. (2010). Mid-latitude calcareous nannofossil biostratigraphy and biochronology across the middle to late Eocene transition. Stratigraphy, 7(4), 229.

Heilmann-Clausen, C. (1988). The Danish Subbasin, Paleogene dinoflagellates. The north west European Tertiary basin: results of the International Geological Correlation Programme, Project, (124), 339-343.

Heilmann-Clausen, C., & Van Simaeys, S. (2005). Dinoflagellate cysts from the Middle Eocene to? lowermost Oligocene succession in the Kysing Research borehole, central Danish Basin. Palynology, 29(1), 143-204.

Hooker J.J., King C., (2018). The Bartonian unit stratotype (S. England): Assessment of its correlation problems and potential, Proc. Geol. Assoc., https://doi.org/10.1016/j.pgeola.2018.08.005

Hooker, J. J. (1986). Mammals from the Bartonian (middle/late Eocene) of the Hampshire Basin, southern England (Vol. 39, No. 4).

Huggett, J. M., & Gale, A. S. (1997). Petrology and palaeoenvironmental significance of glaucony in the Eocene succession at Whitecliff Bay, Hampshire Basin, UK. Journal of the Geological Society, 154(5), 897-912.

Iakovleva, A. I., Aleksandrova, G. N., 2013. To the question on Dinocyst zonation of Paleocene–Eocene in Western Siberia. Bulletin of the Moscow Society of Naturalists, Geological Section 88(1), 59–82. (in Russian)

Iakovleva, A.I. (2017), Detalization of Eocene dinocyst zonation for Eastern Peritethys. Bulletin of Moscow Society of Naturalists. Geological Series, 92, pp. 32-48. (in Russian)

Jovane, L., Sprovieri, M., Coccioni, R., Florindo, F., Marsili, A., & Laskar, J. (2010). Astronomical calibration of the middle Eocene Contessa Highway section (Gubbio, Italy). Earth and Planetary Science Letters, 298(1-2), 77-88.

Keen, M. C. (1993). Ostracods and Late Eocene cycles of sedimentation in southern England. In: Keen, M. C. (ed.) Proceedings of the 2nd European Ostracodologists' Meeting. University Of Glasgow, Glasgow, 213 – 222.

King, C. (2016, January). A revised correlation of Tertiary rocks in the British Isles and adjacent areas of NW Europe. Geological Society of London.

Kirschvink, J. L. (1980). The least-squares line and plane and the analysis of palaeomagnetic data. Geophysical Journal, Royal Astronomical Society, 62(3), 699–718.

Kitazato, H., 1988. Ecology of benthic foraminifera in the tidal zone of a rocky shore. Revue de Paléobiologie, vol. spec. 2 (Benthos'86), p. 815-825.

Köthe, A. (2012). A revised Cenozoic dinoflagellate cyst and calcareous nannoplankton zonation for the German sector of the southeastern North Sea Basin. Newsletters on Stratigraphy, 45(3), 189-220.

Liengjarern, M., Costa, L., & Downie, C. (1980). dinoflagellate cysts from the upper eocene_ lower oligocene of the isle of wight. Palaeontology, 23, 25.

Marino, M., & Flores, J. A. (2002a). Middle Eocene to early Oligocene calcareous nannofossil stratigraphy at Leg 177 Site 1090. Marine Micropaleontology, 45(3), 383-398.

Martini, E. (1971). Standard Tertiary and Quaternary calcareous nannoplankton zonation. In Proc. II Planktonic Conference, Roma 1970, Roma, Tecnoscienza (Vol. 2, pp. 739-785).

Murray, J.W., Wright, C.A., (1974). Palaeogene Foraminiferida and palaeoecology, Hampshire and Paris Basins and the English Channel. Special Papers in Palaeontology 14, 1–129 20 pls.

Okada, H., Bukry, D., (1980). Supplementary modification and introduction of code numbers to the low-latitude coccolith biostratigraphic zonation (Bukry 1973, 1975). Marine Micropaleontology 5, 321–325.

Papazzoni, C. A., Fornaciari, E., Giusberti, L., Vescogni, A., & Fornaciari, B. (2017). integrating shallow benthic and calcareous nannofossil zones: the lower eocene of the monte postale section (northern italy) sb and cn biozonation in the eocene of Monte Postale, italyc. a. papazzoni et al. palaios, 32(1), 6-17.

Plint, A. G. (1988). Global eustacy and the Eocene sequence in the Hampshire Basin, England. Basin Research, 1(1), 11-22.

Powell, A.J., (1992). Dinoflagellate cysts of the Tertiary System. In: Powell, A.J. (Ed.), A Stratigraphic Index of Dinoflagellate Cysts. British Micropaleontological Society Publication Series. Chapman and Hall, London, pp. 155–251.

Prestwich, J. (1847). On the probable Age of the London Clay, and its Relations to the Hampshire and Paris Tertiary Systems. Quarterly Journal of the Geological Society, 3(1-2), 354-377.

Riding, J. B., & Kyffin-Hughes, J. E. (2004). A review of the laboratory preparation of palynomorphs with a description of an effective non-acid technique. Revista Brasileira de Paleontologia, 7(1), 13-44.

Riding, J. B., & Kyffin-Hughes, J. E. (2004). A review of the laboratory preparation of palynomorphs with a description of an effective non-acid technique. Revista Brasileira de Paleontologia, 7(1), 13-44.

Sluijs, A., & Brinkhuis, H. (2009). A dynamic climate and ecosystem state during the Paleocene-Eocene Thermal Maximum: inferences from dinoflagellate cyst assemblages on the New Jersey Shelf. Biogeosciences, 6(8).

Villa, G., Fioroni, C., Pea, L., Bohaty, S., & Persico, D. (2008). Middle Eocene–late Oligocene climate variability: calcareous nannofossil response at Kerguelen Plateau, Site 748. Marine Micropaleontology, 69(2), 173-192.

Wei, W., & Wise Jr, S. W. (1989). Paleogene calcareous nannofossil magnetobiochronology: results from South Atlantic DSDP Site 516. Marine Micropaleontology, 14(1-3), 119-152

Zijderveld, J. D. A. (1967). A. C. demagnetization of rocks: analysis of results. In D. W. Collinson, K. M. Creer, & S. K. Runcorn (Eds.), Methods in Palaeomagnetism (pp. 254–286). Amsterdam, New York: Elsevier.

Chapter 5

General conclusions

The main aim of this thesis work was the investigation of the role played by the high frequency orbital forcing (precession and eccentricity) on the abundance and distribution of calcareous nannofossil assemblages, during the Ypresian and Lutetian Stages (56-41Ma) in the Basque-Cantabrian Basin. Such an approach has been applied to different stratigraphic successions of Eocene period, an investigation that had not been previously performed for this time interval. We carried on the study of three stratigraphic successions, representing different paleoenvironments in the Basque-Cantabrian Basin: the Sopelana, the Oyambre and the Gorrondatxe sections. In the frame of the study of the Eocene, an added goal to the thesis was the multidisciplinary study (nannofossil, smaller and larger benthic foraminifera, dinoflagellate and paleomagnetism) of the Alum Bay section in the Hampshire basin.

In the first part of this thesis work we focused on the analysis of the Sopelana section, producing a calcareous nannofossil biostratigraphy, that allowed us, documenting the *Rhomboaster-Tribrachiatus* lineage, to confirm the stratigraphic continuity and to assign the section to CNE1-CNE3 Zones (early Ypresian). The statistical analysis (Principal Component and Cluster analysis) on the calcareous nannofossil assemblages allowed us to identify the presence of oligotrophic and warm water taxa and well distinct eutrophic and cooler taxa. These two cluster have been interpreted to be dependent from two major components, the temperature and the nutrient supply. Based on time series analysis performed on $CaCO_3$, we have identified cycles, expressed by marl-limestone couplets, organized in bundles, that have been proven to be in phase with Milankovitch frequencies. Particularly, the periodicities may be related with precession (21 ky, marl-limestone couplets) and short eccentricity cycles (100 ky, bundles), influencing fertility and

productivity. An increase of eutrophic taxa is recorded in marly beds, indicating that they can be correlated with high fertility.

In the second part, we applied a similar approach to three specific intervals of the Sopelana, Oyambre and Gorrondatxe sections. The role of the orbital forcing on marl-limestone couplets sedimentation had been proven for the Sopelana section in the first part of our thesis work, while, for the two last sections, this forcing had already been proven (Martinez-Braceras et al., 2017), representing a starting point for our analyses. The three sections, are the expression of different paleoenvironments, allowing us to investigate the role of orbital forcing on calcareous nannofossil assemblages in different depositional conditions. Contrarily to the above mentioned analysis of the Sopelana section, in this study we focused on a discrete eccentricity cycle, expressed by a single bundle, implying a high resolution analysis of calcareous nannoplankton assemblage variations. The depositional model by Martinez-Braceras et al., (2017) is confirmed and supported by our analyses of abundance variations and by our paleoecological studies. Considering all the three investigated sections, the major and most relevant variations of calcareous nannofossil assemblages have been proven to be occurred in correspondence of the maximum eccentricity, as testified by a decrease of oligothrophic warm and stable environment taxa and an increase of meso-euthrophic cooler, lower salinity and stressed environment taxa. The statistical analysis (Principal Component and cluster analyses) applied to the nannofloral content, suggested that the major variables driving the deposition of marly lithology are high nutrients and lower temperatures, whereas, limestones are formed under lower nutrient supply and higher temperatures. This outcomes, confirm, as previously indicated by our general study of the Sopelana section (first part of this thesis work) that marls likely reflect high fertility.

Overall, our study on the entire Sopelana section and on a discrete bundle of the Sopelana, Oyambre and Gorrondatxe sections, proved the role of orbital forcing on calcareous

nannofossil communities, giving information of how they respond to the shift of nutrients/temperatures/salinity parameters, and furnishing an overview of possible environmental conditions in the Basque-Cantabrian Basin during the Ypresian-Lutetian.

In a third part we investigated the Lutetian/Bartonian boundary, with a different aim. Our main goal for this further study was to improve the biostratigraphy and chronology for the Bartonian Stage, for which the definition of the GSSP is still pending. Alum Bay section is the parastratotype for the Bartonian stage, and our objective was to find possible events that can be correlated outside of the Hampshire Basin. Our multiple analyses, allowed us to assign the Alum bay section to calcareous nannoplankton Zones CNE14-CNE15 corresponding to NP16. Basing on our biostratigraphic analysis, *Rhombodinium draco* (dinoflagellate), an important and correlatable event in the Peri-Thetyan domain, is recognized within the section, and correspond to the acme of *Nummulites prestwichianus* (considered the base of the Bartonian Stage in the Barton area). *Rhombodinium draco* was proven to correlate with nannoplankton Zone NP16. Furthermore, considering magnetostratigraphic data, we identified the normal Chron C19n (considered the Base of the Bartonian Stage in absence of a formal GSSP) in the interval 0-5m. Considering the Alum Bay section, even if our work cannot completely solve the correlation problematics for the Bartonian stage, this interdisciplinary effort provides new useful information for the Bartonian GSSP definition.